Blanca Mendiguren Gutiérrez

Morphological evolution of the Guadiana ebb-delta at short time scales

UNIVERSIDADE DO ALGARVE

FACULDADE DE CIÊNCIAS E TECNOLOGIA

2020

Blanca Mendiguren Gutiérrez

Morphological evolution of the Guadiana ebb-delta at short time scales

Master in Marine and Coastal Systems
Work performed under the supervision of:

Erwan Garel

Óscar Ferreira

UNIVERSIDADE DO ALGARVE

FACULDADE DE CIÊNCIAS E TECNOLOGIA

2020

Morphological evolution of the Guadiana ebb-delta at short time scales

Declaração de autoria de trabalho

Declaro ser a autora deste trabalho, que é original e inédito. Autores e trabalhos consultados estão devidamente citados no texto e constam da listagem de referências incluída.

_____

Declaration of authorship of work

I declare to be the author of this work, which is original and unpublished. Authors and works consulted are duly cited in the text and are included in the list of references.

_____

Abstract

The Guadiana estuary (southern Portugal) has undergone drastic changes in the morphology of the ebb-tidal delta and inlet channel due to anthropogenic activities: jetty construction, closure of a major dam and dredging activities. The morphologic evolution of the mixed-energy ebb-tidal delta of the Guadiana estuary and its response to the ocean climate, is examined using a series of sequential satellite images (Sentinel-2) and bathymetric maps spanning six years. To achieve these goals, the outer edge at the three main morphological features of the ebb-delta was identified, namely the updrift lateral bar, the outer shoal and the downdrift complex. The evolution of the sandy shoals was examined over both datasets through six profiles across the ebb-delta, evidencing a series of landwards and seawards migrations. The wave climate was studied independently for southeast (SE) and southwest (SW) swells. Furthermore, storm events were defined based on a significant wave height higher than 2.5 m and a duration of these events of at least 6 hours. A total of 53 storm events were identified and analysed separately according to the dominant incoming direction of the storms. Additionally, the impact of the swells and of the storm events in the behaviour of the sandbars was researched regarding their normalised wave power. This last analysis evidenced a relation with the migration of the ebb-delta shoals. Finally, it was possible to identify the normal behaviour of the ebb-delta shoals under the dominant swells (SE and SW) and the severe impact of extreme storm events (such as Emma storm). The Guadiana ebb-tidal delta morphology displays a strong seasonal pattern due to the strong reliance on the local hydrodynamic conditions, depicting a morphological cyclic recession of the shoals after storm events, which yields a progressive counter clockwise rotation over the ebb-delta.

Keywords: Ebb-delta; Mixed-energy inlet; Morphological evolution; Storm events

Resumo

Mudanças drásticas na morfologia e no canal do delta vazante do estuário do Guadiana (sul de Portugal) ocorreram após a construção de espigões, fechamento de uma grande barragem e atividades de dragagem. A evolução morfológica do delta de maré de energia mista do estuário Guadiana, e a sua reposta ao clima oceânico, incluindo eventos de tempestade, foi investigada por meio de uma serie sequencial de seis anos de imagens de satélite (Sentinel-2) e mapas batimétricos. Visando verificar a evolução morfológica, as principais bordas externas do delta de vazante foram digitalizadas, cuja identificação nas imagens de satélite foram facilitadas pelos mapas batimétricos. A evolução dos bancos de areia do delta vazante foi examinada em seis perfis no conjunto de dados. O clima oceânico foi analisado separadamente para ondas provenientes de sudeste (SE) e sudoeste (SW), e a definição dos eventos de tempestade foi baseada na altura significativa de onda e a duração destes eventos. Foram identificados um total de 53 eventos de tempestade, estes foram examinados separadamente de acordo com a direção dominante. O comportamento dos bancos de areia foi investigado em relação aos impactos das ondas (SE e SW) e dos eventos de tempestade, evidenciando a relação destas variáveis com a migração dos bancos de areia do delta vazante. No presente estudo foi possível identificar o comportamento natural dos bancos de areia do delta de vazante sob a dominância das ondas (SE e SW) e o severo impacto causado por eventos extremos de tempestade (tempestade Emma). O delta de vazante do Guadiana é fortemente dependente das condições hidrodinâmicas locais, mostrando variações sazonais na morfologia. Foi identificada uma recessão cíclica dos bancos de areia apos períodos de tempestade, promovendo uma rotação progressiva em sentido anti-horário do delta de vazante.

Resumo alargado

Os deltas de maré vazante são acumulações de areia em direção ao mar na frente da barra da maré e formam-se principalmente devido as correntes de maré vazante e são modificadas pela ação das ondas. O estuário do Guadiana (sul de Portugal) sofreu drásticas mudanças na morfologia do delta vazante e no canal após uma serie de alterações antropogénicas. O canal foi delimitado pela construção de dois espigões em 1972 e 1974 na barra de maré e também provocou mudanças na morfologia do delta histórico. O aporte de sedimentos ao delta foi reduzido drasticamente na área de estudo por conta do fechamento de uma grande barragem e duas atividades de dragagem, que foram necessárias para habilitar a navegação entre o delta e o canal, sendo em 2015 a última dragagem realizada.

Previamente à intervenção antropogénica na barra de maré, os sedimentos eram incorporados num sistema de banco de areia no delta de vazante histórico, o banco de O'Bril, localizado na margem oeste do estuário. Devido ao clima oceânico, o delta de vazante moderno do estuário Guadiana é considerado de energia mista e está constituído por quatro características principais, nomeadamente: i) o canal, sendo parte mais estreita e profunda da barra de maré, ii) a barra lateral à barlamar, iii) a barra frontal e iv) o complexo à sotamar. As condições de onda nesta área produzem uma deriva longilitoral dominante em direção a Este e os sedimentos acumulam-se na área à barlamar. Estes sedimentos podem-se movimentar para a barra frontal, a qual também recebe materiais do rio Guadiana. O transporte sedimentar para o complexo de barlamar é devido à deriva longilitoral desde a barra à sotamar, este processo é conhecido como *sediment bypassing*. O *sediment bypassing* é descontínuo e depende da frequência das ruturas naturais associadas ao banco de O'Bril, que podem ocorrer gradualmente ou pontualmente devido a fenómenos como tempestades.

A evolução morfológica do delta de maré do estuário Guadiana e a sua reposta ao clima oceânico foi investigado no presente estudo por meio de uma serie sequencial de noventa e sete imagens de satélite (Sentinel-2) e seis mapas batimétricos, abrangendo uma série temporal de seis anos. Visando verificar as alterações morfológicas do delta de maré vazante, as margens externas dos três bancos de areia principais foram digitalizadas (a barra lateral à barlamar, a barra frontal e o complexo à sotamar). A identificação da margem dos bancos de areia ao longo do delta nas imagens de satélite foi facilitada pelos mapas batimétricos, resultando em uma valiosa complementaridade do conjunto de dados. A evolução dos bancos de areia do delta de vazante foi examinada por meio de seis perfis no conjunto de dados. Quatro perfis foram

definidos para os bancos de areia ao oeste e dois perfis para o complexo a sotamar. O clima oceânico usado no presente estudo foi obtido através de dados de uma boia offshore e analisados separadamente para ondas procedentes do sudeste (SE) e sudoeste (SW). Adicionalmente, estudaram-se os eventos de tempestade, os quais foram definidos baseados na altura de significativa de onda (< 2.5 m) e a duração destes eventos (mínimo de 6h). Isto permitiu um último estudo, distinguindo os períodos nos quais aconteceram eventos de tempestade e períodos nos quais não houve tempestade com o objetivo de investigar o comportamento das barras de areia sob o efeito dos diferentes climas oceânicos. O impacto das ondas, já seja durante períodos de tempestades ou sem tempestades, foi fundamentado no poder normalizado das ondas (*Pn*) uma vez que contabiliza com o efeito das marés de sizígia, o qual causa alterações morfológicas no delta principalmente durante as marés baixas.

Os mapas batimétricos permitiram a observação de uma serie de modificações na morfologia dos principais elementos do delta de vazante: o alargamento e migração para o mar da barra lateral à barlamar, a redução no comprimento dos bancos de areia lobados da barra frontal e uma mudança na orientação e posição do canal. Foram realizados uma serie de mapas de diferença vertical anuais, os quais possibilitaram a visualização de migrações dos bancos de areia para à costa e para o mar, destacando essas migrações nos anos 2016-2017 e 2017-2018. Foram identificados um total de 53 eventos de tempestade, os quais foram examinados por separado de acordo com a direção dominante da tempestade. Os impactos das ondas (SE e SW) e dos eventos de tempestade foram investigados em relação ao comportamento dos bancos de areia, evidenciando a relação com a migração dos bancos de areia do delta vazante. Um evento extremo de tempestade foi identificado no estudo, a tempestade Emma, cujo impacto foi severo na morfologia do delta. Embora esse evento extremo de tempestade não ter afetado a barra lateral à barlamar, a localização dos bancos de areia da barra central migraram 38 m para o mar, resultando após esse evento em uma migração de 45 m do complexo a sotamar em direção a costa.

No presente estudo, não foi possível associar a direção das migrações dos bancos de areia com a direção proveniente das ondas que atingiram a costa, em vista que as ondas vindas de sudeste e de sudoeste resultaram em migrações tanto para a costa como para o mar. No entanto, foi possível identificar que é a dominância da direção das ondas o fator que domina o comportamento dos bancos de areia do delta vazante. O delta de vazante do Guadiana exibiu fortes padrões sazonais devido à hidrodinâmica, resultando em morfologias induzidas pela maré durante os meses do verão e morfologias induzidas pelas ondas durante o inverno. O

comportamento normal dos bancos de areia do delta de vazante do Guadiana é diferente na zona Este e Oeste, as barras frontais e laterais à barlamar tendem a migrar para o mar, enquanto o complexo à sotamar migra para a costa. O impacto das tempestades faz com que os bancos de areia migrem em direção oposta à normal, após os quais pode-se observar uma morfologia definida como estado pós-tempestade (*Post-storm state*). Depois destes eventos de tempestade, os bancos de areia passam por um período de transição (*Transitional-phase),* onde não há grandes mudanças na morfologia. Este período de transição finaliza em um estado de calmaria-extensa (*extended-calm),* no qual os bancos de areia retomam as migrações em sentido normal. Esta serie de períodos ou fases criam uma recessão cíclica da morfologia que, além de migrar os bancos de areia, promove uma rotação progressiva em sentido anti-horário do delta de vazante no estuário do Guadiana.

Acknowledgements

I am most grateful to both of my supervisors Erwan Garel and Oscar Ferreira for helping me with any issue I faced working on this thesis. I felt supported by them the whole time, even during a global pandemic and their holidays. I am thankful for the time they have dedicated to me, including the last-minute corrections and the patience in dealing with all my doubts during the time of this project. The detailed comments and feedback I received from them throughout the whole process, resulted in an improvement in knowledge of tidal deltas morphology and a more critical view in the scientific research.

I would like to thank the GUADELTA project for providing the bathymetric maps and, for allowing me to be part of the bathymetric campaign of the Guadiana delta during September of 2020. I would like to acknowledge the Instituto Hidrográfico (IH) for providing the offshore-wave data.

I thank my parents Filis and Marta for not losing the hope, for the constant motivation and interest in my work and for the big support I have always received from them to pursue my dreams, no matter what.

I would like to extend my gratitude to all my Professors part of the MaCS program within the Universidade do Algarve. I would like to thank to all my MaCS classmates and Praia community for the good times and support during the last years. I express special thanks to Lara Mills, Valeria Fanti and Vincent Kümmerer for always being there, for correcting my English and for giving constructive comments. I am very grateful for having shared my days during the 'Estado de alerta','Estado de emergência' and 'Estado de contingência' with Lucas Ramirez, Justine Nathan, Holly Sparks, the boys (Harry and Archie) and the rest of Praia community, who made it feel like a playground. I would also like to thank Iphygenia Giannoukakou-Leontsini for our long-lasting friendship and, for sharing this passion for coastal dynamics. Last but not least, I thank Henri Ringeard for the support, the love and good times we always share.

Contents

List of Figures

List of Tables

1 Introduction and objectives

Ebb-tidal deltas are shallow sandy bodies located at the seaward and bay ends of tidal inlets and folds around the ebb-dominated channel (van der Vegt *et al.*, 2009). Ebb-tidal deltas are complex, highly dynamic, morphologic structures formed by the interaction of tidal and wave-generated flows (FitzGerald, 1984; Dohmen-Janssen and Hulscher, 2019). The comprising ebb-tidal deltas volume, morphology, and sedimentary sequences are a function of tidal prism, nearshore slope, sand bypassing processes, as well as interactions between wave and tidal energy (FitzGerald *et al.,* 2012).

Energetic storm events result in large morphological changes at sandy coasts. These events on their own happen clustered depending on the season, as they occur during winter and have a regional to continental scale effect (Masselink *et al.,* 2016). Even though the morphology of ebb-tidal deltas systems is known to progressively return to ‘‘normal’’ conditions after storm events, these events induce strong perturbations including spit breaching, bypass of large amounts of sand or closure of channels (Balouin *et al.,* 2004). Understanding the morphodynamics of these complex systems under various forcing conditions, is of major importance for management (López-Ruiz *et al.,* 2020), where frequent measurements are required to capture the morphological evolution.

With the purpose of monitoring underwater topography and movement of deposited sediments, an accurate determination of water depth is crucial, as it also supports critical information for producing nautical charts, port facility management, dredging operations as well as to predict channel infill and sediment budget (Gao, 2009). Boat-based acoustic echo soundings generate highly accurate point measurements as well as depth profiles along transects (Gao, 2009). As the in-situ surveying interval enlarges, uncertainties increase regarding its capability to capture the rapid coastal morphological evolution (Bergsma *et al.*, 2020). Alongside, satellite observations provide regular and consistent characterizations of the coastal zone and consequently, offer scientists and coastal engineers key information to comprehend detailed large spatial-scale coastal processes, allowing decision-makers to prevent coastal risk (Bergsma and Almar, 2020). An alternative approach is to combine shipboard echo-sounding and satellite data (Sichoix and Bonneville, 1996), allowing to track the main morphological changes without the need for intensive field work, required during the bathymetric surveys.

The main objectives of the present thesis are firstly, to investigate and comprehend the short-term morphologic evolution of the Guadiana Estuary modern ebb-delta migration (at a weekly to monthly timescale) from 2014 to 2019, in terms of horizontal spatial displacement of the outer edge of the shoals. Secondly, seek any possible relation with the marine climate at the study area, more specifically storm events that could have induced major changes on the ebb delta morphology.

In order to achieve these main objectives, bathymetric maps are combined with satellite imagery in order to fill the periods in between bathymetric surveys leading to a secondary objective: assess the sensibility of Sentinel-2 satellite imagery of capturing underwater features and morphological changes in shallow water deltaic environments.

The results obtained from the present study will provide a key source of reference information for future coastal planning and management, providing stakeholders and coastal managers with baseline data on the current status of the Guadiana ebb delta and, its morphological response to various wave conditions, including storms.

2 Tidal deltas

2.1 General characteristics

Tidal inlets are short narrow waterways that connect a bay, an estuary, or a body of water with a larger water body (i.e. ocean or sea) (Kraus, 2010). Tidal inlets represent an environmental important element they since they keep the dynamic equilibrium of the coastal system (Vila-Concejo *et al.*, 2004), where the inlet channel is primarily maintained by the tidal current (FitzGerald, 2005). As tidal currents flow beyond the constriction of the inlets, the currents expand laterally losing their velocity and their capacity to transport sand, leaving their sediment load as tidal delta shoals (Fisher and Simpson, 1982). Ebb-tidal delta is a sand accumulation seaward of the inlet throat, formed principally by ebb-tidal currents but modified by wave action, whereas the flood-tidal delta is an accumulation of sand landward of the inlet throat, shaped primarily by flood-tidal currents (Boothroyd, 1985). Therefore, the formation of ebb- and flood-tidal deltas is a result of sand deposition by the ebb- and flood-tidal jets, respectively (see Figure 1) (FitzGerald *et al.*, 2012). The terms ebb-tidal delta and flood-tidal delta have also been applied to sediment accumulations that form around tidal inlet channels in barrier island depositional systems (Reinson, 1992).

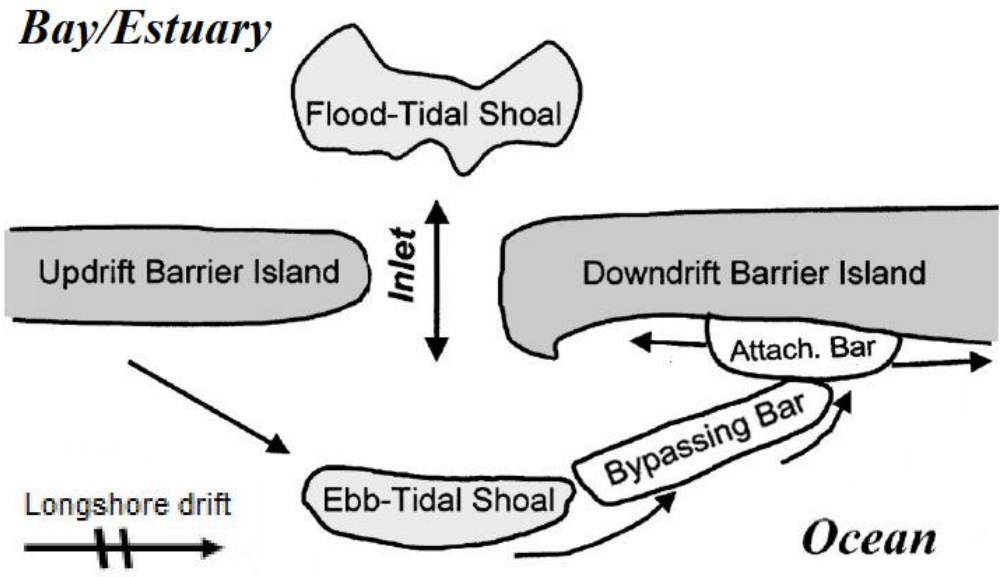

Figure 1.- Inlet morphology showing the flood-delta and ebb-delta. The main components of the ebb-delta are illustrated and sediment pathways (black arrows), adapted from Kraus (2000).

Tidal deltas were first described in detail by Hayes (1975) as extreme complicated sand deposits occurring at the mouth of estuaries, where their morphology is controlled by the interaction of numerous process parameters, primarily by the influence of tide and wave

conditions. Hayes (1975) indicated that the tidal range was the primary control over the distribution and form of the sand deposits, where the sand shoals associated to estuaries with small tidal ranges differed distinctly to the sand shoals occurring in estuaries with large tidal ranges. Three basic models of estuarine sedimentation were proposed: i) Microtidal model (range < 2 m), in which waves and wind dominate as the major processes; ii) Mesotidal model (2-4 m), where a mix of waves and tidal currents dominate and, iii) Macrotidal model (> 4 m), which is dominated by tidal-current deposition. However, a combination of wave and tidal-current energy results in mixed-energy shorelines that are not strictly a product of either process (Boothroyd, 1985). Later, Hayes (1979) further sub-divided these three categories into five. The division of estuarine tidal deltas was incorporated to his coastal classification. This approach to coastal classification by Hayes (1979), uses tidal ranges which do tend to develop similar morphologies through a range of wave climates (see Figure 2):

i. Wave-dominated: microtidal coast (tidal range < 1m).

ii. Mixed energy, wave-dominated: low-mesotidal coast (tidal range 1 – 2m).

iii. Mixed energy, tide-dominated: high-mesotidal coast (tidal range 2 - 3.5 m).

iv. Tide-dominated low: low-macrotidal coast (tidal ranges 3.5 - 5 m).

v. Tide-dominated high: high-macrotidal coast (tidal range > 5 m).

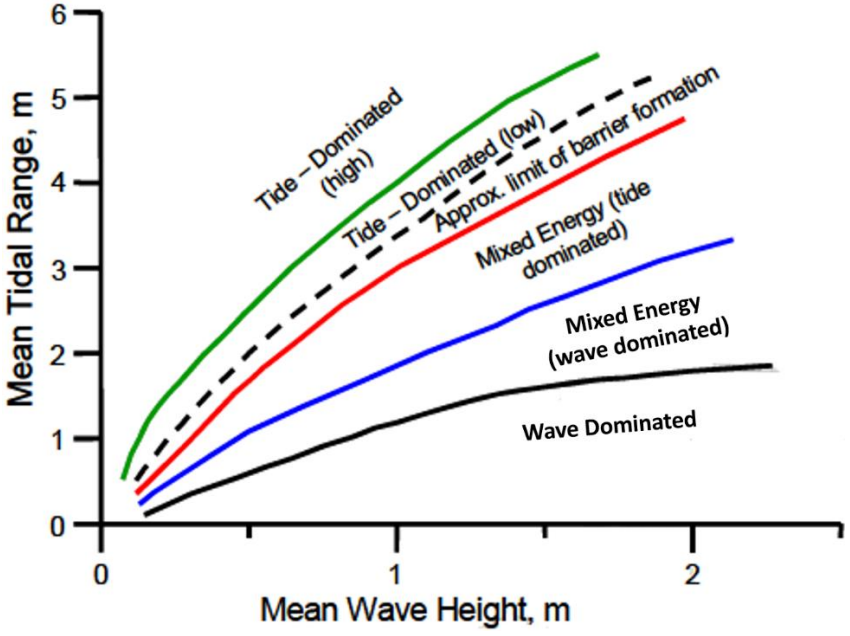

Figure 2.- Classification of tidal inlet morphology (after Hayes, 1979).

However, Davis and Hayes (1984) recognized that tidal prism causes a more direct hydrologic control than the tidal range, emphasizing in the importance of the ratio between tidal range and wave height, particularly along coastlines with moderate wave energy. The tidal prism is the volume of water entering an estuary during the flood or leaving during the ebb (which is about the same). The amplitude difference between spring and neap tides is of great importance in the study of tidal inlets, since an increased amplitude at spring tide leads to an increase in the tidal prism, resulting in an increased tidal current velocity, where a larger volume of water has to ebb and flood within the same time span (Boothroyd, 1985). David and Hayes (1984) finally defined three types of coasts from the perspective of their influencing processes, which linked coastal shape to tidal range and wave height, classifying the coastal energy regimes as: i) Wave-dominated: those dominated by waves, where the shoals are formed parallel to the coast, ii) Tide-dominated: those dominated by tides, where the shoals are formed parallel to the inlet and, iii) Mixed energy: those with a balance between waves and tides, showing variability in the shapes of the shoals. Although the classification of David and Hayes (1984) was broader than the one proposed by Hayes (1979), since it did not relate the dominant process to a particular tidal range or wave parameter, the hypothesis of Hayes (1979) has since been duplicated and adapted by many other authors, remaining a seminal starting point for classifying coastlines (Mulhern *et al.,* 2017).

2.2 Ebb-tidal deltas

Ebb-tidal deltas are large sandy deposits located in front of tidal inlets as a result of the non-linear interaction between waves, tides, sediment supply and possible riverine discharge (Zarzuelo *et al.*, 2019). Typical horizontal size of ebb-tidal deltas range from circa 200 m, as for example the inlets along the Florida coast (Davis, 1997; FitzGerald, 1996), to 5 km which is the case of the Texel delta, located in the Dutch Wadden Sea (Oost and de Boer 1994) or to the more than 7 km of the Guadiana estuary. Ebb-tidal deltas represent an important morphological feature within coastal system since (FitzGerald *et al.*, 2000):

i. They embody huge sand reservoirs.

ii. Wave energy on landward beaches are reduced by sand shoals associated with ebb-tidal deltas.

iii. They affect the bypass process towards downdrift shorelines, thereby influencing coastal change.

iv. The shallow water and dynamic sandbars pose a key hazard to navigation.

The morphology of ebb-tidal deltas is strongly controlled by the tidal prism, a function of the tidal range and the geometry of the enclosed bay, which has been shown to correlate with the volume of sediment contained within the delta (Walton Jr and Adams, 1976; Hicks and Hume, 1996). Other factors including inlet geometry, shoreline configuration, offshore bathymetry, wave climate, tidal flows, littoral drift, sediment supply and size, freshwater runoff, local geology and, anthropogenic modifications (either through engineering of harbour mouths, or as a result of interruption of sediment supplies), exert a control on ebb-tidal deltas morphology and dynamics (Hicks and Hume, 1996; FitzGerald *et al.*, 2000).

Ebb-deltas represent a major sand sink along many of the world's coastlines and are being increasingly seen as potential sources of sand to be used by industries and/or for beach nourishment (Hicks and Hume, 1996). The intricate interactions that take place in ebb-tidal deltas frequently result in large morphological changes, denoted by modifications in the position of the inlet channel as well as development and migration of shoals throughout periods ranging from seasons to decades (Garel *et al.*, 2015). Sediments are introduced to the system through longshore transport, modifying the mass balance by facilitating the growth of the ebb shoal delta and bypassing to the down-drift beach (Hayes, 1980). In this theoretical context, sediments are incessantly reworked through intricate exchanges between waves and tidal currents, shaping the ebb-shoals morphology (Styles *et al.*, 2016). Continuous bypass as well as release (cyclically or episodically) of the sediment contained within ebb-tidal deltas modulate costal changes along downdrift beaches (FitzGerald, 1984), where a key factor in the control on coastal changes is defined by the variability in the sediment supply to coastal areas. Tidal inlets constitute some of the most dynamically active systems in coastal zones (Komar,1996; Hayes, 1980), as they are primary pathways for terrestrial sediments to the ocean: they function as both sources and sinks of sediment and, can disrupt longshore transport pathways modulating the growth, migration and erosion of adjacent shorelines (Styles *et al.*, 2016).

Coastal evolution studies have demonstrated the importance of sediment supply for millennial-scale coastal change (Carter and Woodroffe, 1997), and modelling studies have revealed how human engineering (dams on rivers, groynes, and seawalls on beaches) has profoundly influenced sediment supply and sediment transport over decadal time-scales, with far-reaching impacts on coastal erosion and coastal flooding (Dickson *et al.*, 2007; Dawson *et*

al., 2009). A series of conceptual models were proposed by FitzGerald (1982, 1988) and FitzGerald *et al.*, (2000) to explain sediment by-passing under mixed-energy conditions. These models are based on the relationship between the stability of the inlet throat and the movement of the main ebb channels, showing to be valid for a wide range of mixed-energy tide-dominated inlets (Elias and van der Spek, 2006).

Among these, model 8 explains the sediment bypassing in ebb-tidal deltas where the inlet has been stabilized by jetties (see Figure 3), which is of specific interest for the present study since it is representative of the Guadiana estuary ebb-delta. Traditional engineering solutions to tidal inlet coastal hazards are hard protection techniques such as inlet stabilisation by jetties (Vila-Concejo *et al.*, 2004), where navigable inlets are commonly stabilized by two jetties and dredged to preserve navigable depth and, to protect the channel and the vessels navigating it from sediment shoaling and waves (Kraus, 2010). Even though jetty construction frequently promotes the stabilization of the inlet's position, it breaks with the dynamic equilibrium among the historical ebb-tidal delta morphology and the predominant hydrodynamic conditions (Komar, 1996; Kraus, 2010; Oost *et al.*, 2012).

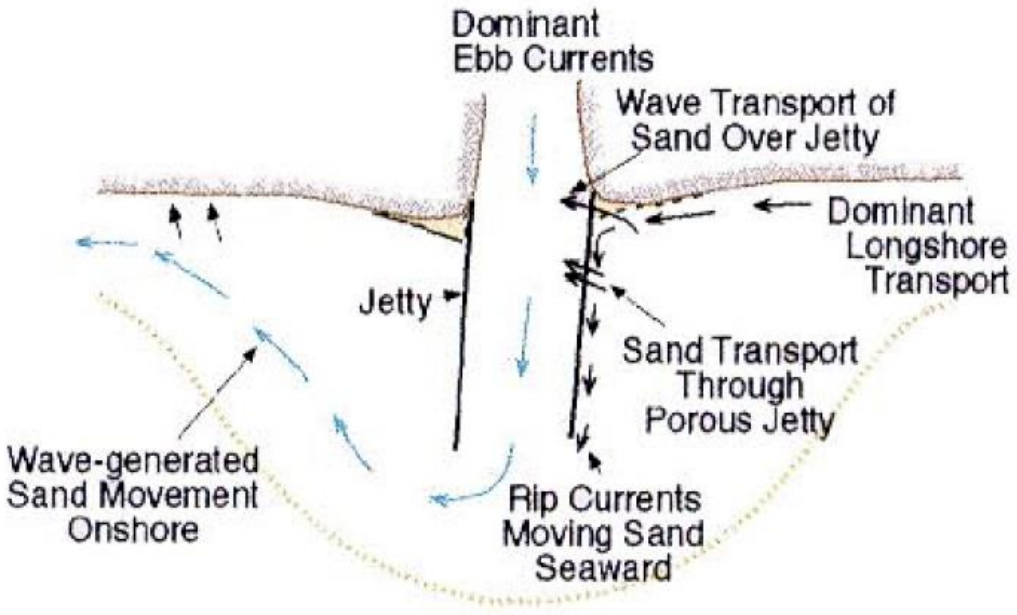

Figure 3.- Model 8 by FitzGerald et al. (2000) illustrating jettied inlet bypassing.

Ebb shoals form under a balance of sediment transport produced by the ebb flow of the inlet and by the longshore current created by waves and wind (Kraus, 2010). Inlets regularly respond with the collapse of parts of the original or historical ebb-tidal delta, where the sand transport induced by waves is no longer opposed by ebb tidal flow and part of the sediments is forced

offshore, resulting in the development of a new ebb-tidal delta in the seaward stream of the stabilized estuarine jet (Garel *et al.*, 2014; Hansen and Knowles, 1988; Pope, 1991; Buijsman *et al.*, 2003; Kraus, 2006). The accumulated sand of the original ebb shoal located in areas where they are no longer affected by the ebb current, will migrate onshore under wave action (Krauss, 2008). The amount of sediment input that is trapped in the system progressively reduces as the delta evolves towards a mature stage, defined by a relatively stable general morphology, increasing its bypassing efficiency, i.e., sediment transported from the updrift to the downdrift lateral bars of the inlet (Byrnes and Hiland, 1995; Garel *et al.*, 2014; Gaudiano and Kana, 2001; Kraus, 2000; Kraus, 2006). Additionally, part of the shoal remaining in front of the now-stronger ebb jet will migrate further seaward (Pope, 1991).

2.3 The Guadiana ebb-tidal delta

The study area comprises the sandy ebb-tidal delta of the Guadiana estuary, located at the southern border between Spain and Portugal (see Figure 4). The Guadiana estuary is an 80 km long estuary and is constituted by a 50-700 m wide single narrow channel (Lobo *et al.*, 2004). The interaction between both fresh and marine waters delimits the Guadiana into three sectors based on distinct hydrological characteristics (Morales, 1993; Chícharo *et al.*, 2001; Gonzalez-Regalado *et al.*, 2013):

i. Marine or Lower Estuary (from the mouth to ~ 10 km), a tide-dominated zone which is strongly influenced by seawater.

ii. Middle or Central Estuary (from ~ 10 to 20 km), the brackish water zone.

iii. Fluvial or Upper Estuary (from ~ 20 km to upstream), filled with freshwater, sediment processed and dominated by riverine transport.

The Guadiana delta has a semi-diurnal mesotidal regime, with a mean tidal range of about 2.1 m and a tidal range oscillating between 3 m during spring tides and 1 m during neap tides (Zazo *et al.*, 1994; Morales and Garel, 2019). The action of waves is significant at the submerged delta, but generally neglected within the estuary, where tidal and riverine processes dominate (Garel *et al.*, 2009). Moderate energy waves dominate the wave climate with a yearly average peak period of 8.2 s (Costa *et al.*, 2001). The dominant incoming SW waves display a yearly mean significant of 1.0 m and represent 71% of occurrences (Costa *et al.*, 2001). SE sea waves embody 23% of the occurrences (Costa *et al.*, 2001). According to these hydrodynamic

characteristics and to the terminology of Hayes (1979), the Guadiana can be defined as a mixed-energy, tide-dominated inlet (Morales, 1993).

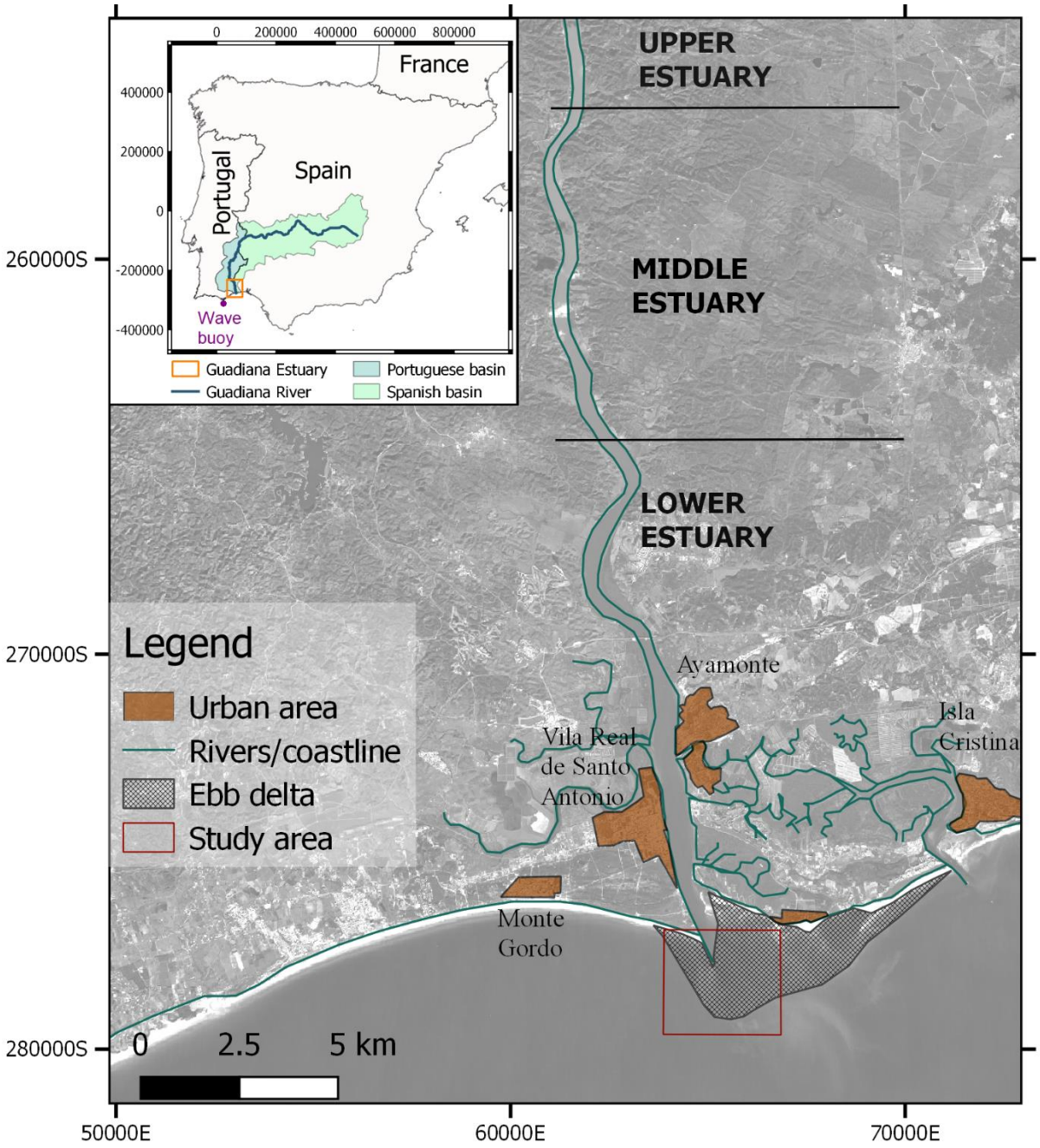

Figure 4 - Top left: The Guadiana hydrographic basin, river, and estuary. Large figure: The Guadiana estuary division and main urban areas. The extension of the ebb-delta is illustrated as the black mesh area. The study area is delimited by the red square (see Figure 6).

Storm conditions correspond to 2% of the offshore wave climate regime (e.g. offshore wave height higher than 3 m) (Costa *et al.*, 2001). Recent studies have considered significant wave heights higher than 2.5 m as storm events for the southern Portuguese coast, where these *Hs* values correspond approximately to two times the annual mean of *Hs* at the location (Oliveira *et al.*, 2018). Storm events in the area concentrate between October and March for southwest

swells, while southeast swells occur more typically between December and March, where December and March present the highest average number of storms per month for SW (1.17) and SE (0.67) events, respectively (Oliveira *et al*, 2018). A total of 177 storm events were identified between 1987 and 2015, where 113 of those events corresponded to SW swells, representing the 63.85% of the occurrence, whilst a total of 64 events stand for SE swells symbolizing the remaining 36.15% (Oliveira *et al.*, 2018).

Although riverine sediments are also supplied to the present Guadiana ebb delta during periods of high river inflows, this source has been drastically reduced with the building of dams since the mid 1950's along the Guadiana estuary (Gonzalez *et al.*, 2001, Dias *et al.*, 2004). The sediment supply to the Guadiana basin was sharply weakened after the Alqueva dam closure, in 2002, which is located approximately 150 km from the river mouth and 60 km upstream from the estuary head (Garel *et al.*, 2009; Garel and Ferreira, 2011). The floodgates closed on the 8th of February 2002, increasing the river flow regulation from 75% to 81% (Morais and Domingues, 2017). Therefore, as a response to sediment retention in dams and decreased freshwater flows at the Guadiana river mouth, coastal erosion is expected to be greater in the future (Morais and Domingues, 2017). The largest discharge events recorded (data available since 1947), occurred in 1996-98 with peak monthly average values up to 10,000 m^3/s, resulting in the significant scouring of the inlet channel (Oliveira *et al.*, 2018). The depth of the channel resulting from this scouring has remained the same throughout the following decades (see Garel *et al.*, 2015).

Prior to the construction of the pair of parallel jetties (the eastern one only being emerged at spring low tide) in 1972 -1974, the historical ebb-delta of the Guadiana estuary was wide, asymmetric eastwards and distinguished by the presence of the O'Bril bank. The O'Bril bank was a large sandy shoal system, situated in front of the estuary mouth that accumulated the littoral drift on the western margin (Gonzalez *et al.*, 2001; Garel *et al.*, 2014). The morphological evolution of the Guadiana historical ebb delta and estuary mouth was first studied by Weinholtz de Bivar (1978) and Morales (1997), who observed a cyclic behaviour of the O'Bril bank. The O'Bril bank used to grow over the course of a few decades on the western margin of the estuary, rotating to the east and partially blocking the mouth of the estuary (Weinholtz de Bivar, 1978; Morales, 1997). Subsequently, a new river channel usually formed close to the western margin splitting the bank into two (or more) segments, which produced the intermittent bypass of a large volume of sediments as well as intricate and hazardous boat access (see Figure 5) (Gonzalez *et al.*, 2001; Dias *et al.*, 2004, Garel *et al.*,

2014). The construction of the jetties, to artificially stabilize the entrance of the channel perpendicular to the coast and to improve the navigability, had an immediate effect analogous to the natural breaching of the O'Bril bank and consequent bypass of a large volume of sand to the downdrift area (Garel *et al.*, 2015). As a response, the eastern area of the historical delta collapsed as the modern ebb delta began to form , narrow and more symmetrical, off the mouth caused by the stabilization of tidal flows by the jetties (Garel *et al.*, 2014; Garel *et al.*, 2015).

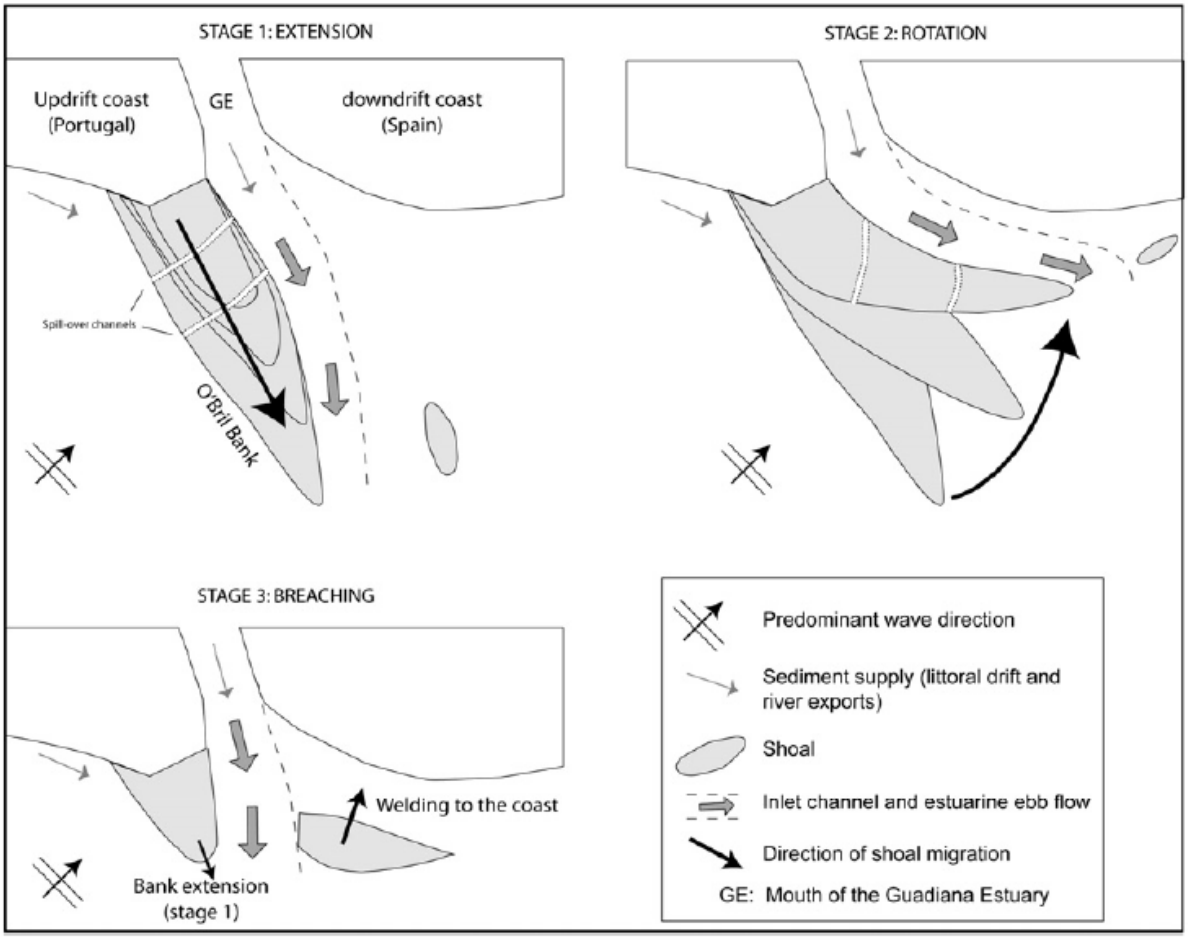

Figure 5.- Conceptual model of evolution of the O'Bril bank by Garel et al. (2014), adapted from the model of ebb-tidal delta breaching by Fitzgerald et al. (2000).

Recent studies have focused their research following the progression of the sedimentation processes towards the present modern ebb delta (e.g. Garel and Ferreira, 2011; Garel *et al.*, 2014; Garel *et al.*, 2015; Garel, 2017; Garel, 2017b, Garel *et al.*, 2019; Morales and Garel, 2019). The modern delta developed into an inlet channel scoured into the O'Bril bank, bounded by sand storage sandy shoals that were relict of the O'Bril bank (Garel *et al.*, 2019). The main morphological features of the modern ebb-delta were already identified in 1977 (i.e. the first map available after the jetties installation), although their boundaries have a variable position

through time (Garel *et al.*, 2019). It is constituted by four main areas with distinct morphological features (Figure 6):

i. An inlet channel.

ii. An updrift lateral area, moderately straight and constituted with bars sub-parallel to the west jetty.

iii. An outer shoal, or ebb shoal 'proper' following Kraus's (2000) terminology, which developed relatively rapidly (few years) due to a large contribution of local sand eroded from the O'Bril bank (Garel, 2017).

iv. A broad downdrift complex, corresponding to the swash platform of the historical delta, submitted to pronounced widespread erosion (Garel *et al.*, 2014; López-Ruiz *et al.*, 2020).

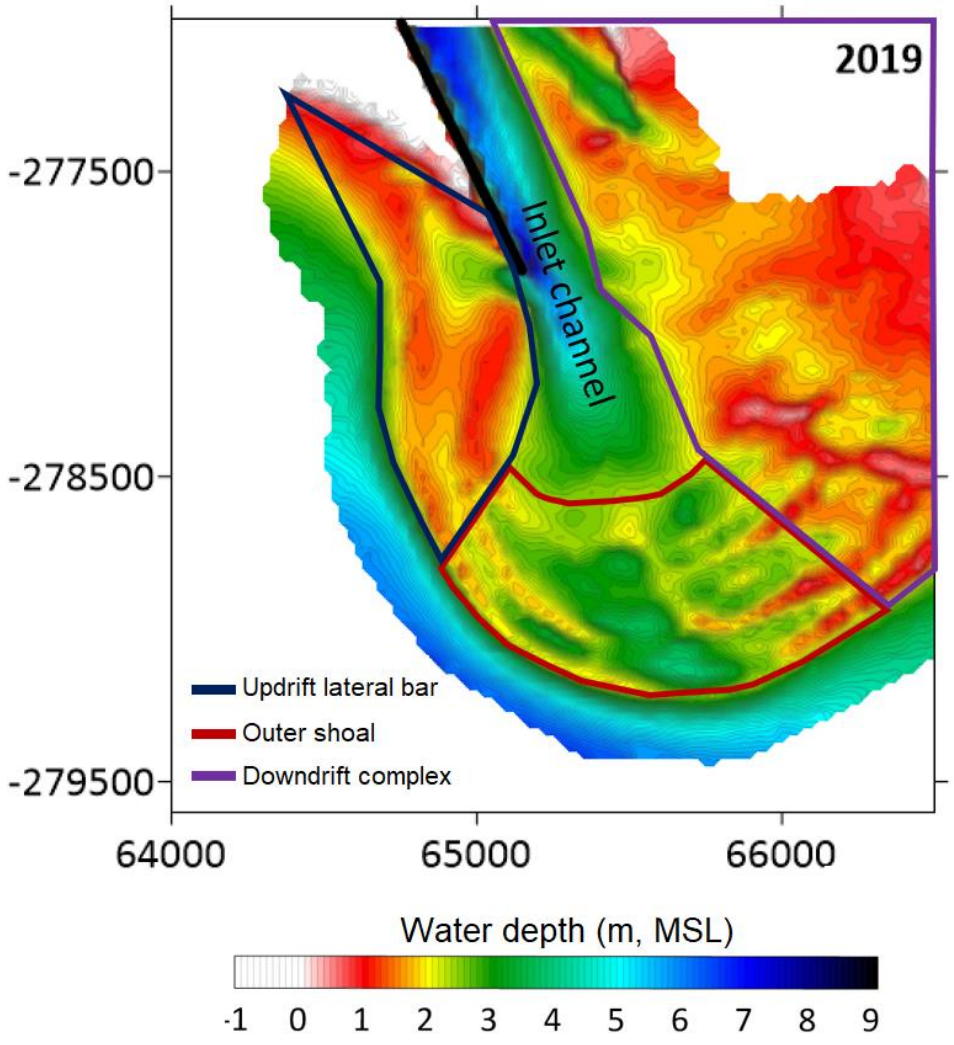

Figure 6.- Map of the Guadiana modern ebb-tidal delta in 2019, showing the location of the inlet channel, updrift lateral bar, outer shoal and downdrift complex (mixed, blue, red and purple boundaries, respectively).

The subparallel lobate swash bars off the mouth correspond to the outer shoal, which is limited laterally by the transition from the lobate bars of the outer shoal to the broader, shallower and straighter bars of the lateral areas, corresponding to the updrift (in the west) and the downdrift (in the east) areas (Garel *et al.,* 2019). The inlet channel area is limited on the sides by the jetties, the updrift lateral bar and the downdrift complex as it extends seawards until linking with the outer shoal (Garel *et al.,* 2019). From a top view, the outer shoal presents a typical horseshoe shape marked by a series of sub-parallel lobate swash bars (Morales and Garel, 2019). The development of these sub-parallel bars (mainly from the 2000's) has diminished locally the depth of the entrance channel to less than 5 m, referred to mean sea level (López-Ruiz *et al.,* 2020). Previous studies on the Guadiana ebb-tidal delta found that the bathymetry of the ebb-shoal was relatively smooth from 1986 to 2001, with a similar average water depth of 4 to 5 m in 2014 presenting a higher variability due to the presence of sand bars (Garel *et al.,* 2015). Shallow water depths present a series of navigational hazards, justifying the dredging operations performed in 1987 and 2015 (Garel, 2017). This recent dredging reached a minimum depth of 5.5 m and the area comprising it had a length of 1,250 m and was 60 m wide (Garel, 2017).

The updrift lateral bar and outer shoal define a major path for sand transport from the updrift coast to the downdrift complex (Morales and Garel, 2019). Part of the updrift material pass the western jetty reaching the inlet channel, from where it can be transported towards the outer shoal together with river-borne sediment by ebb jets (Morales and Garel, 2019). As a result of the ocean climate present in the area, the average transport rate from the updrift lateral bar to the outer shoal is 11,000 m^3/year (Garel *et al.*,2019). On the other side, close to the submerged jetty, the sand is transported westward due to the wave refraction over the swash platform and to the protection provided by the jetties (Garel *et al.,* 2014). In general, the sand deposited at the modern ebb delta is remobilized by wave action primarily during storms events (Morales and Garel, 2019). Bathymetric studies showed that the modern delta was still growing and migrating offshore at a rate of 7 m/year (Garel *et al.*, 2019). Although, the local sediment source from the relict sediments of the O'Bril bank, will drain out in the next few decades as a result of the total collapse of the historical delta, leading to a significant erosion of the downdrift coast, several decades after jetty construction (Morales and Garel, 2019).

Concerning the morphological processes, relatively slow but continuous bypassing of sediments takes place, although not comparable with the irregular (cyclical) bypassing of large volume of sand associated to breaching of the historical delta (Morales and Garel, 2019). The

incoming SW waves induce a prominent eastward littoral drift (Garel *et al*, 2015) and, the direction of the longshore sediment transport (LST) is always reported to be from west to east (CEEPYC, 1979; Granja *et al.*, 1984; Andrade, 1990; Cuena, 1991; Bettencourt, 1994; Gonzalez *et al.*, 2001; Vicente and Pereira, 2001; Santos *et al.*, 2014). The usual behaviour of the sand transport at ebb deltas where jetties construction controls the inlet channel position is a temporary inhibition of sediment bypass that causes downdrift erosion, where the downdrift part of the swash platform is controlled by onshore wave-induced transport (Garel *et al.*, 2019). The erosion induced by the waves in the historical delta, may result in the development and landward migration of shoals that eventually connect to the downdrift coast (Kana *et al.*, 1999; Gaudiano and Kana, 2001). This erosion is well-evidenced with the landward migration of shoals over the swash platform (Garel *et al.*, 2014). Although the pathways followed by the material that reached the downdrift complex and, that are transported landwards under wave action, are not specifically defined (Morales and Garel, 2019). An increase in deposition was noticed at the updrift beach as a result of the cross-shore transport (as shoal) of a large volume of local sand (released from the erosion of the O'Bril bank) in addition to LST trapping (Garel *et al.*, 2015).

The littoral transport is one to two orders of magnitude higher than the riverine contribution to the ebb delta development (Garel and Ferreira, 2011). The average rate of LST is ~85,000 m^3/year since the jetty construction, where the yearly longshore sediment transport ranges from ~25,000 m^3 (westward) to ~245,000 m^3 (eastward), and the yearly riverine export is ~4,000 m^3 (for low discharges) (Garel *et al.*, 2019). Consequently, this last one is usually neglected except during rarely high discharge events (Garel and Ferreira, 2011). Large river discharges increase sediment mobility as well as large morphodynamic changes, although river flow regulation due to the Alqueva dam construction, has limited the peak river discharges to a maximum water outflow of 2,500 m^3/s (López-Ruiz *et al.*, 2020). The area with mobile sediments has been reduced up to 3 times, for peak value of flood events decreasing from 10,000 (before the Alqueva dam) to 2,500 m^3/s (López-Ruiz *et al.*, 2020). In the present, the Guadiana ebb-delta tends to remain in a dynamic equilibrium with the riverine forcing, while expecting to feature a smoothed large-scale morphological evolution, suggesting that the decrease of river discharge could have increased the control of waves on the delta evolution (López-Ruiz *et al.*, 2020).

3 Material & Methods

The morphological evolution of the Guadiana ebb delta was analysed based on 6 bathymetric maps from 2014 to 2019 complemented with a timeseries of Sentinel-2 satellite images from July 2015 to November 2019. Wave rider buoy data was used to characterize the ocean climate from 2014 to 2019 and the corresponding tidal levels were computed to complement the characteristics of the storm events. The following chapter contains the description of the datasets used, along with the description of the methodology carried out to process the bathymetric maps, satellite images and ocean climate data (Figure 7).

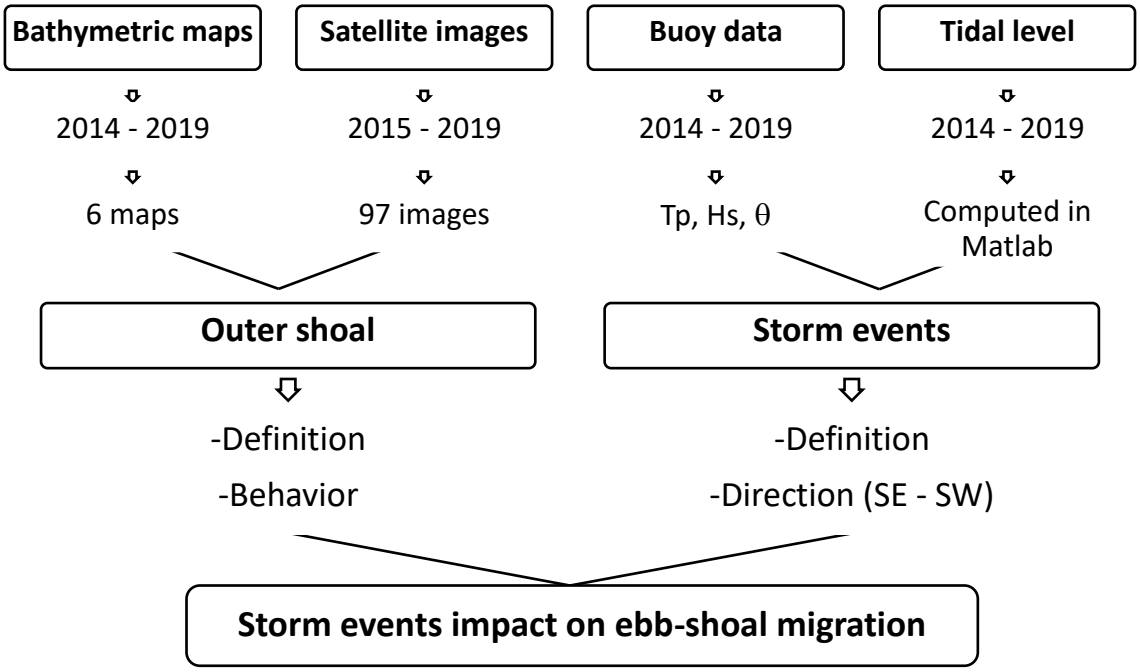

Figure 7.- Work flow followed to achieve the objectives proposed.

3.1 Bathymetric maps

The bathymetric data used in the present study covers a timeframe of 6 years, with yearly maps surveyed in May, June or September. The grid data from 2014 to 2019 were provided by PhD. Erwan Garel, from the GUADELTA project of the University of the Algarve (UAlg). The GUADELTA project aims to monitor the morphodynamic evolution of the Guadiana Estuary delta based on bathymetric maps, consisting of a total of 19 maps which are available since 1969 until 2019 and with yearly maps since 2014, available through the website https://www.cima.ualg.pt/cimaualg/index.php/pt/producao-de-dados/guadelta.

The bathymetric data provided by the GUADELTA project from the years 2014 to 2019 were collected with a single beam echo sounder in 50 m transect intervals, in RTK with a base

station at the end of the west jetty to correct the tidal level at each measurement and pre-processed with HyPack® software to exclude errors associated to the sampling (Figure 8). Such errors occur due to the rotational motion of the boat and consequent loss by the sonde of the pulse reflected. The grids produced and provided for the present study were generated using the Surfer® mapping software, gridded at 25 m cell-size (Garel *et al.*, 2015), referenced to the mean sea level (MSL) and processed in ETRS89, Portugal TM06 coordinate system.

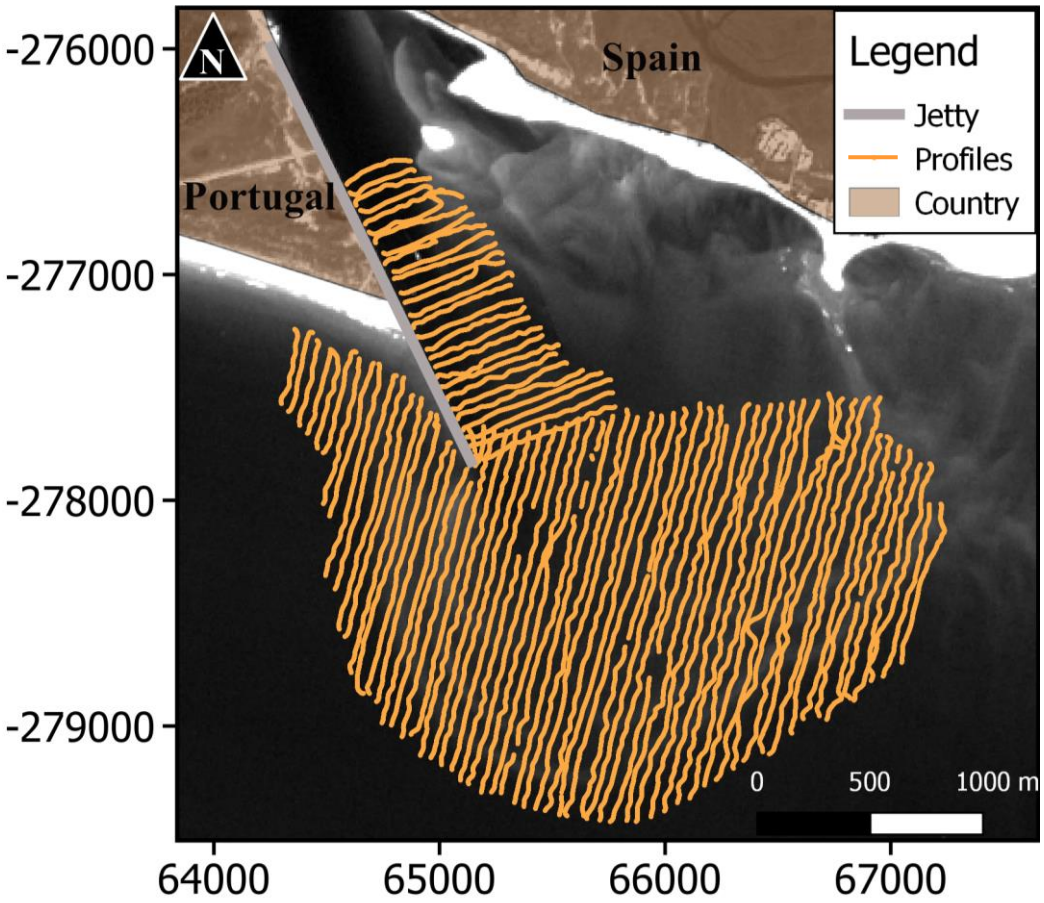

Figure 8- Representation of the transects collected during the bathymetric survey of 2020, after being processed in HyPack. Background satellite image from Sentinel-2 and map composition made through QGIS.

The bathymetric surveys were carried out under diverse climate conditions and the grids were pre-processed by the GUADELTA project team to make reliable data sets. To ensure the inexistence of errors in the vertical datum among the grids, a yearly comparison was carried out for the present study between the 5 consecutive maps. Particular interest was given to the areas located most offshore as possible from the delta, where depth values are expected to be relatively constant in time (see Figure 31 in **Annex I**). Vertical displacements among grids may happen due to errors in the sonde calibration, depth of the transducer, height of the GPS stations, tide correction, orthometric height, etc.

Two polygons were selected located sea wise of the updrift lateral bar, acting as reference areas where there is no higher or lower vertical displacement of 0.1 m or -0.1 m respectively between years, which are expected to be were the seafloor maintains its depth through time in order to validate the vertical displacements between grids (see Figure 31 in **Annex I**). Areas with vertical displacements higher than 0.1 and -0.1 m represent bigger changes in bathymetry such as erosion or deposition of the shoals. Grids of 2018 and 2019 originally presented a vertical displacement of 0.15 and 0.05 m respectively, to which these values were added the entire grids to obtain a difference of about 0 m. A series of maps of yearly vertical differences were processed to focus on the main changes, as well as to highlight the erosion and deposition occurring in between surveys. The morphological changes were considered significant only when variations were higher than 0.5 m.

3.2 Satellite imagery

The satellite imagery chosen in the present study is from the Copernicus Programme, which is coordinated and managed by the European Commission and implemented in partnership with the Member States, the European Space Agency (ESA), the European Organisation for the Exploitation of Meteorological Satellites (EUMETSAT), the European Centre for Medium-Range Weather Forecasts (ECMWF), EU Agencies and Mercator Océan.

Copernicus is served by a set of dedicated satellites, the Sentinel families. Sentinel-2 provides high-resolution optical imagery for land and water services such as imagery of vegetation, soil and water cover, inland waterways and coastal areas. Sentinel-2 meets the necessities for coastal areas evolution monitoring over large regions, possibly with lower accuracy than local in-situ measurements, while offering suitable repeatability to assess global seasonal morphological evolution at unrivalled spatial scales (Bergsma and Almar, 2020).

The twin satellites, Sentinel-2A and Sentinel-2B, were respectively launched on 22 June 2015 and on 7 March 2017. Sentinel-2 data are acquired on 13 spectral bands in the visible and near-infrared (VNIR) and Short-wavelength infrared (SWIR) spectrum, as shown in Table 1. The selection of the optimal spectral bands that can provide better insight of underwater features is crucial and, the key factor governing is their capability in penetrating the aquatic environment. In theory, the spectrum comprised between 0.45 – 0.52 μm (blue spectrum) presents the suitable characteristics for optically sensing bathymetry due to its strong penetration capabilities and lower attenuation of electromagnetic radiation (Gao, 2009). However, this spectrum has not been universally accepted as the ideal for estuaries, where the

water bodies present higher turbidity, therefore longer radiation ranging between 0.5 - 0.6 µm (Warne, 1972) and 0.77- 0.80 µm (Kumar *et al.*, 1997) has been designated as optimum for these environments.

Table 1.- Spectral and spatial resolution characteristics of Sentinel-2 images, modified from Luo (2018).

Band	Spatial Resolution (m)	Wavelength range (nm)	Band width (nm)	Purpose
B01 Coastal aerosol	60	433 - 453	20	Aerosol detection
B02 Blue	10	458 - 523	65	Soil and Vegetation discrimination
B03 Green	10	543 - 578	35	Clear and turbid water, vegetation
B04 Red	10	650 - 680	30	Identifying vegetation, soils, and urban features
B05 Red edge	20	698 - 713	15	Vegetation classification
B06 Red edge	20	733 - 748	15	Vegetation classification
B07 Red edge	20	773 - 793	20	Vegetation classification
B08 VNIR	10	785 - 900	115	Vegetation classification
B08A VNIR	20	855 - 875	20	Mapping shorelines and biomass content
B09 Water vapour	60	935 - 955	20	Detecting water vapour
B10 SWIR/Cirrus	60	1360 - 1390	30	Detecting cirrus clouds
B11 SWIR	20	1565 - 1655	90	Moisture content of soil vegetation, snow and clouds
B12 SWIR	20	2100 - 2280	180	Snow/ice/cloud discrimination

The band B03-Green from the Sentinel-2 twin satellites performs under a wavelength range between 543 and 578 nm, which is ideal for turbid water bodies, and provides a 10 m imagery resolution, delivering high-quality data to perform the present research. Therefore, Sentinel-2A and -2B images from the band B03-Green were chosen in the present study to evaluate the migration of the Guadiana ebb delta. The ESA Copernicus database provides the imagery data on their open access website https://scihub.copernicus.eu/dhus/#/home. A total of 495 images were available in the period from 12/07/2015 until 16/11/2019, from which only 202 were downloaded for a future classification. From the 202 downloaded images, a total of 97 images were chosen to study the morphological evolution of the Guadiana ebb-tidal delta, with variability in the quantity of yearly images (see Table 2). The remaining 105 images were discarded due to the high percentage of cloud coverage, reflectance or presence of surface waves which precluded the possibility to perceive the morphology of ebb-tidal delta with clarity.

Table 2.- Yearly and total amount of satellite images analysed for the period between 2014 and 2019.

	2014	**2015**	**2016**	**2017**	**2018**	**2019**	**Total**
Images	0	7	14	22	24	30	97

The analysis of datasets through geographic information systems (GIS) offers a monitoring tool for environmental changes and a funding for verdicts for future coastal planning actions while aiding to answer questions concerning both geographical patterns and processes (Gao, 2009; Malczewski, 2004). Therefore, each image was examined separately with the help of the QGIS software initially by checking the clarity of the ebb delta, followed by imaging characteristics modulation (saturation and lighting) if required, to have a more accurate view of the outer limits and shape of the ebb-delta.

The outer limit of the shoals on the satellite images were defined as the demarcation line between the shoals sandbar and the ocean, also named as the boundary of the shoal sandbar (Zhang et *at.*, 2020), as shown in Figure 9 with a blue line. The outer limit was selected as the location with stronger contrast between black (deep water) and white (shallow water). These determinations form the basis for obtaining information on lagoon, tidal inlets, and sandbars (Zhang et *at.*, 2020). The outer edge of the shoals was digitized through QGIS software.

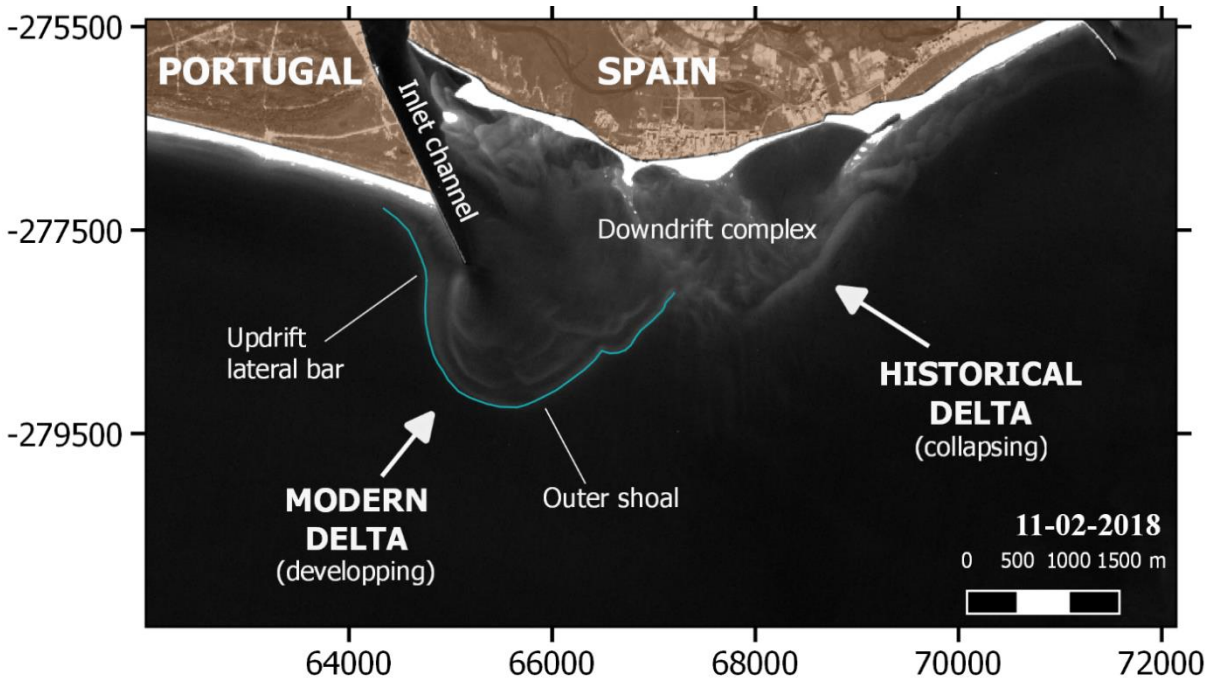

Figure 9.-Main morphological components of Guadiana ebb delta as seen from a Sentinel-2 image. Blue line represents the boundary of the sandy shoal.

3.3 Shoals displacement

Prior to the analysis of morphological changes observed in the satellite imagery through QGIS software, the satellite images were referenced to the coordinate system of the bathymetric maps (ETRS89, Portugal TM06). This correction allowed the superposition of both types of datasets. Table 3 presents the dates of the satellite images with their corresponding tidal level (referred to MSL) that were immediate or closest to the dates of the bathymetric surveying.

Table 3.- Bathymetric survey dates and immediate satellite image capture dates with their corresponding tidal level (MSL).

Bathymetric surveys	Satellite imagery	Tidal level (m)
12/06/2015	12/07/2015	0.9548
31/05/2016	06/06/2016	-0.6473
31/05/2017	02/05/2017	-0.3062
21/09/2018	22/09/2018	0.737
04/06/2019	06/06/2019	-1.0072

The comparison between both datasets supported the localization and definition of the outermost shoal depth, where the 4.5 m contour line nearly superimposed with the boundary of the shoal sandbar (Figure 10). The first satellite image available from Sentinel-2 was from

the 12th of July of 2015 and consequently, it was not feasible to visually compare the bathymetric map of 2014 and a corresponding satellite image (Figure 10).

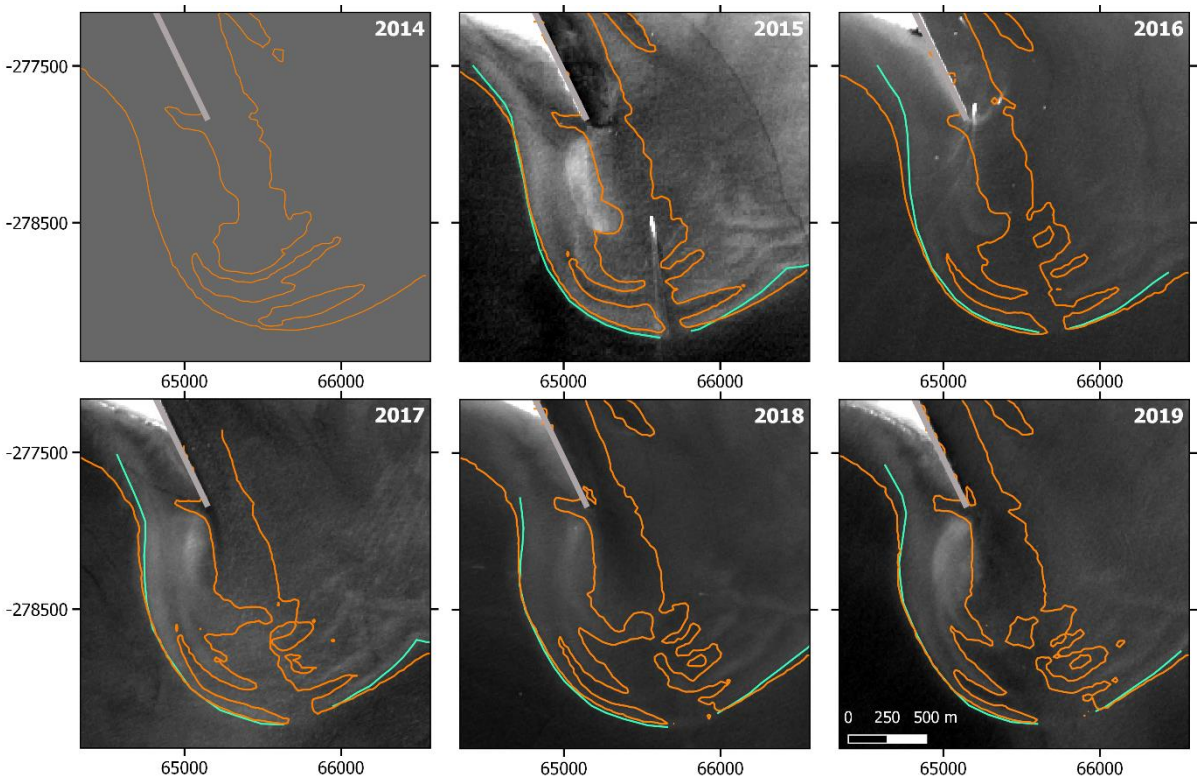

Figure 10.- Superposition of the bathymetric maps and the immediate corresponding satellite image. Shoals edge represented in orange (4.5 m contour) and blue (delineation) and west jetty represented in grey.

The analysis of the significant changes between 2014 and 2019 was evaluated through a total of 6 profiles across the outer shoal, where profile 1 represents to the updrift lateral bar, profiles 2, 3 and 4 to the outer shoal itself and profiles 5 and 6 correspond to the easternmost part of the shoal, representing the downdrift complex (Figure 11). Profiles 1, 2, 3 and 4 start from a common point of origin (65418.16, -278367.80) which allows a wider coverage of the western region of the ebb delta, with a maximum length of 900 m that make a 30º angle with the next profile from the vertex. Profiles 5 and 6 also began in a common point of origin (65796.87, -278445.30) having a maximum length of 800 m and with an angle of 15º with each other (Figure 11).

Even though it is not possible to assume a common depth for the outermost bar along the 6 profiles and 6 years covering the present study at a depth of 4.5 m, this depth was selected as an average measure, based on the literature, to facilitate the characterization of the migration of the ebb-shoal. The displacement of the outer shoals was evaluated by measuring the distance from the origin point to the 4.5 m contour line for the bathymetric maps; for the satellite images

it was measured between the same origin and the previously defined boundary of the shoal sandbar.

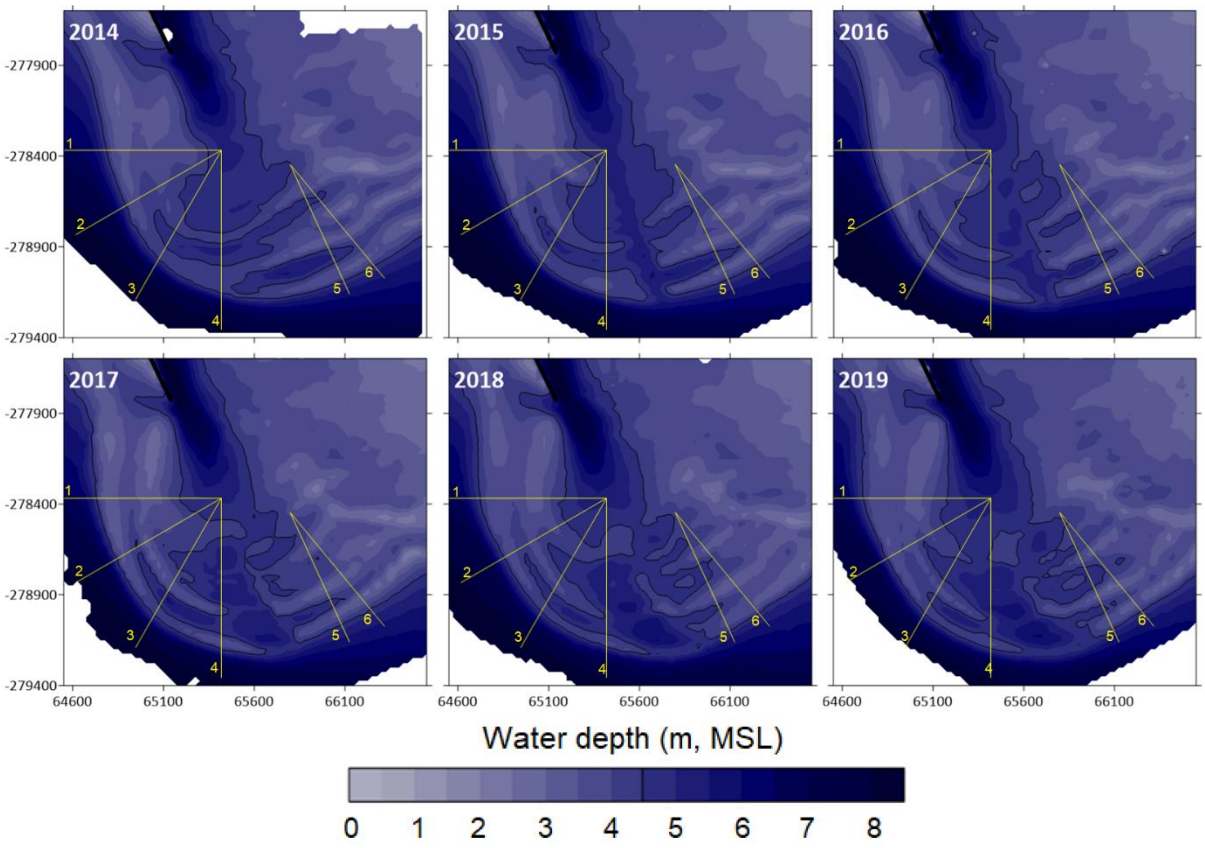

Figure 11.- Yearly bathymetric maps with 0.5 m interval showing the location of the 6 profiles across the Guadiana ebb delta and the shoal depth definition (4.5m, dark contour line).

To estimate the error between the field data and the satellite data, the length of the profiles to the 4.5 contour line in the bathymetric maps, were compared to the length of the profiles to the boundary of the shoal's sandbars in the satellite images. The satellite images used for the error estimate analysis, where the immediate ones to the bathymetric surveys (dates presented in Table 3). The error estimate analysis included the root mean square error (RMSE), the average error (also known as bias) and the correlation coefficient (R^2).

The rate of migration was calculated at each of the profiles, by measuring the highest displacement recorded along the study period (6 years). The offshore migration of the ebb-delta was measured following Stauble (1998) and Garel (2017b), along the line extending seawards from the western jetty until the external boundary of the outer shoal (white dashed line in Figure 12). To understand the main changes experienced by the shoals along the 6 profiles since 2014, the distance from the origin point to the 4.5m contour line of 2014 were subtracted from all the measurements from both the satellite images and the bathymetric maps.

Consequently, 2014 was established as the first distance value and therefore, set at 0 m. Positive displacement of the shoal represents a seaward movement, while negative values stand for a landward migration. Errors associated to the data characteristics were included as error-bars, namely the size of the grid cell, which is 25 m (± 12.5 m) and the pixel size of the satellite images is 10 m (± 5 m).

3.4 Ocean climate

Morphological evolution of ebb deltas is controlled by the action of waves and tides as primary factors (Morris *et al.*, 2001). Hydrodynamic data were obtained from the Portuguese Hydrographic Institute (IH), deep-water directional wave-rider buoy located off Santa Maria Cape (36º 54.3' N, 07º 53.9' W), c.a. 50 km eastward of the estuary and moored at a depth of 93 m (see Figure 4). The buoy accounts values of significant wave height (*Hs*), spectral peak wave period (*Tp*) and mean wave direction at peak frequency (θ) for 20 min every 3 hours in 2014 and for the period 2015-2019 the records were taken hourly, except during storm periods, where the oceanographic data were recorded every half hour (Almeida, 2012). Tidal level series were computed for each of the wave records at a given latitude at the mouth of the estuary, in between the jetties, (37° 10' 1.2" N) using the tidal harmonics of the Guadiana mouth (provided by PhD. Erwan Garel from the GUDELTA project) for the T_TIDE function (Pawlowicz, *et al.*,2002) in MATLAB.

3.5 Storm event definition and impact on ebb-shoal migration

A series of thresholds were selected to define the characteristics of a storm in the study area based on wave parameters and duration of such attributes. For a storm event to be considered as such, significant wave height had to be higher than 2.5 m (Oliveira *et al.*, 2018) and with a duration of at least 6 hours (Almeida *et al.*, 2012). As storms develop, they can lose power and the significant wave height can drop to less than 2.5 m and then build up stronger characteristics afterward. To consider these decreasing and increasing intervals, it was assumed that significant wave heights not lower than 2 m for a maximum period of 5 hrs would be considered as the same storm.

The identified storms were separated into southeast and southwest angles of incidence to reflect the strong bimodal character of the wave climate in the region (Pires, 1998; Morris *et al.*, 2001). This allowed the distinction between southwest Atlantic generated storms ($\theta \geq 180^{o}$), and southeast Levante storms ($\theta < 180^{o}$), which are mainly generated somewhere

between the Strait of Gibraltar and the study area (Oliveira *et al.*, 2018). Exceptions were made when the storms shifted from one direction to the other, as it happens when SW conditions are dominant followed by Levante winds that get stronger until they prevail or vice versa. In such cases, the dominant direction from the overall storm was considered as the prevailing for the analysis.

The modification of the wave power formulated by Morris *et al.* (2001) to include a coefficient that reflects the magnitude of the tidal range was applied, aiming to consider the combination of large waves (>Hs) and low tides, which can cause major impacts in submerged structures such as sand bars or shoals. The linear wave theory was applied to the wave data in order to provide an estimation of the deep-water incident wave power (*P*), followed by the computation of the normalised wave power (P_n) from Morris *et al.* (2001), defined as:

$$P_n = P\left(\frac{\eta_{dtr}}{\eta^*_{dtr}}\right) \qquad \text{Equation (1)}$$

Where η_{dtr} is the daily tidal range and η^*_{dtr} is the maximum tidal range, consequently at spring tides $P_n \approx P$ and at neap tides $P_n \approx 0.3P$. This parameter conveniently indicates the increased potential impact during spring tides (for the delta morphological changes mostly during low tides) without completely denying the possibility of some impact during storm conditions at lower tidal range.

A further understanding of the behaviour of the ebb delta towards storm events was carried out first by analysing the periods in between sampling, i.e. the dates of bathymetric surveys and when the satellite images were captured, in terms of occurrence or non-existence of a storm event and the apparent displacement of the ebb shoal. This apparent displacement can be described as the distance that the ebb shoal has dislocated at each sampling time regarding the previous measurement. The apparent displacement along the profiles was averaged to analyse the 3 main structures of the ebb delta as:

- Updrift lateral bar: profile 1.
- Outer shoal: average of profiles 2, 3 and 4.
- Eastern outer shoal area: average of profiles 5 and 6.

Regarding the periods in between samplings where storm events took place, a complementary exploration of the ebb delta behaviour was carried out by differentiating SW from SE storm events with the aim of researching any potential trend of migration. The

evolution of the Guadiana ebb delta was studied in terms of normalised wave power impact, where only maximum P_n in between samplings was considered. This procedure does not integrate the total power of the storm events and neglects the maximizing impact that multiple storm events could have in between samplings on the ebb delta.

The storm impact is presented in the results section separately mainly in three graphs, showing the maximum normalised wave power of the periods where storm events took place and the periods when there were no storm events and, their relation with the displacement of the shoals. Afterwards, an analysis of the periods where no storm events happened was carried out separating the swells in SE and SW, followed by the recorded impact of the storm events in between samplings. These last two analyses present the maximum *Pn* of the southeast swells in negative values, with the aim of visually observe any possible trend among the SE and SW swells.

4 Results

In this chapter, the results obtained from the bathymetric grids, the delineation of the satellite imagery and the processed ocean climate data analysis are presented, along with the relation between ebb delta migration and storm events in the Guadiana Estuary.

4.1 Morphological evolution of the Guadiana ebb-delta

The series of bathymetric maps allowed the identification of the four main features of the ebb-delta: the updrift lateral bar, the ebb-shoal, the downdrift complex and, the tidal channel. In the present study, the tidal channel itself is not deeply studied, while the evolution of ebb-flow channel is analysed, since it provides more information regarding the morphological evolution of the outer shoal.

Between 2014 and 2019, the updrift lateral bar shows a migration towards the west, shifting its area offshore as well as widening the inlet channel area (Figure 12). The updrift parallel sandbars show a more defined shape in 2019 when compared to 2014. The lobate sandbars of the outer shoal show a reduction in their length in 2019 on both sides, although more significantly towards the downdrift complex. Both these changes are as a result of the dredging of 2015 that separated these formations.

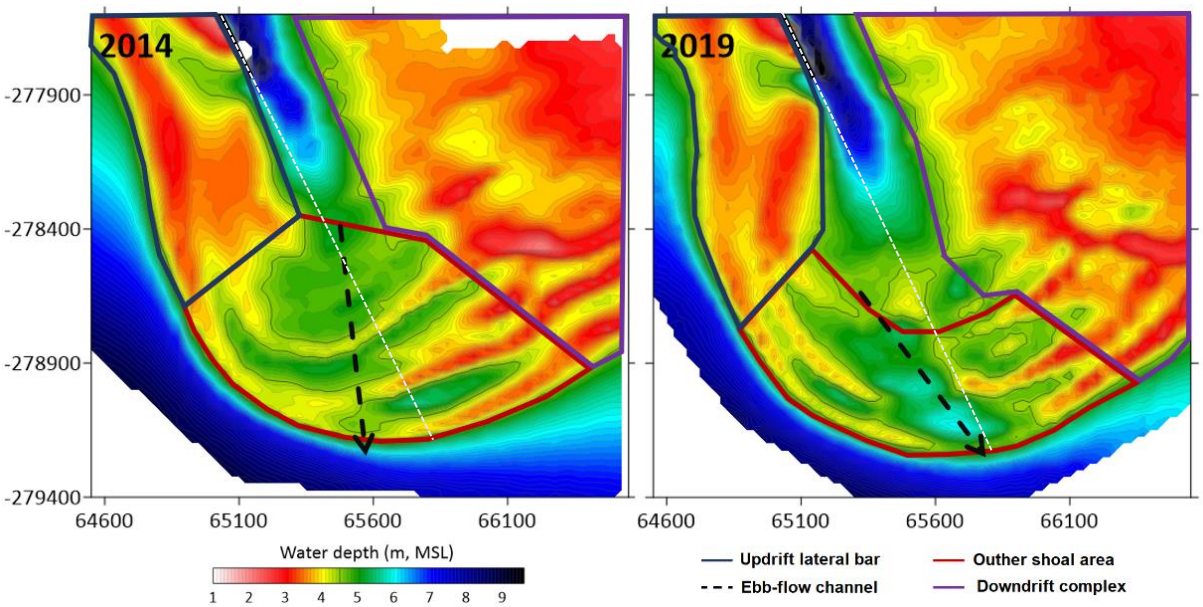

Figure 12.- Bathymetric maps of 2014 and 2019 with 0.1 m contour interval. Morphological structures of interest for the present study are highlighted. White dashed line represents the line where the ebb-delta migration was measured following Stauble (1998).

A slightly curved and elongated bar of sediment deposition up to 2 m was observed along the updrift lateral bar and the ebb-shoal, followed by an erosion of around -2 m towards the inlet channel, illustrating the horseshoe shape of the ebb-delta (Figure 13). A series of deposition and erosion areas can be observed as well towards the downdrift complex. The delta presents in its central area a 'drop-shaped' region of 0.5 to 1.5 m of erosion leaning towards the south from the edge of the west jetty.

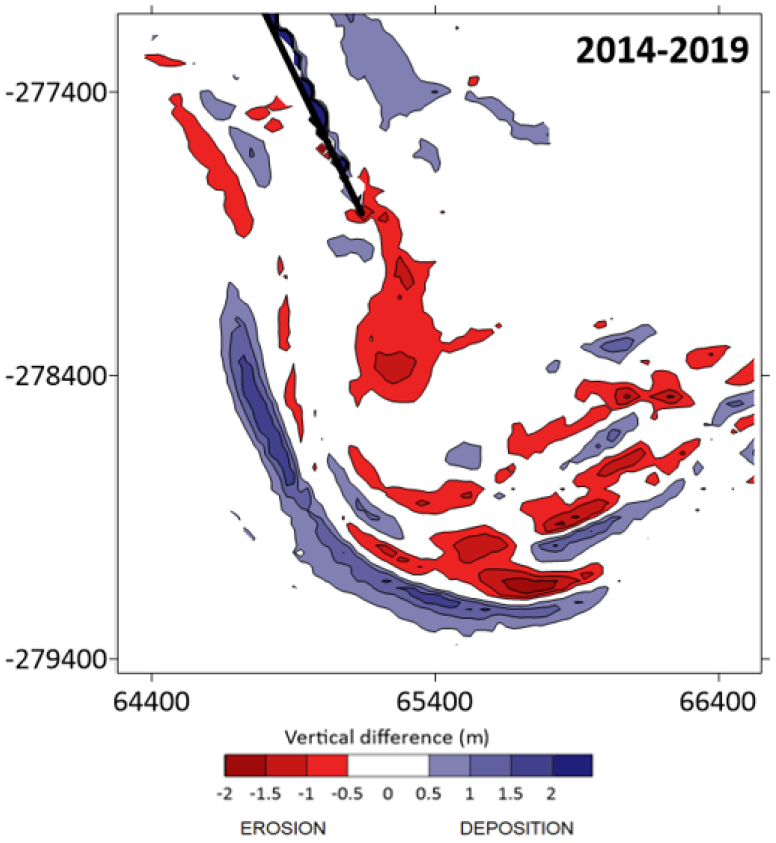

Figure 13.- Vertical difference map between 2014 and 2019. Red areas represent erosion processes, while blue areas represent deposition of sediments.

The recent dredging can be easily visualized by comparing the 2014 and 2015 maps, where the 5 to 6 m deep ebb-flow channel crosses the ebb-shoal in the Southern area in 2015 and 2016, as it later shifts its position towards the East from 2017 onwards (Figure 14). The lobate bars of the outer shoal start to reconnect at a depth of 5 m, off the ebb-flow channel, in 2017. The lobate bars seem to be attached at the South South-East area at a depth of 5 m. The central area of the ebb-delta (landward area of the outer shoal), where the dredging of the tidal channel took place, presents an increment in sand volume from 2015 to 2017 which persists in the same location in 2018 and 2019. Among this accretion, a lobe from the outer shoal, closer to the western side of the inlets channel, elongates towards the east (see 2015 and 2016 map; Figure 14) crosses the tidal channel (see 2017 and 2018 maps; Figure 14) until it finally separates in

2019 posing navigational hazards due to the depth and location of the structure. Following the ebb-flow channel seawards through the outer shoal, it is possible to observe in the most recent years that this accretion is followed by erosional processes in the outermost part of it, creating a series of crests and troughs that might pose navigational hazards due to the centric location and shallow depth (4 m at the crest) (Figure 14).

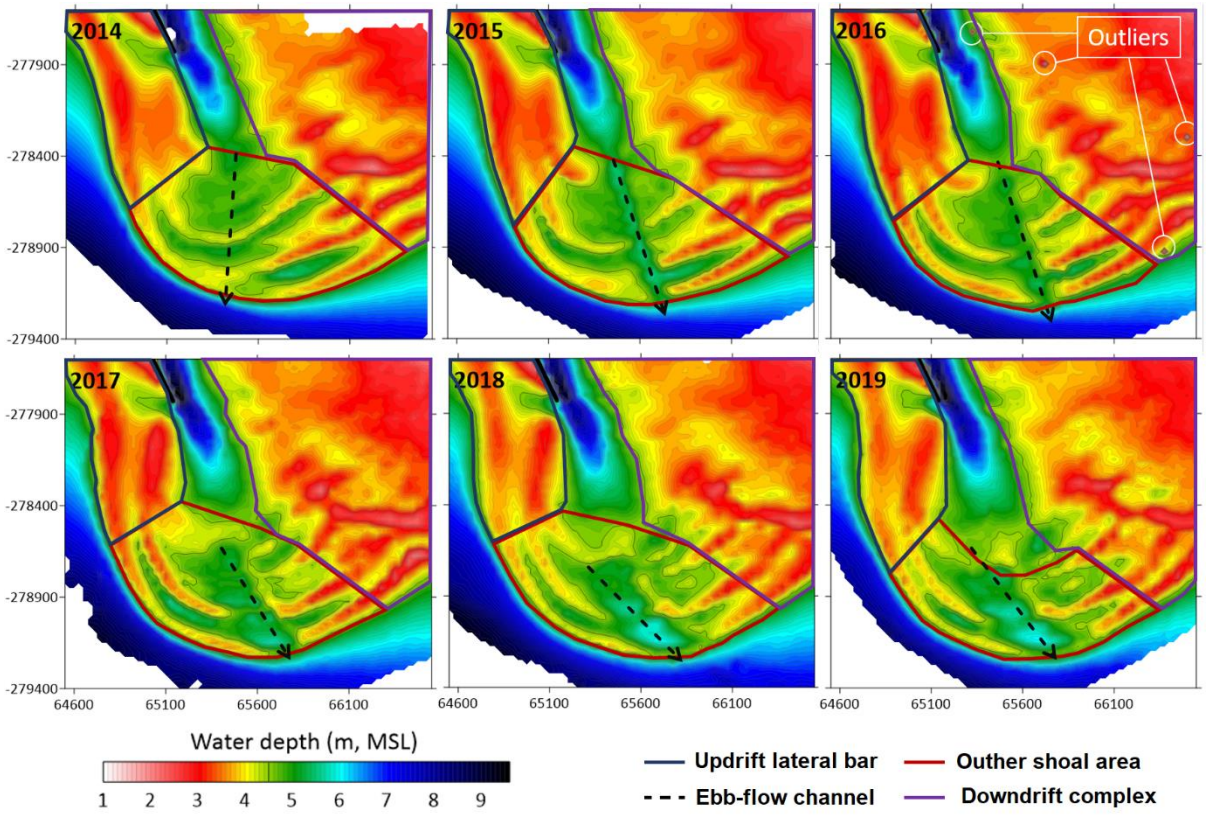

Figure 14.- Yearly bathymetric maps with 0.1 m contour interval of the Guadiana ebb-delta. The main morphological features are highlighted through lines.

Variations on the ebb-flow channel can be observed in the map comparing 2014 and 2015 due to the dredging, showing a track of erosion (see Figure 15), where a series of parallel depositional bars occur perpendicular to the ebb-flow channel. No remarkable changes were found between 2015 and 2016 other than few parallel elongated areas of deposition, perpendicular to the sides of the ebb-flow channel. Of special interest are the major changes involving 2017, where between 2016 and 2017 there is an increment of 1 to 1.5 m in height of the updrift lateral bar and the outer shoal followed by an adjacent erosion of 1 m landwards as well as smaller areas of alternated erosion and deposition in both eastern and western shoals. These morphological shifts suggest that a seaward migration occurred on the western side of the ebb delta (black arrows in Figure 15), while a landward displacement took place on the downdrift area (green arrows in Figure 15). An opposite migration can be observed on the

downdrift area in the 2017-2018 map, where the displacement is, in this case, seawards (black arrows in Figure 15). These morphological changes along the delta, pose a key uncertainty concerning what happened between 2016 and 2018. Finally, there were no significant changes between 2018 and 2019.

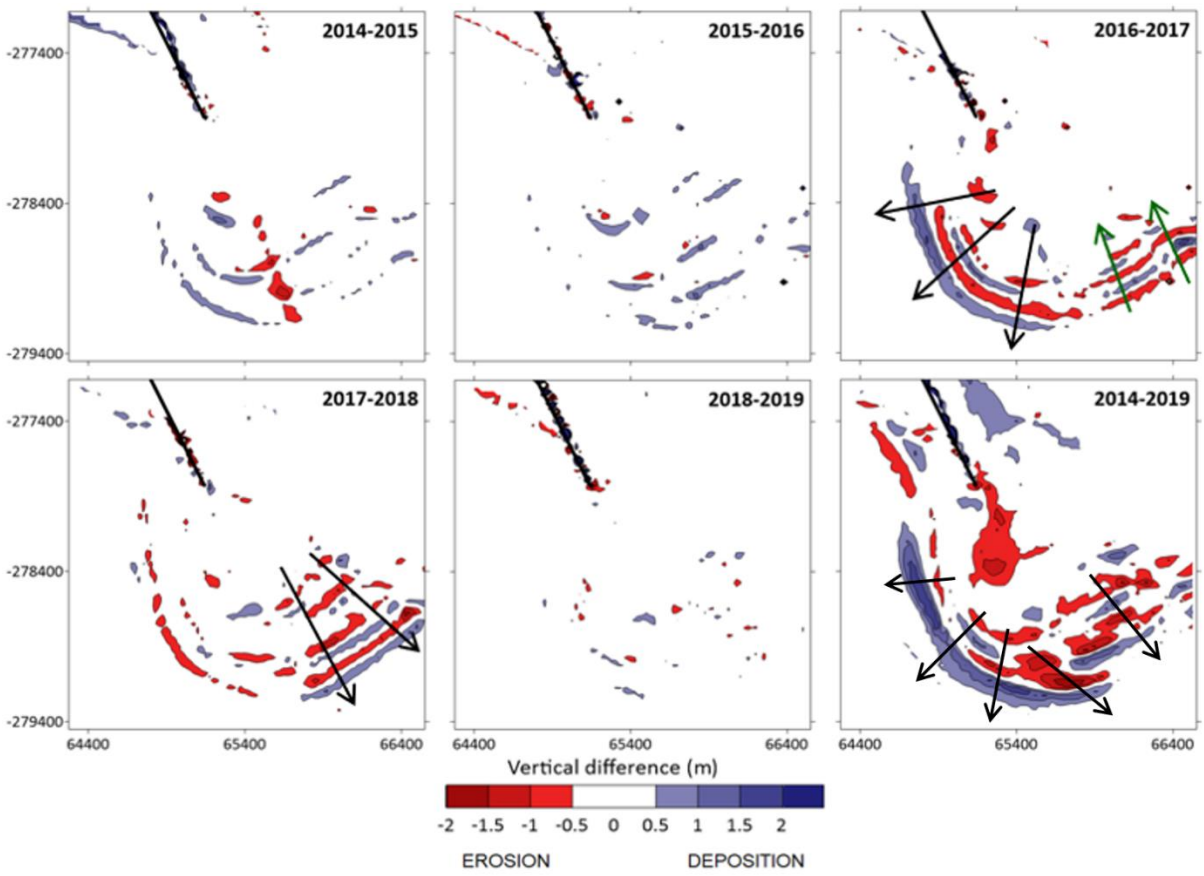

Figure 15.-Yearly bathymetric vertical difference maps of the successive grids and between 2014 and 2019. Red areas represent erosion and blue deposition. Black arrows show the offshore migration of the subparallel bars, while green arrow represent landward migration.

4.2 Morphological evolution along the profiles

Later to the yearly characterization, the morphological evolution was examined along the 6 profiles to observe more precisely the vertical and horizontal changes, based on the bathymetric maps, furnishing additional information to the vertical difference maps where erosional and depositional processes were evaluated. The depth-length profiles provide critical evidence on the movement of sand deposits along the subparallel bars (Figure 16).

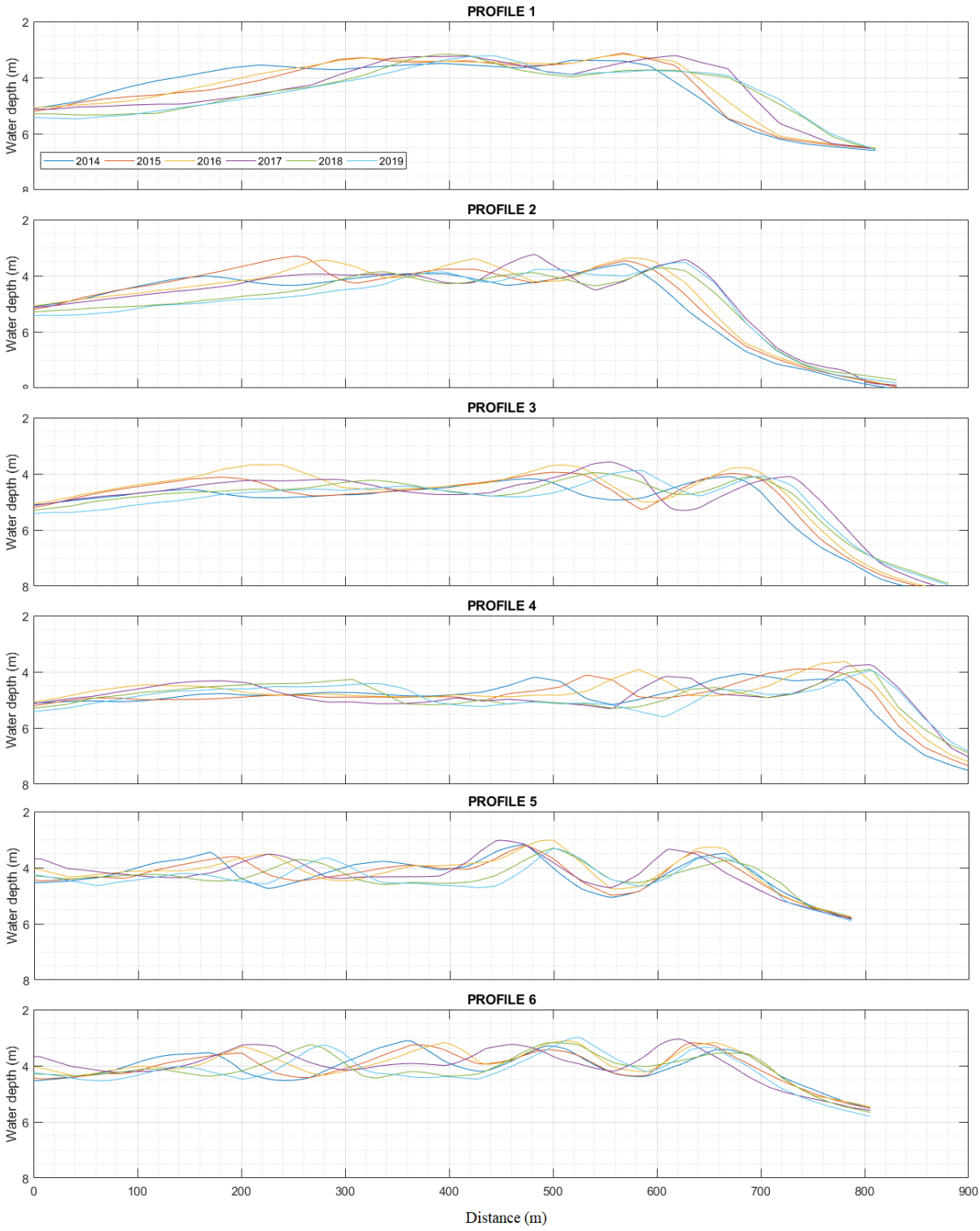

Figure 16.- Depth-length evolution of the 6 profiles along the study period.

The updrift region, represented by Profile1 (Figure 16), shows a very smooth seafloor marked by a seaward migration of the outermost sandbar. In 2014 the crest of the sandbar was at 3.5 m depth and 500 to 600 m from the origin point, showing a small accretion in 2015 that lasted until 2016. In 2017, this vertical structure can be observed circa 45 m seawards (westward). A decrease on the depth of the sandbar crest can be observed in 2018 that lasted until 2019, with a final depth of almost 4 m.

Profile 2 (Figure 16) shows that the outermost sandbank nearly stayed steady between 2014 and 2016, followed by a circa 40 m seaward migration in 2017, after which was stabilized on the location. In terms of crest height, there is a series of slow but continuous accretion until 2018, where the sandbar deeper from 3.5 m to roughly 4 m and recovered its depth almost entirely through depositional processes by 2019.

Similar results can be observed between profiles 3 and 4 (Figure 16). Although, in profile 3 the 40 m seaward migration of 2017 was followed by a recession of the position of the outermost shoal of circa 40 m. While in profile 4, there is an accretion of almost 0.5 m in the outermost sandbar between 2014 and 2016, where the final crest height is at 4 m depth. The parallel bars of the outer shoal show more morphological variability through time along the 3 profiles.

In profiles 5 and 6 (Figure 16) it is observable that the downdrift complex endured a landward migration of the outermost sandbar and swash lobate bars in 2017 of around 30 m, followed by a seaward displacement in 2018 held until 2019. The seaward migration of the lobate bars was more accentuated in the easternmost area and it was accompanied by a decrease in height of all the sandbars crest.

To summarize the evolution observed in the bathymetric maps along the profiles shown in Figure 16, Table 5 presents the main morphological changes that occurred at the outer edge and at the crest of the outer sandbars of the ebb-delta. The morphological changes presented in Table 4 show those values which imply significant morphological changes, namely, erosion and deposition at the crest of the sandbar and, onshore and offshore migrations measured at the outer edge of the sandbar, that were higher than 0.5 m.

Table 4.- Yearly sedimentary processes on the edge of the outer shoals along the profiles. The values presented for 2015 are referenced to the morphology in 2014, while the values shown for 2016, 2017, 2018 and 2019 are referenced to the previous year. The limit of the sandbars is measured at the 4.5 m contour line.

		Morphological changes on the edge of the shoals			
		Limit of the sandbars		**Crest of the sandbars**	
Profile	**Year**	Landward migration	Seaward migration	Erosion (decrease in height)	Deposition (increase in height)
1	**2015**	-	5 m	-	>0.5 m
	2016	-	20 m	-	-
	2017	-	25m	-	-
	2018	-	20m	0.5 m	-
	2019	-	10 m	-	-
2	**2015**	-	15 m	>0.5 m	-
	2016	-	15 m	>0.5 m	-
	2017	-	25 m	-	-
	2018	10 m	-	-	>0.5 m
	2019	-	10 m	>0.5 m	-
3	**2015**	-	15 m	>0.5 m	-
	2016	-	5 m	>0.5 m	-
	2017	-	30 m	-	>0.5 m
	2018	20 m	-	-	-
	2019	5 m	-	-	-
4	**2015**	-	15 m	-	>0.5 m
	2016	-	5m	-	>0.5 m
	2017	-	25 m	>0.5 m	-
	2018	20 m	-	>0.5 m	-
	2019	5 m	-	-	-
5	**2015**	>5 m	-	-	-
	2016	>5 m	-	-	>0.5 m
	2017	15 m	-	>0.5 m	-
	2018	-	40 m	0.5 m	-
	2019	-	25 m	-	>0.5 m
6	**2015**	-	20 m	-	>0.5 m
	2016	-	-	-	-
	2017	20 m	-	-	>0.5 m
	2018	-	20 m	0.5 m	-
	2019	-	20 m	-	>0.5 m

4.3 Error estimate of the datasets

The regression analysis, conducted between the two datasets, evidenced a good agreement between both sets of survey data with a correlation coefficient (R^2) of 0.942 (see Figure 17).

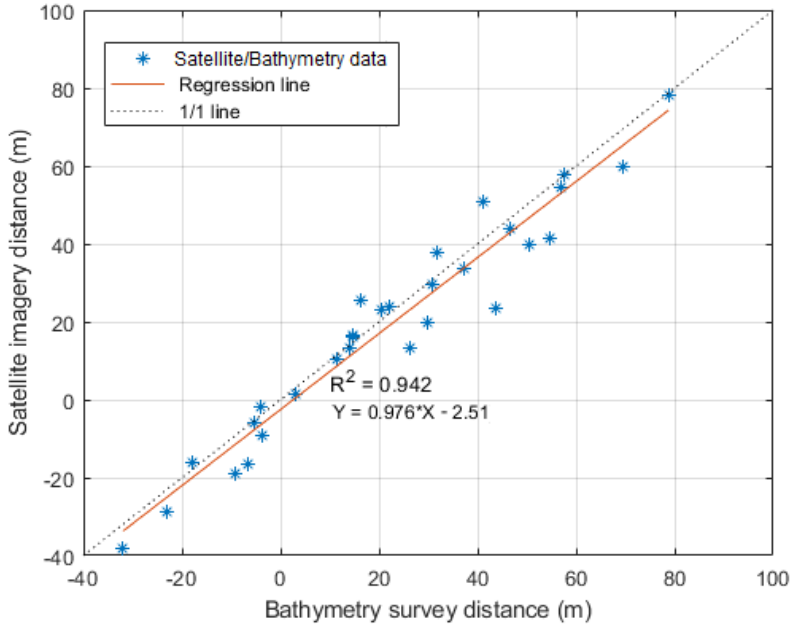

Figure 17.- Regression analysis between satellite and bathymetry survey data on the outer edge of the ebb-delta shoals. Dashed line represents the 1:1 linear fit.

The RMSE obtained in the analysis was of 6.68 m and the average error is 3.061 m, being both values lower than the error associated to the satellite imagery, which is 10 m (pixel size). These values can be considered in good agreement for the proposed analysis, encouraging and allowing the quantitative analysis of the morphological evolution of the ebb-tidal delta outer shoals.

4.4 Ocean climate

The ocean climate characteristics (*Hs, Tp, θ* and tidal level) timeseries show that the average significant wave height recorded by the offshore-buoy is 1.02 m with a peak period of 8.4 s, where SW waves were the most dominant governing 74.75% of the wave climate with an average significant wave height of 0.95 m and peak period of 9.13 s (Figure 18).

Sea waves incoming from the SE represent 25.25% of the occurrences with an average significant wave height of 1.25 m and peak period of 6.33 s. The maximum tidal level computed at the Guadiana river mouth, corresponds to a high spring tide of 1.84 m while the lowest tide recorded was -1.78 m, during low spring tide.

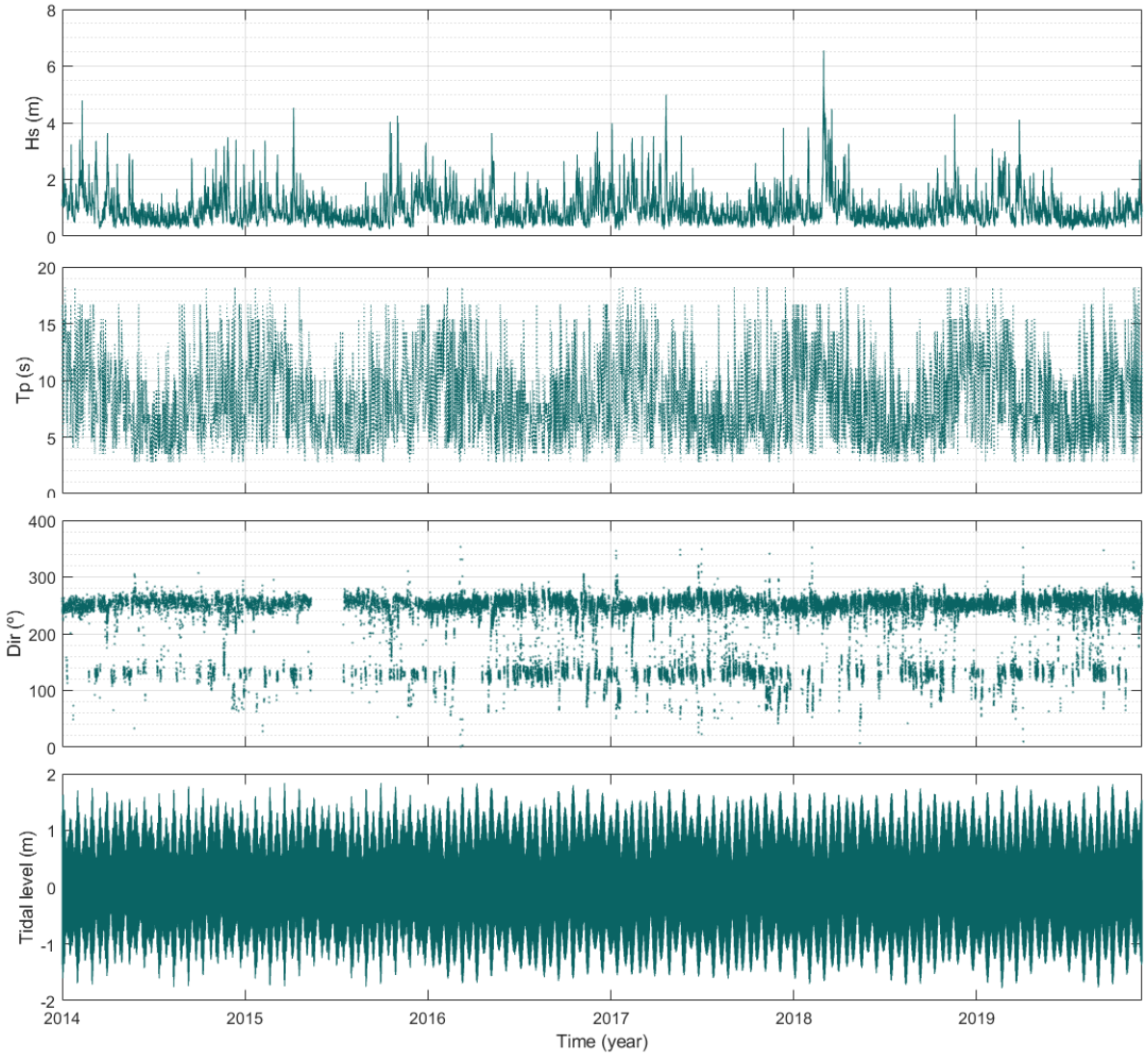

Figure 18.- Ocean climate characteristics between 2014 and 2019.

To consider the effects of spring tides, which enhance the impact of waves during low tide in submerged structures due to the reduction in height of the water column, the daily tidal range data was computed to normalise the wave power using Equation (1). The maximum tidal range used was 3.7 m, based on the values provided by the Instituto Hidrográfico for Vila Real de Santo António. A clear example on how the consideration of the tidal level can adjust the wave power, as suggested by Morris *et al.* (2001), is highlighted in Figure 19 where two different storm events took place with a difference of almost 60,000 J/s m^2 and, when considering the tidal level at each timing of the storm, both storms result in almost equal *Pn* of ~1.58x10^5 J/s m^2.

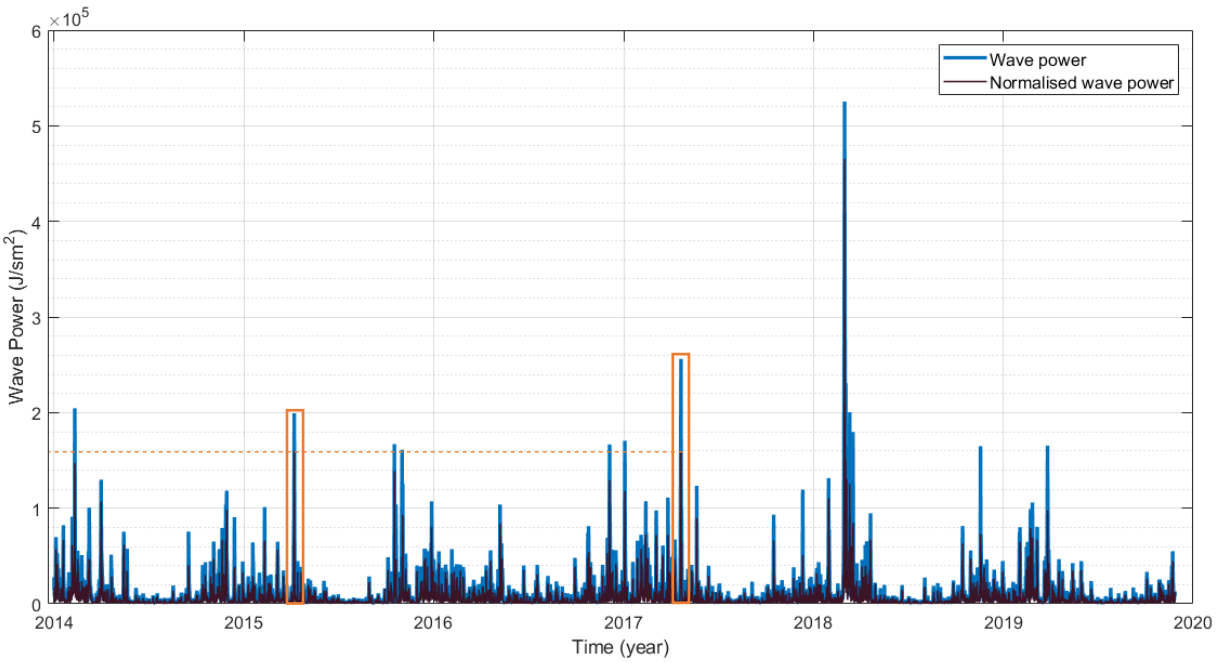

Figure 19.- Wave power and normalised wave power calculated for 2014 to 2019. Rectangles show two storm events with same normalised wave power. Dashed line marks the 1.58x10^5 J/s m^2.

A total of 53 storms took place in the 6 years considered in the present study, where the vast majority occurred during winter and fall months (Figure 20). Although 12 storms occurred in 2014, for which only the bathymetric map was available to understand possible effects on the shoals, the following years were supplied with a yearly increasing number of satellite images.

It was not until March 2017 that Sentinel-2B mission was launched and this is depicted on the availability of images from 2015 and 2016, with a total of 13 storms between both years that overlapped with the times when less images were possible to explore, due to high cloud coverage. Once the twin satellites were orbiting, it was possible to analyse a minimum of one image per month, excluding June 2017 and the period comprising between the end of February and end of April of 2018 due to high cloud coverage and, later suspended sediments and turbidity, which is when a cluster of storms took place (rectangle in Figure 19). The characteristics of all storm events (duration, max H_s, mean H_s, mean T_p, mean θ, max P and P_n) are provided in **Annex II**

Storm events with significant wave height higher than 2.5 m (following the threshold selected for the present study) represent 4.59% of the offshore wave climate regime. The average maximum H_s of all the storm events is 3.43 m, whereas the maximum significant wave height recorded in the period studied was of 6.55 m, occurring in the winter of 2017/2018, more precisely the 28th of February of 2018 (Figure 19). This peak matches the development of Emma storm, at SW of the Iberian Peninsula, which lasted until the 3rd of March of 2018 and

with a total duration of 151 hours. Emma storm followed a similar track of some of the most energetic and devastating storms in the southern Portuguese coast (Ferreira *et al.*,2019) (see **Annex III**).

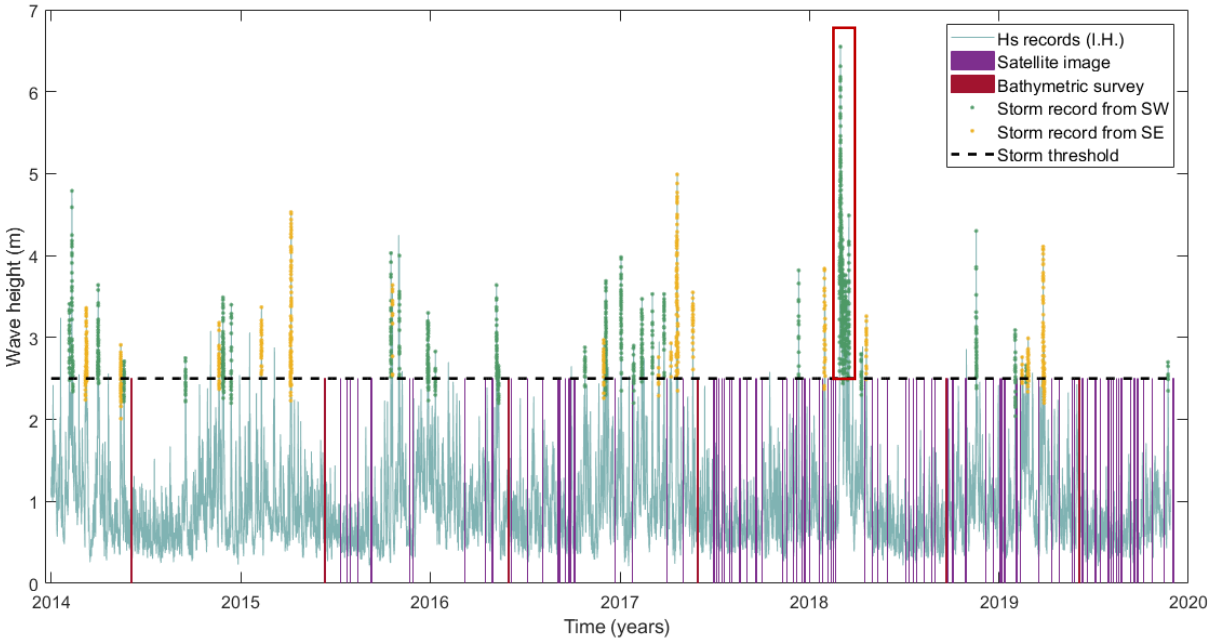

Figure 20.- Satellite images and bathymetric survey dates along with the significate wave height recorded from 2014 to 2019. Storm events from the SW are shown in green and from SE in yellow. Storm cluster shown in the red rectangle.

Following Emma storm, which had a maximum wave power of 5.25×10^5 J/m^{2}s and a maximum normalized wave power of 4.72×10^5 J/m^{2}s, two other storms were recorded in the study area with significantly lower characteristics, as shown in Figure 21. These consecutive events are however, of high interest due to the small timeframe between them, their possible impact in the Guadiana ebb-shoal and the fact of being the only remarkable storm cluster that happened during the study period.

Table 5.- Cluster of storms recorded during winter 2007/2018 and their main characteristics. (Avg.=Average; Dir.=Direction; Max.=Maximum)

Date	Duration	Max. Hs	Avg. Hs	Avg. Tp	Avg. Dir.	Dir.	Max. P	Pn
28/02/2018	151H	6.55	4.01	10.78	241.05	SW	525227.15	472470.16
09/03/2018	61H	3.76	3.14	11.53	248.45	SW	200358.20	63694.60
14/03/2018	10H	3.44	3.03	8.22	249.00	SW	92717.44	52827.82

From the 53 storms recorded in the study period, a total of 32 storms were incoming from the SW corresponding to 60.37%, while the storms from the SE represent 39.63% with a total of 21 events (Figure 21-a). Emma storm, represented as event nº 39 in Figure 21-a, has an estimated return period of about 16 years (Ferreira *et al.*,2019). To understand what the

characteristics of the typical storm events that reached the Guadiana ebb-delta during the study period, the frequency of such events was evaluated without accounting for Emma storm, including the separation of the storm events based on their direction.

The most frequent storm events that occurred in the timeframe of the present study are of a magnitude in between $3x10^4$ and $6x10^4$ J/m^{2}s of normalised wave power, from both SE and SW direction, representing 39.6% of the storm activity (Figure 21-c and Figure 21-d). The less frequent storms documented between 2014 and 2019, are of the order of $1x10^5$ J/m^{2}s to $1.5x10^5$ J/m^{2}s, displaying a 3.7% of the recorded storm events, and which can also be expected from both directions (Figure 21-c and Figure 21-d). Storm events with a *Pn* of $6x10^4$ J/m^{2}s up to $1.21x10^5$ J/m^{2}s are significantly more frequent from the SW direction (Figure 21-d).

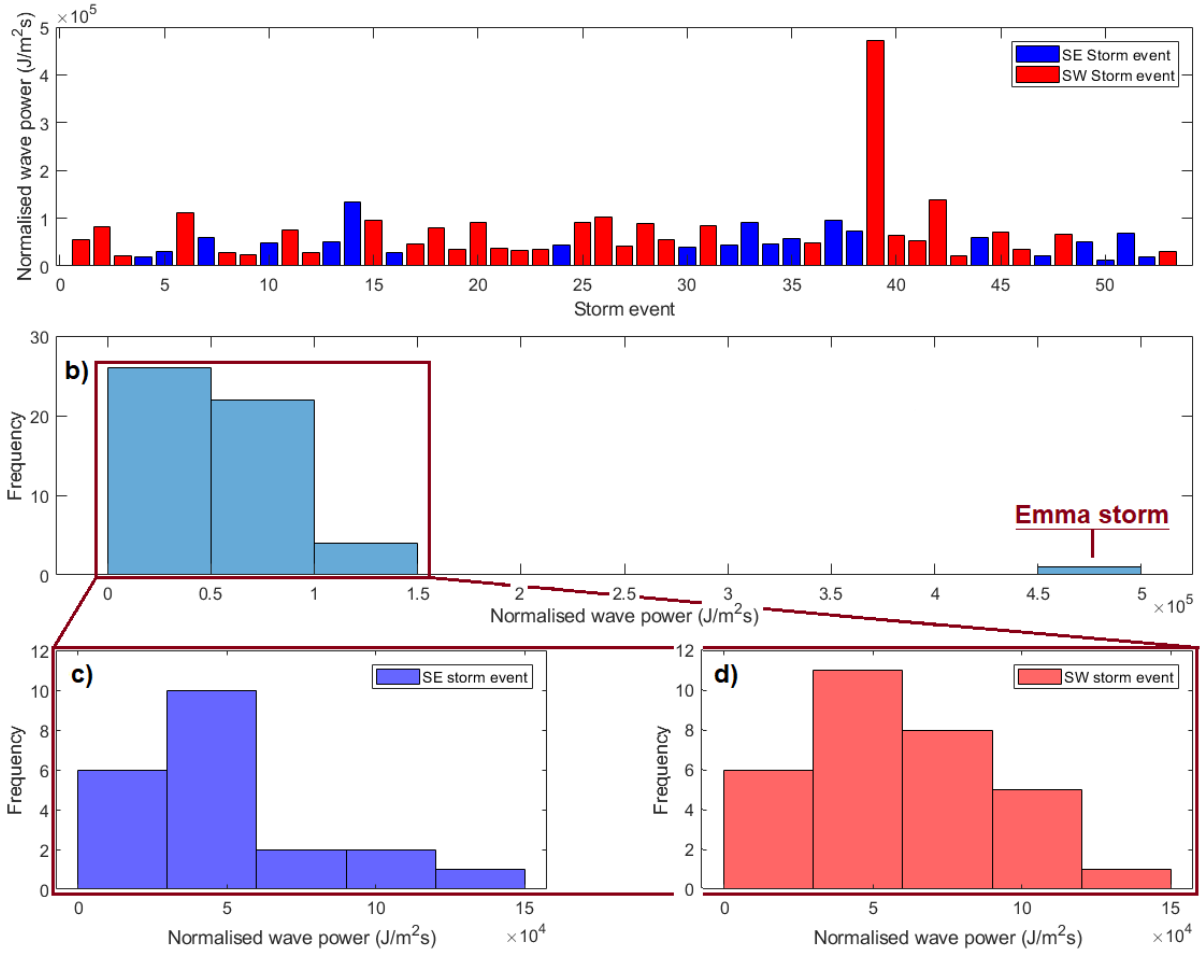

Figure 21.-a) Maximum normalised wave power of the 53 storm events recorded between 2014 and 2019 (SE in blue and SW storms), b)Frequency of the 53 storm events regarding their maximum normalised wave power and, frequency of the storm events without considering Emma storm for: c) SE storm events and d) SW storm events.

4.5 Storm events impact on ebb-shoal migration

The results of the displacement of the ebb-delta's outer edge along the profiles show: i) a seaward migration of the order of 40 to 60 m of the western shoal from 2017 onwards, represented by positive values (black dashed arrows in Figure 22); ii) Profile 1 shows a different morphological evolution from profiles 2, 3 and 4 that present similar outcomes among each other in terms of displacement (Figure 22); iii) a cyclical recession of the downdrift lateral bar towards the coast until the cluster of storms of 2018 took place (dashed curved arrows in Figure 24) and lastly, major displacements closer to 40 m occurred in the beginning of 2017, visible in the eastern shoal, and in 2018 easily recognisable in both lateral bars (purple arrows in Figure 22 and Figure 24).

Lower migration rate of the lateral bar can be observed from 2017 onwards in Profile 1 (Figure 22), in agreement with was observed at the depth-length analysis of the profiles (Figure 16), when compared to the other profiles of the western shoal where higher migration rates can be observed. This can be associated to a more perpendicular position of Profile's 1 location on the shoal when referenced to the shoreline. Approximately at the time the bathymetric survey of May 2016 was carried out, a progressive progradation of the updrift lateral bar began and displaced it almost 40 m. This progressive progradation ceased when a series of 12 separate storm events occurred in the winter of 2016/2017. The storms concerning winter 2016/2017 correspond to the storm events 23 to 35, with an average normalised wave power of 63401.96 J/m^2s and, a maximum *Pn* of 103014 J/m^2s for event 26. The shoal maintained it position until summer 2018, when a progressive offshore migration of circa 25 m took place until summer 2019, after which its position receded around 20 m towards the coast.

No significant changes were observed along the outer shoal until the end of 2016 (Profiles 2, 3 and 4 in Figure 22). The progressive offshore migration observed in 2016 along the updrift bar (Profile 1 in Figure 22) could not be observed along the outer shoal profiles. Instead, the evolution of the outer shoal presented different results during the storms of winter 2016/2017 compared to the updrift lateral bar. Profiles 2 and 3 show a progressive seawards migration after the SE storm events, with final migration of 45 m and 35 m, respectively. Profile 4 first shows a landward migration of ~15 m followed by an offshore migration of around 30 m.

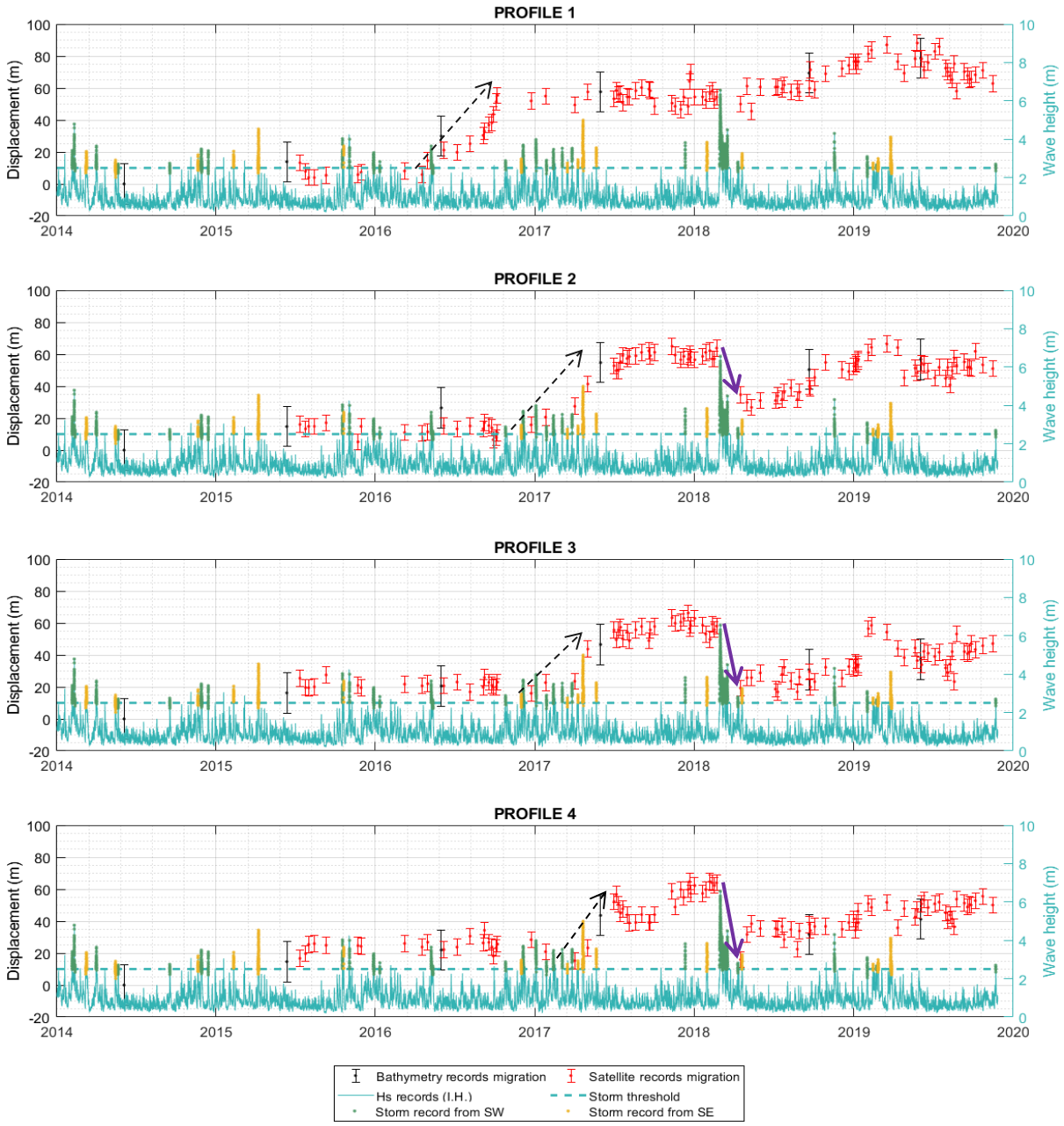

Figure 22.- Updrift lateral bar and ebb-shoal displacement based on satellite (red error-bars) and bathymetric (black error-bars) measurements. Right axes represent significant wave height and storm events (SE and SW). Storm threshold (2.5 m) is represented through a blue dashed line.

Only profile 4 shows a significant variation on the position through 2018, with a 15 m recession followed by a 25 m progradation (Figure 22). Even though two storm events took place during these shifts, none of them seems to have had an impact on the shoal. The impact of the storm cluster of winter 2017/2018 was noticeable throughout the outer shoal, with a retrogradation of the sandbar of 30 m, 40 m, and 50 m along profiles 2, 3 and 4, respectively. After such events, the outer shoal returns to its natural offshore migratory pattern that is again affected by the storm events taking place in the following winter. The storm events occurring in the winter of 2018/2019 are of significantly lower characteristics compared to the previous

winter, which is reflected in the recession of the outer shoal position of an order of 10 m, 20 m and 15 m along profiles 2, 3 and 4, respectively. During 2019 profiles 3 and 4, which have a more southern direction, show a slight retrogradation followed by a progradation, to which no storm event can be attributed for.

The storm events occurring in the winter of 2018/2019 are of significantly lower characteristics compared to the previous winter, which is reflected in the recession of the outer shoal position of an order of 10 m, 20 m and 15 m along profiles 2, 3 and 4, respectively (Figure 22). During 2019 profiles 3 and 4, which have a more southern direction, show a slight retrogradation followed by a progradation, to which no storm event can be attributed for.

The digitation of the outer edge of the shoals before and after the cluster of storms that took place in winter 2017/2018 (including Emma storm), shows the progradation of the updrift lateral bar and outer shoal as well as the landward migration effect on the downdrift complex (Figure 23). It is possible to observe a widening on the edge of the ebb-flow channel as well as a shift on its position.

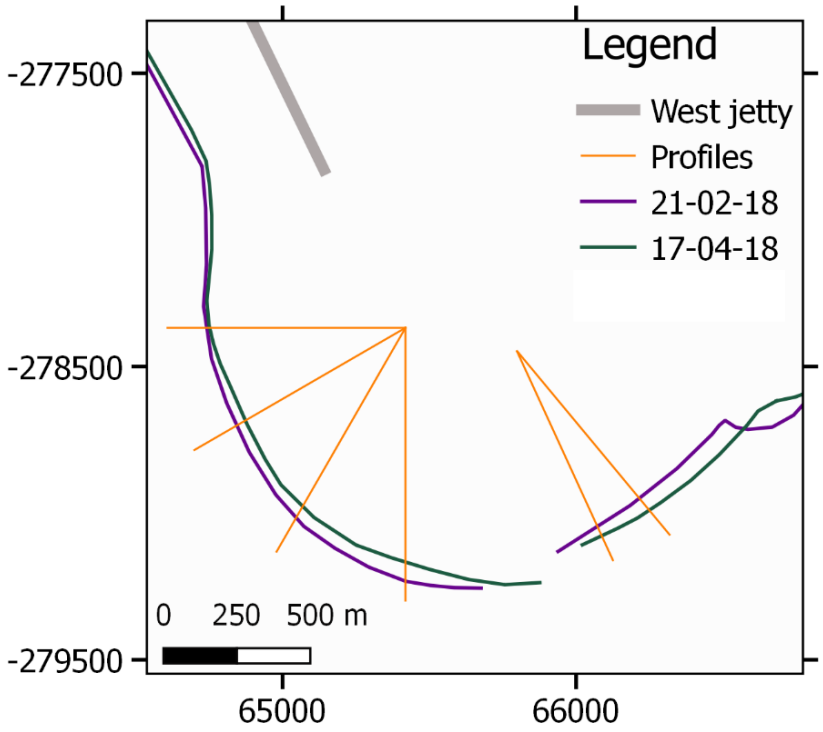

Figure 23.-Ebb-delta outer digitation of the shoals position before (21-02-18) and after (17-04-18) the storm cluster, including Emma storm.

The downdrift complex displacement through time show a very similar behaviour between profiles 5 and 6, although profile 6 shows a higher retrogradation (Figure 24). The storm events in the winter of 2016/2017 had an opposite effect in this area in comparison with the updrift

lateral bar (Figure 22 and Figure 24). After the bathymetric survey of 2016, the sandbars of the downdrift area migrated almost 35 m landwards and, in profile 5 we can observe a stabilization of the lateral bar, while in profile 6 there is an additional 10 m landward migration followed by a 20 m progradation of the bar after the storm events. The behaviour of the downdrift complex resembles a cyclical recession(see dashed curved arrows in Figure 24), where the impact of the storm events results in an impediment to the natural retrogradation of the historical ebb delta.

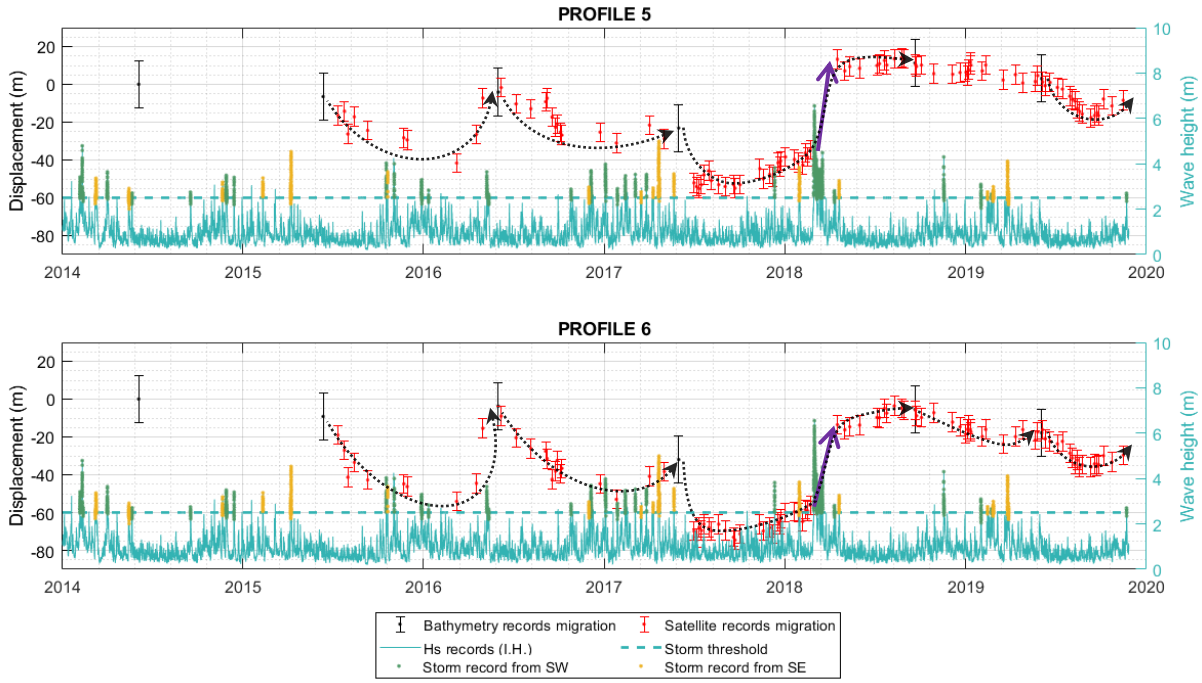

Figure 24.- Downdrift complex displacement based on satellite (red error-bars) and bathymetric (black error-bars) measurements. Right axes represent significant wave height and storm events (SE and SW). Storm threshold (2.5 m) is represented through a blue dashed line.

The updrift lateral bar shows a maximum displacement of 88.2 m through the 6 years analysed in the ebb-delta, which represents a seaward migration of 14.7 m/year. The outer edge of the shoals in profiles 2, 3 and 4 displaced a maximum distance in between 64.73 m and 66.38 m. Therefore, the 3 profiles of the outer shoal were averaged, showing a seaward migration rate of 10.96 m/year. Lastly, the maximum distance migrated along profiles 5 and 6 was -55.18 m and -74.54 m, resulting in a landward migration rate of 9.19 m/year and 12.42 m/year, respectively. The offshore migration at the outer shoal measured following Stauble (1998) (dashed line in Figure 12), shows a displacement of the bar of around 41 m between 2014 and 2019, with a rate of migration of 6.83 m/year.

The graphs showing the migration across the six profiles (Figure 22 and Figure 24) can be found without the wave climate data in **Annex IV**.

4.6 SE / SW swells and storms impact in between surveys

Stormy periods represented 17.47% of the total analysed periods between surveys with a total of 18 storms (Figure 25). A total of 85 periods without storm events were recorded, representing the 82.53%. Storm events had maximum normalised wave power higher than $0.5x10^5$ J/m^{2}s, except for one event of weaker characteristics of the order of $3.5x10^4$ J/m^{2}s (Figure 25). The maximum normalised wave power is from the period when the storm cluster occurred, with a P_n of $4.72x10^5$ J/m^{2}s corresponding to Emma storm. The maximum normalised wave power for the periods without storm events was lower than $4.11x10^5$ J/m^{2}s, apart from two periods that show similar characteristics to those with stormy times. These exceptions are a consequence of the thresholds previously selected for the storm events. Less powerful storms had a higher impact on the bar. The maximum offshore migration effects of the order of 15.6 m and 15.5 m were caused by storm events of $0.8x10^4$ J/m^{2}s and $1.6x10^4$ J/m^{2}s, respectively. The updrift bar migrated similar distances (i.e. 15 m offshore) when under low ($8.13x10^3$ J/m^{2}s) or high ($1.99x10^5$ J/m^{2}s) wave power conditions. The impact of storm events along each of the 6 profiles can be found in **Annex V** ant the characteristics of the periods with and without storm in **Annex VI**.

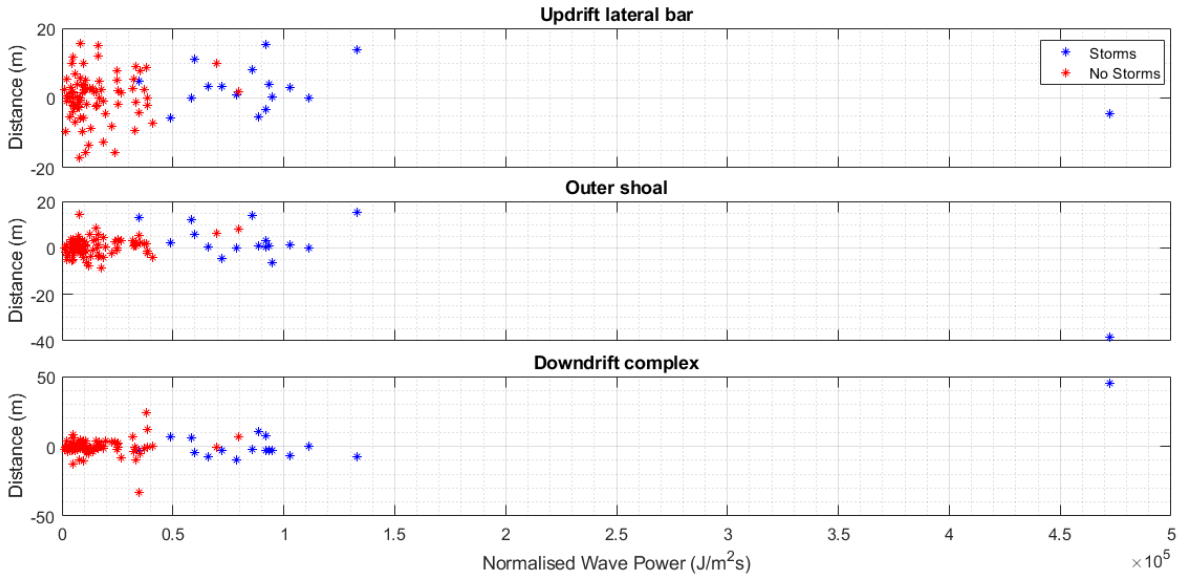

Figure 25.- Maximum normalised wave power in between surveys. Storm events are shown in blue while periods without storms are shown in red. Positive values of distance correspond to seaward migration, negative values refer to landward migration of the shoals.

The updrift lateral bar showed the lowest distances migrated due to storms from the whole ebb-delta, although it presents higher variability among the registered migrations (Figure 25). The periods without storm events show comparable landward (circa -20 m) and seaward (almost +20 m) migration when under similar wave conditions. These displacements depict the

natural movement of the shoal, although an offshore displacement tendency was inferred from the previous analysis, where the displacement of the shoal was examined through the whole dataset (Profile 1 in Figure 22). Emma storm did not pose a high impact on the updrift shoal, causing a 5 m landward migration which is in agreement with the analysis performed through the whole dataset (Profile 1 in Figure 22). The immediate effect after the storm cluster of 2018 on the outer shoal was a retrogradation of the order of -38 m, representing the highest migration recorded on the shoal. The downdrift complex shows the highest displacement effect due to Emma storm along the ebb-delta, with an offshore migration of 45 m. It is possible to observe that all the storm events considered in the present study had maximum *Hs* higher than 3 m and, that two of the periods without storm events reached a higher significant wave height of the 2.5 m, considered as a threshold for storm events (Figure 26). Periods without storm events and periods considered as stormy, show similar displacement values along the ebb-delta. The highest migrations are a result of lower *Hs* (illustrated as no storm periods) as can be observed in the downdrift complex, where maximum *Hs* of ~2.5 m result in shoal migrations above 20 m (black circles in Figure 26).

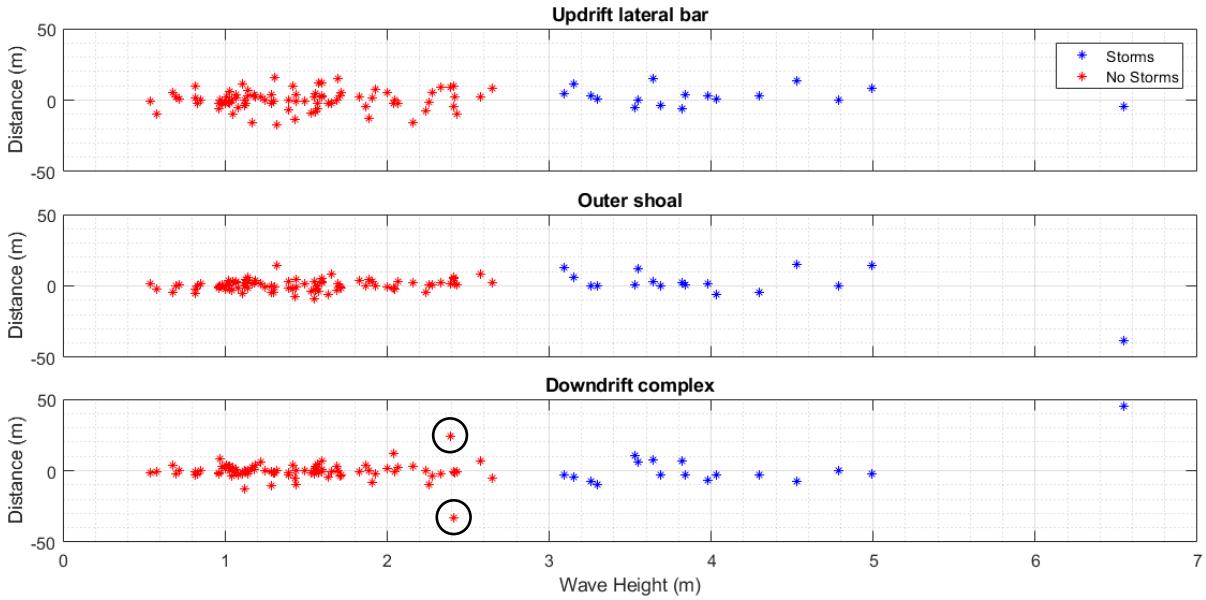

Figure 26.- Maximum significant wave height in between surveys. Storm events are shown in blue while periods without storms are shown in red. Positive values of distance correspond to offshore migration, while negative values refer to landward migration of the shoals.

The wave impact of the periods in which there occurred no storm events were analysed based on their incoming direction, where 88.24% of the incoming event were from the SW, congregated in 75 events. The remaining 11.76% were incoming from the SE, illustrating 10 events. The analysis of the periods without storm events showed that the most powerful swell recorded was from the SE, with a *Pn* of 7.9×10^4 J/m^{2}s, resulting in a displacement of less than

10 m along the ebb-delta (shown with black arrows in Figure 27). The highest displacement recorded over the outer shoal (~15 m) was caused by a SE swell (green circle in Figure 27). The incoming waves with a *Pn* higher than $3x10^4$ J/m^2s only occurred under SW swells, resulting in significant impacts in the downdrift area, with displacements shifting between ~35 m landwards and 25 m seawards (black circles in Figure 27). The updrift lateral bar migrated similar distanced under SE and SE swells, although due to the dominance of the southwest swells, it is possible to infer that the ebb-delta natural evolution is mainly disturbed by the SW swells.

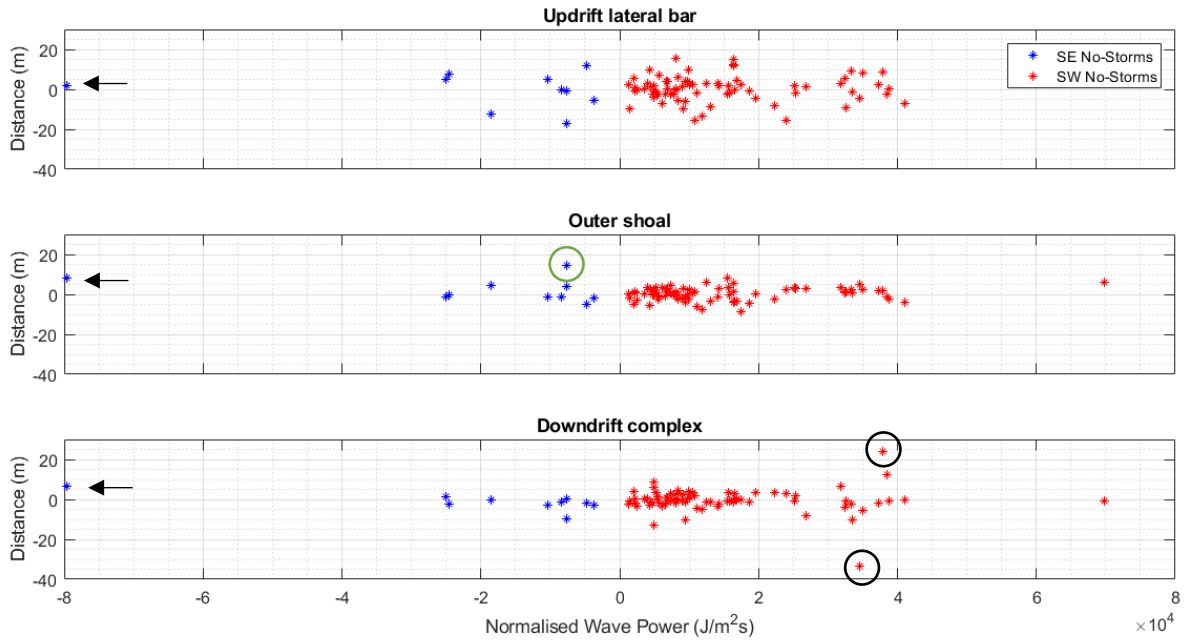

Figure 27.- Maximum normalised wave power in between surveys during periods without storms. SE incoming waves are shown in negative (blue) and SW in positive (red).

The impact of typical storm events was examined to represent the behaviour of the ebb-delta under frequent storm conditions (without accounting with Emma storm, see Figure 28). SE and SW storm events caused migrations of the order of 15 m at the updrift lateral bar and at the outer shoal when under low or high normalised wave power (black and orange circles in Figure 28). Results show that as the *Pn* increases, the updrift lateral bar and outer shoal migrate longer distances offshore (orange circles in Figure 28). Only one SE storm event resulted in a landward migration of the updrift lateral bar and the outer shoal (green circle in Figure 28. SW storm event resulted in a more variable response from the updrift and outer shoal areas. The downdrift complex did not show any significant migration under SE or SW storm events (<10 m migrations).

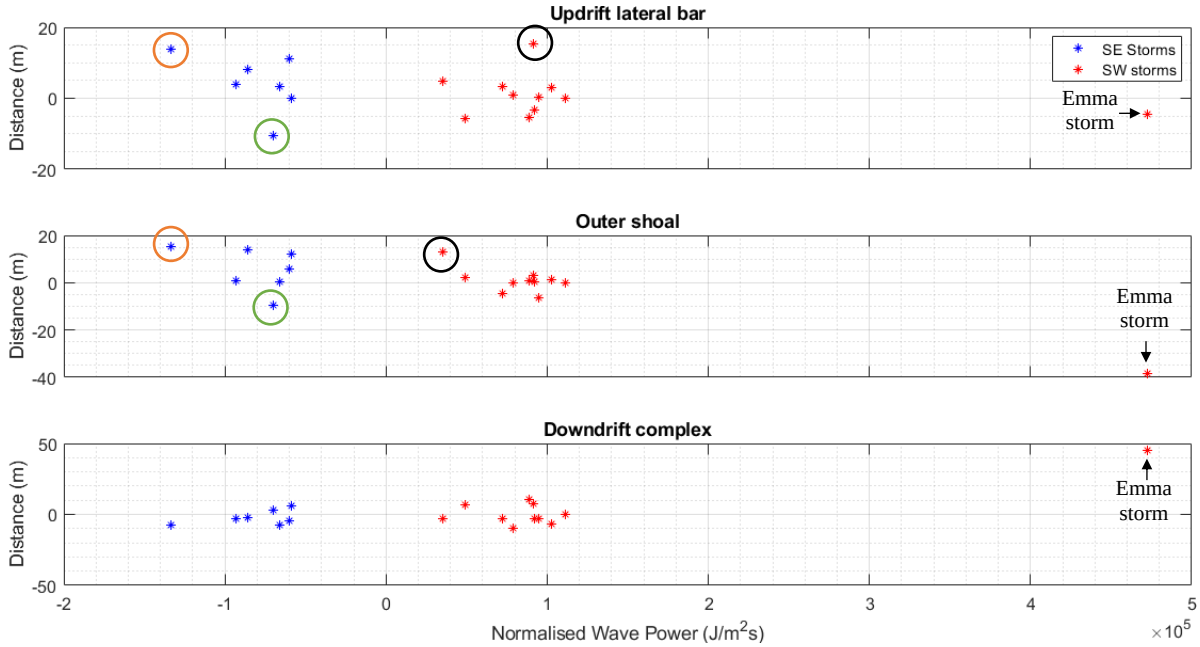

Figure 28.- Maximum normalised wave power in between surveys during storm events. SE incoming waves are shown in negative (blue) and SW in positive (red).

However, variations on the position of the ebb-delta shoals, in terms of displacement or apparent displacement, pose an uncertainty on the veracity of these values due to the errors associated to the datasets characteristics, where the pixel size is 10 m and the grid size is 25 m. Table 6 summarizes the main morphological effects observed in the Guadiana ebb-delta along the study due to the impact of SE and SW waves during the periods where storm events were identified and the periods when no storm events occurred and, extreme storm events.

Table 6.- Main impact observed in the morphological evolution of the ebb-delta due to the incoming swells.

Morphological feature	**SE waves**		**SW waves**		**Extreme event impact (Emma storm)**
	No-storm impact	**Storm impact**	**No-storm impact**	**Storm impact**	
Updrift lateral bar	Variable direction	Seaward migration	Variable direction	Variable direction	Landward migration
Outer shoal	Slightly seaward	Seaward migration	Oscillating behaviour	Slightly seaward	Landward migration
Downdrift complex	Oscillating behaviour	Slightly landward	Variable direction	Oscillating behaviour	Seaward migration

5 Discussion

5.1 Morphological evolution of the Guadiana ebb-delta

The morphological evolution of the ebb-delta, including the lobate and parallel bars, was analysed through the present study. Along the yearly difference maps, it is possible to observe a series of alternated erosional and depositional areas (Figure 15). The sediments from the eroded areas are in fact located in the depositional bars, illustrating the landward or seaward migration of the sandbars. For example, between 2016 and 2017, the areas of alternated erosion and deposition show the seaward migration of the western side of the ebb delta, while the a landward displacement took place on the downdrift area (Figure 15). These results are in agreement with the results obtained by Garel *et al*. (2015), that show a seaward migration of the updrift lateral bar and the ebb-shoal (outer shoal) between 2005 and 2015. An opposite migration was observed on the downdrift area between 2017 and 2018, where the displacement was seawards. This change in the direction of the migration was a result of the impact of Emma storm, which affected greatly this area of the delta (see Figure 23) and additionally, explains the migration of the downdrift complex lobate sandbars shown in the vertical difference maps between 2014 and 2019 (Figure 13). The delta also presented a 'drop-shaped' region of 0.5 to 1.5 m of erosion which is explained by the collapse of the tip of the western jetty, that occurred in March 2019 and that has already been rebuilt (Figure 13). Finally, the migration of the lobate sandbars at the outer shoal, between 2015 and 2016, would be visible with a lower variability interval (< 0.5 m), showing the wider alternated red (erosion) and blue (accretion) bars (Figure 15).

According to the literature (Morales, 1997; Gonzalez *et al.,* 2001; Garel *et al.,* 2015; Garel *et al.,* 2014; Garel *et al.,* 2019; Morales and Garel, 2019), the sediment pathways in the Guadiana ebb-delta and across the four main morphological elements are explained as follows: i) sediments from the longshore transport feed the updrift lateral bar, from where they are transported towards the outer shoal and within the inlet channel by wave and current actions; ii) the inlet channel additionally receives sand exported from the Guadiana River estuary; iii) the material from both the updrift lateral bar and the inlet channel feeds the outer shoal, from where sand is transported towards the downdrift complex. The migration of the shoals along the profiles showed that the updrift bar migrated seawards after June 2016 (Figure 22), where the updrift bar is also fed by sand from the outer shoal under SE wave regime. The outer shoal did not show such migration after the bathymetric surveys of 2016 (Figure 22). This could be

associated to the dredging of the inlet channel in 2015. Close to the submerged jetty, the sand is transported westward, due to the wave refraction over the swash platform and to the protection provided by the jetties. These sediments along with the usually supplied from the inlet channel to the outer shoal, could be trapped within the channel explaining the lack of sand available in 2016 required for the seaward migration of the shoal.

The sequence of storm events that occurred from 2014 to 2019, along with the dates when the bathymetric surveys took place and the dates when satellite images were captured, shows the complementarity of the datasets towards the research of coastal morphological changes (Figure 20). The information provided by the satellite images, also allowed the identification of the highest migrations of the ebb-delta along the profiles. Whilst the migration rate calculated following Stauble (1998) resulted in a rate of displacement of 6.83 m/year (calculated along the dashed line shown in Figure 12), which is similar to the values obtained by Garel *et al.* (2019), the other values here presented for the rate of displacement were calculated based on the highest displacements of the shoals along the profiles (Table 6). These values double the 7 m/year presented in the literature Garel *et al.* (2019) (Table 6). This increase was promoted by the power of displacement associated to extreme storm events, such as Emma storm and additionally, because the highest displacements were recorded along the satellite images, not over the bathymetric maps as in Garel *et al.* (2019). Therefore, the use of regular satellite observations has proven to offer key information to capture the morphological evolution of the coastal zone, as recognised by Bergsma and Almar (2020).

5.2 Ocean climate

The dominance of SW waves during the study period and the significant wave heights were in agreement with the literature (Costa *et al.,* 2001), confirming the eastern prominent littoral drift and longshore sediment transport formerly described by Garel *et al.* (2019). The average significant wave height of 1.25 m and peak period of 6.33 s from SE waves, with an occurrence of 25.25% for the study period, also show similar values to the ones presented in the study by Costa *et al*. (2001). Even though the ocean climate study carried out by Costa *et al.* (2001) covered 14 years with a total of 23,863 records, the present ocean climate study was based on a total 41,565 records for a period of 6 years, due to the increase in frequency sampling of the buoy from 2015 onwards. Events defined by significant wave height higher than 3 m represented 1.46% of the occurrences, similar to the 2 % stated by Costa *et al.* (2001). The 53 storms identified in the present study for a significant wave height higher than 2.5 m, have a

SW dominance (60.37% of the occurrence), while SE storms represent 39.63% of the occurrences (Figure 21-a). These values show a slightly lower dominance of storm events from SW swells, compared to the 63.85% documented in the literature. Accordingly, SE storm events have a higher percentage of occurrence when compared to the 36.15% recorded by Oliveira *et al.* (2018). The yearly occurrence of storm events is higher for the present study (8.83 storms/year) compared to the literature (6.32 storms/year, according to Oliveira *et al.*, 2018). It is important to note that the timeframe regarding the present study is just 6 years, while the study of Oliveira *et al.* (2018) covered a period of 28 years, with a total of 177 storms identified. A total of 17.47% of the periods in between bathymetric surveys or satellite images were considered stormy periods by including one or more storms within those periods (Figure 22).

The tidal level relation with the timing of the storm have been proven to contribute to the enhancement of the storm effects (Plomaritis *et al.*, 2018; Ferreira *et al.*, 2019). The same is valid for the present study as low spring tides during the storm peak pose a higher influence on underwater features. The maximum tidal range computed resembles the values provided by the Instituto Hidrográfico for Vila Real de Santo António, the closest town to the Guadiana mouth, with a maximum high tide of 1.96 m and a minimum low tide of -1.74 m.

In the present study, the 6-year timeframe was divided into periods with and without storm events. These periods where analysed based on the highest maximum normalised power recorded in the intervals. Storms occur during the winter months and can be aggregated in storm clusters (Masselink *et al.*, 2016), and it is during these stormy periods is when less images are viable to analyse due to cloud coverage or resuspended sediments. Due to these facts, from the 53 storm events identified in the study, only 18 events represented the periods with storm used for the analysis in terms of storm event impact (Figure 25).

5.3 Sandbar migrations due to the impact of swells and storm events

The ebb shoal has a dominant role in inducing the depth deprivation of the waves causing them to break and, limiting the wave propagation and energy penetration to the inner part of the estuaries (Olabarrieta *et al.*, 2014). Diverse studies based on field measurements and numerical models have also emphasised the importance of wave-induced (surf zone) circulations in the ebb shoal area when under energetic offshore wave conditions. Robin *et al.* (2009) analysed the importance of different hydrodynamic processes on ebb delta bar migration using morphological and hydrodynamic measurements, suggesting that the sediment transport

and the modification in bar morphology were induced mainly by surf zone processes and associated littoral currents where during high surf conditions the mean flows were directed onshore. The study from Bertin *et al.* (2009) at the Obidos Inlet (Portugal), resolved that wave driven currents were the responsible for the infilling the inlet during storm conditions.

The analysis of the morphology through satellite images in the present study, allowed the documentation of a series of temporal progradations in the downdrift complex, which appear to be triggered by storm events. The natural behaviour of the downdrift complex is a retrogradation since it is part of the historical ebb delta. The impact of the storm events results in an impediment to the natural landward migration of the ebb shoal, causing these series of seawards migrations. This morphological behaviour of the downdrift area resembles the cyclical evolution of the Ancão Inlet, at the Ria Formosa barrier-island system (located updrift of the study area), described by Morris (2002).

Two main morphological states were described by Morris (2002): The Post-storm and Extended-calm states, separated by a transitional period of highly variable morphology, the Transitional-phase. Following Morris, the Guadiana ebb-delta would be at the Post-storm state after one or more storm events, which usually occur between October and March (Oliveira *et al.,* 2018) (see Figure 22 and Figure 24). During this state, is where the major seaward migrations can be observed, such as during the winter of 2016/2017 and 2017/2018 (see Figure 22 and Figure 24). During late Spring, the ebb-delta begins a period of transition, the Transitional-phase, leading to the Extended-calm state that mostly takes place during the summer months (see Figure 22 and Figure 24). This period of Extended-calm state represents the prevailing morphological evolution of the ebb-tidal delta, which is the natural retrogradation of the downdrift complex (see Figure 24). It was not possible to infer such cyclical behaviour at the updrift and outer shoal areas, perhaps due to the faster migratory rates of these sandbars. Summarizing, this leaded to the hypothesis that the temporal evolution of the Guadiana ebb-delta morphology is cyclic in nature.

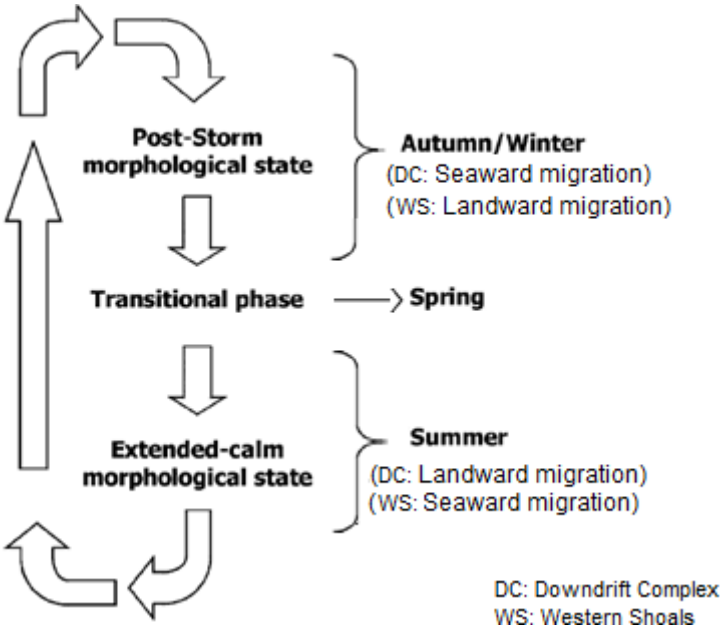

Figure 29.- Scheme of the cyclical morphological evolution of the Guadiana ebb-delta, modified after Morris (2002).

Extreme storm events, such as the Emma storm, have the power to significantly relocate the submerged sandbars of the Guadiana ebb-delta: the progradation of the updrift lateral bar and outer shoal and, the landward migration effect on the downdrift complex (Figure 23). The relocation of the shoals at the Guadiana ebb-delta after the storm cluster (38 m landwards and 45m seawards), could be explained as a result of the southwest direction of Emma storm and, the morphology of the ebb-delta, where the shape, location and orientation of the shoals play a key role in the interaction.

Following the sediment pathways in the Guadiana ebb-delta aforementioned (Morales, 1997; Gonzalez *et al.*, 2001; Garel *et al.*, 2015; Garel *et al.*, 2014; Garel 2019; Morales and Garel, 2019), the sedimentation on the western margin of the jetty is controlled by the littoral drift and wave activity, where the waves are mainly responsible for the migration and accretion of swash bars building the accreting margin. The SW waves are expected to break parallel to the updrift lateral bar and the outer shoal, due to the horseshoe shape and the refraction of the waves caused by the depth deprivation towards the coast. The sediment transport from the updrift area passes the western jetty reaching the inlet channel, from where it can be transported towards the outer shoal together with river-borne sediment by ebb jets (Morales and Garel, 2019). This would explain the 38 m retrogradation of the outer shoal (Figure 22 and Figure 23). The sedimentation on the eastern margin is controlled by the combined action of ebb-tidal and river current, and wave refraction (Morales, 1997). Sand deposited at the modern ebb delta has been documented to be remobilized by wave action primarily during storms events (Morales and Garel, 2019), as in the study by Bertin *et al.* (2009) where the onshore-directed

wave-induced flows in Obidos inlet (Portugal) contributed to the infilling of the inlet during storm conditions. After the waves break, the sediments are suspended and relocated following the eastern drift pattern of the area, where they can end deposited closer to the inlet channel or towards the downdrift complex, explaining the 45 m offshore migration shown in the downdrift area after the storm cluster (Figure 23 and Figure 24).

Regarding the remaining periods when storm events occurred, it was observed a higher variability on the behaviour of the sandbars. The impact of typical storm events was examined to depict the behaviour of the ebb-delta under frequent storm conditions (without accounting with Emma storm). It was observed that SW storm events can cause migrations of the order of 15 m at the updrift lateral bar and at the outer shoal when under low or high normalised wave power (black circles in Figure 28). While a similar effect was observed under SE storm events, the relation with the normalised wave power showed that as the *Pn* increases, the updrift lateral bar and outer shoal migrate longer distances offshore (orange circles in Figure 28). Only one SE storm event resulted in a landward migration of the updrift lateral bar and the outer shoal (green circle in Figure 28), suggesting that these morphological features mostly migrate offshore under SE storm events. SW storm event resulted in a more variable response from the updrift and outer shoal areas. Therefore, it was not possible to define a typical behaviour of the sandbars under these storm characteristics.

Even though López-Ruiz *et al.* (2020) suggested that the decrease of river discharge could have increased the control of waves on the delta evolution and, although it is presumable that dominant wave conditions are the ones that in fact dominate the overall behaviour of the ebb delta evolution (apart from high energy storms or storm groups that disrupt or enhance that evolution), it was not possible to determine the exact behaviour of the shoals under the different swells based on the analysis (see Table 6). The temporal distribution of storms defines the cyclic behaviour of such environments, making the system more dynamically active over the winter months. The opposite occurs during summer periods when less energetic conditions lead to slower morphological changes. Two conceptual models were designed to illustrate the main factors observed that depicted the morphodynamic evolution of the Guadiana ebb-delta (see Figure 30), following the states defined by Morris (2002): the impact of extreme storm events (based on Emma storm effect) and the overall expected behaviour of the sandbars.

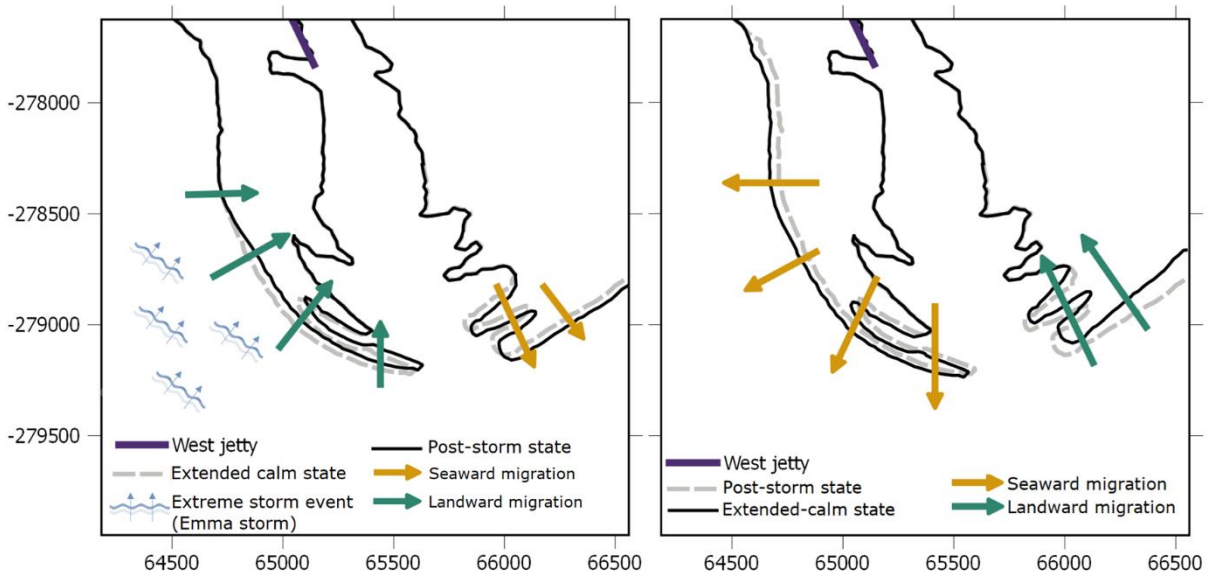

Figure 30.- Morphological evolution of the Guadiana ebb-delta after an extreme storm event showing the Post-storm state (left) and the natural cyclic behaviour, where the sandy shoals return to the Extended-calm state along with the rotation of the ebb-delta (right)

The series of facts hereafter presented created an uncertainty regarding the adequacy of the thresholds selected to define storm events that are needed to promote sand bank movements at the Guadiana ebb-delta. The impact of swells, in terms of significant wave height, showed the highest seaward migration (25 m) and landward migration (30 m) at the downdrift complex, occurred during periods when no storm events happened (Figure 26). These migrations occurred with a maximum wave height of 2.4 m. Similar results were observed in the updrift lateral bar, where a swell with a maximum *Hs* of 1.3 m resulted in the highest landward migration (~20 m) (Figure 26). Therefore, it is not possible to infer that swells with higher significant wave heights, result in larger migrations (except for Emma storm). Furthermore, it was observed that the updrift bar can migrate similar distances, i.e. 15 m offshore, under low (8.13×10^3 J/m^{2}s, no storm recorded) or high (1.99×10^5 J/m^{2}s, storm event) wave power conditions (Figure 25). Moreover, from the periods when storm events occurred, the less powerful SW storm event did in fact have the biggest impact in the outer shoal, with an offshore migration of ~13 m (black circle in Figure 28). This may suggest that the considered significant wave height or duration selected as threshold for storm events, must be revaluated when considering potential storm impacts on submerged structures. Even though a storm definition based on a wave-height threshold (e.g., maximum significant wave height H_s) is highly site-specific and depends strongly on the modal wave conditions, from a marine geological point of view, a more appropriate approach to define storms, identify storm thresholds and investigate storm statistics, might be considering the hydrodynamic forcing (wave conditions

and water level) in the context of coastal change, which has been suggested to be more useful to coastal managers (Masselink and van Heteren, 2014). An alternative could also be not selecting thresholds, but instead consider the accumulated normalised wave power (even for no storm conditions). Other studies that have researched the behaviour of sandbars due to the wave climate, emphasize that the response is particularly sensitive to the water depth above the bar crest, the wave steepness and to the angle of wave incidence, since these variables largely control the amount of waves breaking on the sandbar and, additionally the strength and cross-shore distribution of the associated longshore current (i.e. Thiébot *et al., 2012;* Phillips *et al., 2017*).

6 Conclusions

The morphological evolution of the Guadiana ebb-tidal delta was researched through bathymetric maps and Sentinel-2 satellite images. The wave climate analysis allowed the examination of the effects caused by the typical swells and storm events over the shoals. Satellite data provided key information of the morphological evolution of the ebb tidal delta by addressing the shortcomings of yearly bathymetric surveys. The regression analysis between the datasets were in excellent agreement and allowed the quantitative analysis of the morphological evolution of the ebb-tidal delta. The Guadiana mixed-energy ebb-tidal delta is composed by four main morphological features: the inlet channel, the updrift lateral bar the outer shoal and the downdrift complex.

Extreme storm events, such as Emma storm, have the power to significantly relocate the submerged sandbars of the Guadiana ebb-delta up to 38 m landwards for the western shoals and 45m seawards for the downdrift complex. The direction of these events and the morphology of the ebb-delta, mainly the shape, location, and orientation of the shoals, play a key role in the interaction.

The natural migrations of the shoals tend to dominate the overall morphological evolution of the ebb-tidal delta: the offshore migration of the western shoals and the landward migration of the downdrift complex. Opposite directions in the migrations of the shoals were reported to be caused by storm events. This was only detected due to the additional information provided by the satellite imagery. The short-term analysis of the morphological evolution depicted a cyclical morphologic nature: the shoals tend to recover the natural morphology and migration patterns after being altered by storm events.

Overall, this work shows that the cyclical morphological migrations of the shoals yields a progressive anticlockwise rotation of the Guadiana ebb-delta, which additionally results in the sifting of the ebb-flow channel towards the southeast. Regarding the research of the impact of storm events in underwater sand bodies, the importance of integrating the wave power should be considered in future studies, in order to account the accumulative effect of contiguous storms or storm clusters. These events (or more energetic events) can cause changes in orders of tens of meters. Therefore, the prediction of the evolution of the submerged sandbars is highly important, since they may cause severe changes that might affect navigational channels or cause threats to navigation.

7 References

Almeida, L. P., Vousdoukas, M. V., Ferreira, Ó., Rodrigues, B. A., & Matias, A. (2012). Thresholds for storm impacts on an exposed sandy coastal area in southern Portugal. *Geomorphology*, 143, 3-12.

Andrade C. (1990). O ambiente de barreira da ria formosa Andrade. In *Departamento de Geologia*. Universidade de Lisboa: Lisbon; 645.

Balouin, Y., Morris, B. D., Davidson, M. A., & Howa, H. (2004). Morphology evolution of an ebb-tidal delta following a storm perturbation: assessments from remote sensed video data and direct surveys. *Journal of coastal research*, *20*(2 (202)), 415-423.

Bergsma, E. W., & Almar, R. (2020). Coastal coverage of ESA' Sentinel 2 mission. *Advances in Space Research*.

Bergsma, E., Almar, R., Garlan, T., Kestenare, E. (2020). Global beach evolution; a review. Submitted to Nature Sci. Rep. `

Bertin, X., Fortunato, A. B., & Oliveira, A. (2009). A modeling-based analysis of processes driving wave-dominated inlets. *Continental Shelf Research*, *29*(5-6), 819-834.

Bettencourt P. (1994). Les environnements sédimentaires de la côte Sotavento (Algarve, Sud Portugal) et leur évolution Holocène et actuelle. Univeristé de Bordeaux I: Bordeaux; 586.

Byrnes, M.R., Hiland, M.W. (1995). Large-scale sediment transport patterns on the continental shelf and influence on shoreline response: St. Andrew Sound, Georgia to Nassau Sound, Florida, USA. Mar. Geol. 126, 19–43

Boothroyd, J. C. (1985). Tidal inlets and tidal deltas. In *Coastal sedimentary environments* (pp. 445-532). Springer, New York, NY.

Buijsman, M.C., Kaminsky, G.M. & Gelfenbaum, G. (2003). Shoreline change associated with jetty construction, deterioration and rehabilitation at Grays Harbor, Washington. Shore Beach 71 (1), 15–22.

Carter, R. W. G. & Woodroffe, C. D. (1997). "Coastal Evolution: Late Quaternary Shoreline Morphodynamics." *Sedimentary Geology* 102.3 (1996): 305-305.

CEEPYC (1979). *Plan de estudio de la dinámica litoral de la Provincia de Huelva*. Dirección General de Puertos y Costas: Madrid; 37.

Chícharo, M. A., Chícharo, L., Galvão, H., Barbosa, A., Marques, M. H., Andrade, J. P., *et al* (2001). Status of the Guadiana estuary (south Portugal) during 1996–1998: An ecohydrological approach. *Aquatic Ecosystem Health Management*, 4, 1–17.

Costa, M., Silva, R., & Vitorino, J. (2001). Contribução para o estudo do clima de agitação marítima na costa portuguesa. In: *Proceedings of 2as Jornadas Portuguesas de Engenharia Costeira e Portuária*. International Navigation Association PIANC, Sines, Portugal.

Cuena, G. J. (1991). Proyecto de regeneración de las playas de Isla Cristina. *Servicio de Costas, MOPT*, 100.

Dalrymple, R. W., & Choi, K. (2007). Morphologic and facies trends through the fluvial–marine transition in tide-dominated depositional systems: a schematic framework for

environmental and sequence-stratigraphic interpretation. *Earth-Science Reviews*, *81*(3-4), 135-174.

Davis Jr, R. A., & Hayes, M. O. (1984). What is a wave-dominated coast?. *Marine geology*, *60*(1-4), 313-329.

Dawson, R.J., Dickson, M.E., Nicholls, R.J., Hall, J.W., Walkden, M.J., Stansby, P.K., ... Milligan, J., 2009. Integrated analysis of risks of coastal flooding and cliff erosion under scenarios of long term change. *Clim. Chang*. 95 (1–2), 249–288.

Dias, J. M. A., Gonzalez, R., & Ferreira, Ó. (2004). Natural versus anthropic causes in variations of sand export from river basins: an example from the Guadiana river mouth (southwestern Iberia). *Polish Geological Institute Special Papers*, *11*(95), e102.

Dickson, M.E., Walkden, M.J., Hall, J.W., 2007. Systemic impacts of climate change on an eroding coastal region over the twenty-first century. Clim. Chang. 84 (2), 141–166. https://doi.org/10.1007/s10584-006-9

Dohmen-Janssen, C. M., & Hulscher, S. J. (2019). The role of suspended load transport for the equilibrium of tide-dominated ebb-tidal deltas. In: *River, Coastal and Estuarine Morphodynamics: RCEM 2007, Two Volume Set* (pp. 60-67). CRC Press.

Elias, E. P., & van der Spek, A. J. (2006). Long-term morphodynamic evolution of Texel Inlet and its ebb-tidal delta (The Netherlands). *Marine Geology*, *225*(1-4), 5-21.

Ferreira, Ó., Plomaritis, T. A., & Costas, S. (2019). Effectiveness assessment of risk reduction measures at coastal areas using a decision support system: Findings from Emma storm. *Science of the Total Environment*, *657*, 124-135

Fisher J.J. & Simpson E.J. (1982) Tidal deltas. *Beaches and Coastal Geology. Encyclopedia of Earth Science*. Springer, Boston, MA.

Fitzgerald, D. M. (1984). Interactions between the ebb-tidal delta and landward shoreline; Price Inlet, South Carolina. *Journal of Sedimentary Research*, *54*(4), 1303-18.

Fitzgerald, D.M., Kraus, N.C., Hands, E.B. (2000). Natural Mechanisms of Sediment Bypassing at Tidal Inlets. CHETN-IV-30. U.S. Army Corps of Engineers, Vicksburg, MS.

FitzGerald, D., Buynevich, I., & Hein, C. (2012). Morphodynamics and facies architecture of tidal inlets and tidal deltas. In *Principles of Tidal Sedimentology* (pp. 301-333). Springer, Dordrecht.

FitzGerald, D. M., & Miner, M. D. (2013). 10.7 Tidal Inlets and Lagoons along Siliciclastic Barrier Coasts. Treatise on Geomorphology Volume 10, 2013, Pages 149-165

Gao, J. (2009). Bathymetric mapping by means of remote sensing: methods, accuracy and limitations. *Progress in Physical Geography*, *33*(1), 103-16.

Garel, E. (2017). Efficient dredging strategy for channel maintenance of the Guadiana ebb-delta. *Proceedings of Coastal Dynamics 2017*, *232*, 1-10.

Garel, E. (2017b). Present dynamics of the Guadiana estuary. In: D. Moura, A. Gomes, I. Mendes, J. Anílbal (Editors.), *Guadiana River estuary - investigating the past, present and future*. 1st edition. University of Algarve. Faro, pp. 15–37.

Garel, E. & Ferreira, Ó. (2011). Effects of the Alqueva dam on sediment fluxes at the mouth of the Guadiana estuary. *Journal of Coastal Research*, 1505-1509.

Garel, E. & Ferreira, Ó. (2013). Fortnightly changes in water transport direction across the mouth of a narrow estuary. Estuar. Coasts 36 (2), 286–299

Garel, E., Pinto, L., Santos, A. & Ferreira, Ó. (2009). Tidal and river discharge forcing upon water and sediment circulation at a rock-bound estuary (Guadiana estuary, Portugal). *Estuarine, Coastal and Shelf Science*, *84*(2), 269-281.

Garel, E., Sousa, C., Ferreira, Ó., & Morales, J. A. (2014). Decadal morphological response of an ebb-tidal delta and down-drift beach to artificial breaching and inlet stabilisation. *Geomorphology*, *216*, 13-25.

Garel, E., Sousa, C., & Ferreira, Ó. (2015). Sand bypass and updrift beach evolution after jetty construction at an ebb-tidal delta. *Estuarine, Coastal and Shelf Science*, *167*, 4-13.

Garel, E., López-Ruiz, A., & Ferreira, Ó. (2019). A method to estimate the longshore sediment transport at ebb-tidal deltas based on their volumetric growth: Application to the Guadiana (Spain–Portugal border). *Earth Surface Processes and Landforms*, *44*(13), 2557-2569.

Gaudiano, D.J., Kana, T.W. (2001). Shoal bypassing in mixed energy inlets: geomorphic variables and empirical predictions for nine South Carolina inlets. J. Coast. Res. 17 (2), 280–291.

Gonzalez, R., Dias, J. A. & Ferreira, Ó. (2001). Recent rapid evolution of the Guadiana Estuary mouth (southwestern Iberian Peninsula). *Journal of Coastal Research*, 516-527.

Gonzalez-Regalado, M. L., Ruiz, F., Borrego, J., Abad, M., Garcia, E. X., & Toscano, A. (2013). The mesocosm marsh ecology of two southwestern Spanish estuaries: Applications. *Marshes: Ecology, Management and Conservation*, 91-102.

Granja, H., Froidefond, J. M., & Pera, T. (1984). Processus d'evolution morpho-sedimentaire de la Ria Formosa (Portugal). *Bulletin de l'Institut de géologie du Bassin d'Aquitaine Bordeaux*, (36), 37-50.

Hansen, M. & Knowles, S. (1988). Ebb-tidal delta response to jetty construction at three South Carolina Inlets. In: Aubrey, D., Weishar, L. (Eds.), Hydrodynamics and Sediment Dynamics of Tidal Inlets. Lecture Notes on Coastal and Estuarine Studies. Springer, New York, pp. 364–381.

Hayes, M.O. (1975). Morphology of sand accumulation in estuaries: an introduction to the symposium. In: L.E. Cronin (Editor), *Estuarine Research, Vol II.* Academic Press, New York, pp. 3 – 22.

Hayes, M. O. (1979). Barrier island morphology as a function of tidal and wave regime. In: Leatherman SP (ed) Barrier Islands. *Academic Press, New York*, *1*, 27.

Hayes, M. O. (1980). General morphology and sediment patterns in tidal inlets. *Sedimentary geology*, *26*(1-3), 139-156.

Hayes, M. O., Montello, T. M., Schrader, R. J., & Levine, E. A. (1999). Tidal Inlets—A Major Hurdle to Effectively Protecting Sensitive Coastal Resources. In *International Oil Spill Conference* (Vol. 1999, No. 1, pp. 1239-1243). American Petroleum Institute.

Hicks, D.M., Hume, T.M. (1996). Morphology and size of ebb tidal deltas at natural inlets on open-sea and pocket-bay coasts, North Island, New Zealand. J. Coast. Res. 12 (1), 47–63.

Hume, T. M., & Herdendorf, C. E. (1988). A geomorphic classification of estuaries and its application to coastal resource management—a New Zealand example. *Ocean and Shoreline Management*, *11*(3), 249-274.

Kana, T. W., Hayter, E. J., & Work, P. A. (1999). Mesoscale sediment transport at Southeastern US tidal inlets: Conceptual model applicable to mixed energy settings. *Journal of Coastal Research*, 15(2), 303–313.

Komar, P. D. (1996). Tidal-inlet processes and morphology related to the transport of sediments. *Journal of Coastal Research*, 23-45.

Kraus, N.C. (2000). Reservoir model of ebb-tidal delta evolution and sand bypassing. J. Waterw. Port Coast. Ocean Eng. 126 (3), 305–313.

Kraus, N.C. (2006). Coastal inlet functional design: anticipating morphological response. In: ASCE (Ed.), Proceedings Coastal Dynamics 05, Barcelona, p. 13

Kraus, N.C. (2010). Engineering of tidal inlets and morphologic consequences. In: Kim, Y.C. (Ed.), Handbook of Coastal and Ocean Engineering. *World Scientific*, Singapore, pp. 867–901.

Kumar, K. V., Palit, A., & Bhan, S. K. (1997). Bathymetric mapping in Rupnarayan-Hooghly river confluence using IRS data. *International Journal of Remote Sensing*, *18*(11), 2269-70.

Lobo F.J., Plaza F., González R., Dias J.M.A., Kapsimalis V., Mendes I., Díaz del Río V. (2004) – Estimations of bedload sediment transport in the Guadiana Estuary (SW Iberian Peninsula) during low river discharge periods. *Journal of Coastal Research* 41, 12-26.

López-Ruiz, A.; Garel, E., and Ferreira, Ó., 2020. The effects of high river discharges on the morphodynamics of the Guadiana ebb-tidal delta. In*:* Malvárez, G. and Navas, F. (eds.), Global Coastal Issues of 2020. *Journal of Coastal Research*, Special Issue No. 95, pp. 558-562. Coconut Creek (Florida).

Luo, Y. (2018). Mapping Plant Communities in the Intertidal Zones of the Yellow River Delta Using Sentinel-2 Optical and Sentinel-1 SAR Time Series Data. (Master thesis, University of Twente).

Malczewski, J. (2004). GIS-based land-use suitability analysis: a critical overview. *Progress in planning*, *62*(1), 3-65.

Masselink, G., & van Heteren, S. (2014). Response of wave-dominated and mixed-energy barriers to storms. *Marine Geology*, *352*, 321-347.

Masselink, G., Castelle, B., Scott, T., Dodet, G., Suanez, S., Jackson, D., & Floc'h, F. (2016). Extreme wave activity during 2013/2014 winter and morphological impacts along the Atlantic coast of Europe. *Geophysical Research Letters*, *43*(5), 2135-2143.

Morais, P. & Domingues, R.B. (2017). A brief journey along time in the Guadiana estuary. In: D. Moura, A. Gomes, I. Mendes, J. Anílbal (Eds.), Guadiana River estuary - investigating the past, present and future. 1st edition. University of Algarve. Faro, ISBN 978-989-8859-18-1, pp. 105–11.

Morales J.A. (1993). Sedimentologia del Estuario del Rio Guadiana (S.W. España-Portugal). Ph.D. Thesis, University of Sevilla, Serv. Publ. Univ. Huelva (1995), 274 p.

Morales, J. A. (1997). Evolution and facies architecture of the mesotidal Guadiana River delta (SW Spain-Portugal). *Marine Geology*, *138*(1-2), 127-148.

Morales J.A., Delgado I. & Gutierrez-Mas J.M. (2006) – Sedimentary characterization of bed types along the Guadiana Estuary (SW Europe) before the construction of the Alqueva dam. Estuarine. *Coastal and Shelf Science* 70, 117-31.

Morales, J. A., & Garel, E. (2019). The Guadiana river delta. In: *The Spanish Coastal Systems* (pp. 565-581). Springer, Cham.

Morales, J. A., Pendon, J. G., & Borrego, J. (1994). Origen y evolución de flechas litorales recientes en la desembocadura del estuario mesomareal del rio Guadiana (Huelva, SW España). *Revista de la Sociedad Geologica de Espana*, 7, 155–67.

Morales, J. A., Ruiz, F., & Jiménez, I. (1997). Papel de la sedimentación estuarina en el intercambio sedimentario entre el continente y el litoral: el estuario del río Guadiana (SO de España-Portugal). *Revista de la Sociedad Geológica de España*, *10*(3-4), 309-25.

Morris, B. D., Davidson, M. A., & Huntley, D. A. (2001). Measurements of the response of a coastal inlet using video monitoring techniques. Marine Geology, 175(1-4), 251-272.

Mulhern, J. S., Johnson, C. L., & Martin, J. M. (2017). Is barrier island morphology a function of tidal and wave regime?. *Marine Geology*, *387*, 74-84.

Olabarrieta, M., Geyer, W. R., & Kumar, N. (2014). The role of morphology and wave-current interaction at tidal inlets: An idealized modeling analysis. *Journal of Geophysical Research: Oceans*, 119(12), 8818-8837.

Oost, A.P., Hoekstra, P., Wiersma, A., Flemming, B., Lammerts, E.J., Pejrup, M., Hofstede, J., van der Valk, B., Kiden, P., Bartholdy, J., van der Berg, M.W., Vos, P.C., de Vries, S., Wang, Z.B., 2012. Barrier island management: lessons from the past and directions for the future. *Ocean Coastal Manag*. 68, 18–38

Pawlowicz, R., Beardsley, B., & Lentz, S. (2002). Classical tidal harmonic analysis including error estimates in MATLAB using T_TIDE. *Computers & Geosciences*, *28*(8), 929-937.

Phillips, M. S., Harley, M. D., Turner, I. L., Splinter, K. D., & Cox, R. J. (2017). Shoreline recovery on wave-dominated sandy coastlines: the role of sandbar morphodynamics and nearshore wave parameters. *Marine Geology*, *385*, 146-159.

Pope, J. (1991). Ebb Delta and Shoreline Response to Inlet Stabilization, Examples from the Southeast Atlantic Coast, Proceedings, 1991 Coastal Zone. National Oceanic and Atmospheric Administration, pp. 643–654

Reinson, G.E., 1992. Transgressive barrier island and estuarine systems. In: Walker, R.G., James, N.P. (Eds.), Facies Models: Response to Sea Level Change. *Geological Association of Canada*, St. John's, pp. 179–194.

Robin, N., Levoy, F., & Monfort, O. (2009). Short term morphodynamics of an intertidal bar on megatidal ebb delta. *Marine Geology*, 260(1-4), 102-120.

Santos, F. D., Lopes, A. M., Moniz, G., Ramos, L., & Taborda, R. (2014). Gestão da Zona Costeira–O Desafio da Mudança. *Relatório do Grupo de Trabalho do Litoral: Lisbon, Portugal.*

Sichoix, L., & Bonneville, A. (1996). Prediction of bathymetry in French Polynesia constrained by shipboard data. *Geophysical research letters*, *23*(18), 2469-2472.

Stauble DK. (1998). Techniques for measuring and analyzing inlet ebbshoal evolution. In *Coastal Engineering Technical Note IV-13. U.S. Army Engineering Research and Development Center, Coastal and Hydraulics Research Laboratory*: Vicksburg, MS.

Styles, R., Brown, M. E., Brutsché, K. E., Li, H., Beck, T. M., & Sánchez, A. (2016). Long-term morphological modeling of barrier island tidal inlets. *Journal of Marine Science and Engineering*, *4*(4), 65.

Thiebot, J., Idier, D., Garnier, R., Falqués, A., & Ruessink, B. G. (2012). The influence of wave direction on the morphological response of a double sandbar system. *Continental Shelf Research*, *32*, 71-85.

Tronvig, K.A. (2005) Near-shore bathymetry. Hydro International 9, 24–25.

Van der Vegt, M., Schuttelaars, H. M., & De Swart, H. E. (2009). The influence of tidal currents on the asymmetry of tide-dominated ebb–tidal deltas. *Continental Shelf Research*, *29*(1), 159-74.

Vicente, C., & Pereira, M. C. (2001). *Estudo das condições ambientais no estuário do Guadiana e zona costeira adjacente. 2ª Fase: componente de dinâmica costeira*. Relatório 74/01-NET, Laboratorio Nacional de Engenharia Civil.

Vila-Concejo, A., Ferreira, Ó., Morris, B. D., Matias, A., & Dias, J. M. A. (2004). Lessons from inlet relocation: examples from Southern Portugal. *Coastal engineering*, *51*(10), 967-990.

Vörösmarty, C.J., Sharma, K.P., Balázs, M.F., Copeland, A.H., Holden, J., Marble, J., And Lough, J.A. (1997). The storage and aging of continental runoff in large reservoir systems of the world: Ambio, v. 26, p. 210– 219.

Walton Jr., T.L., Adams, W.D. (1976). Capacity of inlet outer bars to store sand. In: Coastal Engineering, pp. 1919–37 (1977).

Warne, D. K. (1978). Landsat as an aid in the preparation of hydrographic charts. *Photogrammetric engineering and remote sensing*, *44*(8), 1011-16.

Weinholtz, M. B. (1978). Rio Guadiana: Elementos para o estudo da evolução da sua embocadura. *Relatório da Direcção-Geral de Portos, Lisboa, 11p.*

Zazo, C., Goy, J. L., Somoza, L., Dabrio, C. J., Belluomini, G., Improta, S., ... & Silva, P. G. (1994). Holocene sequence of sea-level fluctuations in relation to climatic trends in the Atlantic-Mediterranean linkage coast. *Journal of Coastal Research*, 933-45.

Zhang, H., Li, D., Wang, J., Zhou, H., Guan, W., Lou, X., ... & Ren, L. (2020). Long time-series remote sensing analysis of the periodic cycle evolution of the inlets and ebb-tidal delta of Xincun Lagoon, Hainan Island, China. ISPRS Journal of Photogrammetry and Remote Sensing, 165, 67-85.

8 Annexes

8.1 Annex I

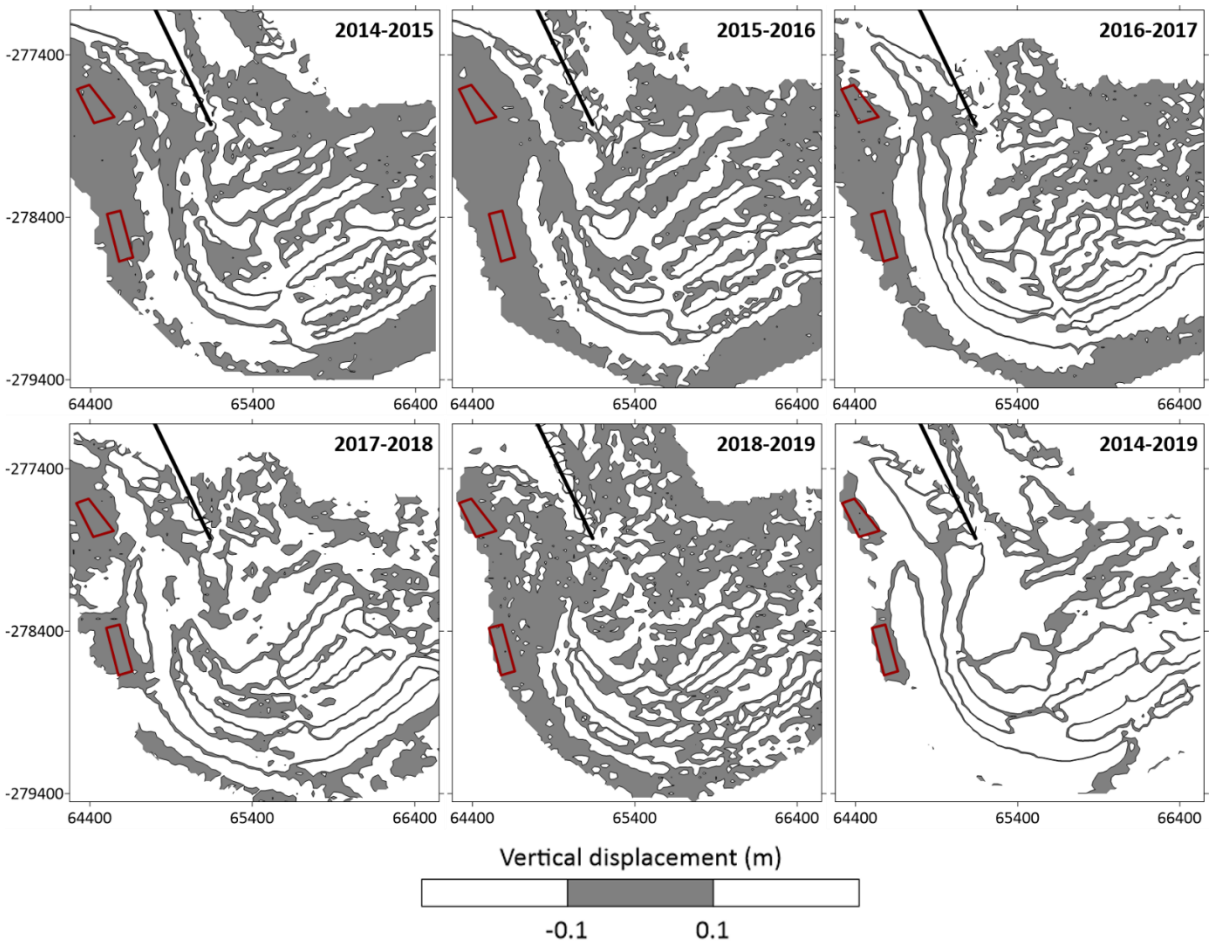

Figure 31.- Yearly difference maps showing vertical displacement between grids. Steady areas are shown in grey and varying areas in white. West jetty in black.

8.2 Annex II

Table 7.- The 53 storm events identified in the present study

Event	Date	Duration	Max Hs (m)	Mean Hs (m)	Mean Tp (s)	Mean Dir (°)	Dir	Max P (J/m^2s)	Pn (J/m^2s)
1	04/02/2014	11h 30'	3.41	2.98	7.59	239.08	SW	91107.33	55597.62
2	09/02/2014	19h	4.79	3.37	9.30	245.72	SW	204487.60	81236.72
3	11/02/2014	6h	2.71	2.55	7.54	253.15	SW	55438.03	21734.52
4	08/03/2014	9h	2.65	2.46	7.89	129.53	SE	55021.99	19618.73
5	09/03/2014	27h 30'	3.36	2.80	8.17	128.16	SE	100617.73	29951.92
6	31/03/2014	42h 30'	3.64	2.82	8.96	229.30	SW	129764.93	111172.37
7	14/05/2014	22h	2.91	2.51	8.60	128.07	SE	75471.32	58746.34
8	21/05/2014	17h	2.71	2.48	7.83	242.51	SW	57541.76	27387.84
9	16/09/2014	12h 30'	2.75	2.46	9.83	246.19	SW	75523.56	23177.97
10	20/11/2014	14h	3.18	2.69	7.74	148.80	SE	79231.67	47318.87
11	27/11/2014	51h 30'	3.49	2.74	10.28	243.18	SW	118247.33	75277.72
12	13/12/2014	11h	3.4	2.72	8.10	214.13	SW	90573.76	28105.77
13	09/02/2015	18h	3.37	2.90	8.20	124.35	SE	101217.53	49987.28
14	06/04/2015	47h	4.53	3.21	8.37	125.11	SE	199208.40	133230.29
15	17/10/2015	20h 30'	4.03	3.03	9.24	194.15	SW	167014.41	94781.86
16	20/10/2015	6h	3.64	3.24	7.63	165.15	SE	103811.94	27868.09
17	02/11/2015	12h	4	3.11	7.92	239.50	SW	125361.60	46686.13
18	28/12/2015	41H	3.3	2.70	8.96	182.14	SW	107185.70	78895.40
19	11/01/2016	7h	2.83	2.50	7.07	235.47	SW	54906.72	34283.91
20	07/05/2016	26h 30'	3.64	2.85	8.66	230.04	SW	103811.94	91706.29
21	10/05/2016	6h	2.66	2.47	8.76	244.46	SW	63060.76	37026.71
22	11/05/2016	11h 30'	2.65	2.46	8.46	235.33	SW	60712.34	33624.97
23	25/10/2016	11h	2.88	2.63	9.41	221.43	SW	81234.32	34181.86
24	30/11/2016	15h	2.97	2.67	7.90	125.03	SE	69112.63	44599.91
25	03/12/2016	41h 30'	3.69	2.86	10.15	227.37	SW	166692.98	91780.60
26	02/01/2017	22H 30'	3.98	3.29	10.52	226.28	SW	170477.83	103014.02
27	26/01/2017	27h	2.9	2.58	8.08	231.64	SW	65893.19	42786.96
28	11/02/2017	21H 30'	3.47	2.86	7.99	182.05	SW	107313.63	88625.20
29	04/03/2017	8h	3.53	2.94	7.75	247.69	SW	97632.40	55526.58
30	15/03/2017	9H	2.76	2.52	7.20	123.10	SE	59684.66	38843.43
31	26/03/2017	13H 30'	3.53	3.17	8.46	215.68	SW	111056.85	83385.38
32	09/04/2017	8H	2.93	2.74	7.89	127.33	SE	67263.55	44793.92
33	19/04/2017	37H 30'	4.99	3.74	9.50	125.57	SE	256061.89	90917.46
34	21/04/207	13H 30'	3.36	2.94	8.32	124.64	SE	100617.73	47259.41
35	21/05/2017	13H 30'	3.55	3.17	9.16	123.44	SE	123427.31	58510.71
36	11/12/2017	8H	3.82	3.12	8.35	250.00	SW	119387.30	49005.44
37	29/01/2018	16H	3.84	3.07	8.38	123.30	SE	131419.07	95794.82
38	30/01/2018	8h	3.39	2.96	8.01	124.78	SE	90041.75	73067.59
39	28/02/2018	151H	6.55	4.01	10.78	241.05	SW	525227.15	472470.16
40	09/03/2018	61H	3.76	3.14	11.53	248.45	SW	200358.20	63694.60
41	14/03/2018	10H	3.44	3.03	8.22	249.00	SW	92717.44	52827.82

42	17/03/2018	24H	4.49	3.30	8.54	250.92	SW	179675.40	139488.82
43	10/04/2018	13H	2.8	2.54	8.17	252.29	SW	61427.18	21761.70
44	20/04/2018	17H	3.26	2.90	8.56	129.72	SE	94717.70	59061.27
45	17/11/2018	21H	4.3	2.97	8.95	216.43	SW	164790.76	71976.20
46	01/02/2019	16H	3.09	2.55	7.80	247.88	SW	74810.32	34941.15
47	14/02/2019	8H	2.76	2.56	8.00	120.56	SE	59684.66	22489.69
48	22/02/2019	6H	2.66	2.55	13.43	247.14	SW	99095.49	65961.35
49	25/02/2019	22H	2.99	2.64	9.20	151.30	SE	105917.33	50812.97
50	26/02/2019	6H	2.79	2.60	7.71	126.43	SE	60989.20	11699.18
51	26/03/2019	32H 30'	4.11	3.05	8.43	127.36	SE	165439.12	69758.33
52	28/03/2019	12H 30'	2.89	2.47	7.88	129.73	SE	65439.54	18755.75
53	22/11/2019	6H	2.7	2.54	7.86	236.29	SW	55021.99	29289.19

8.3 Annex III

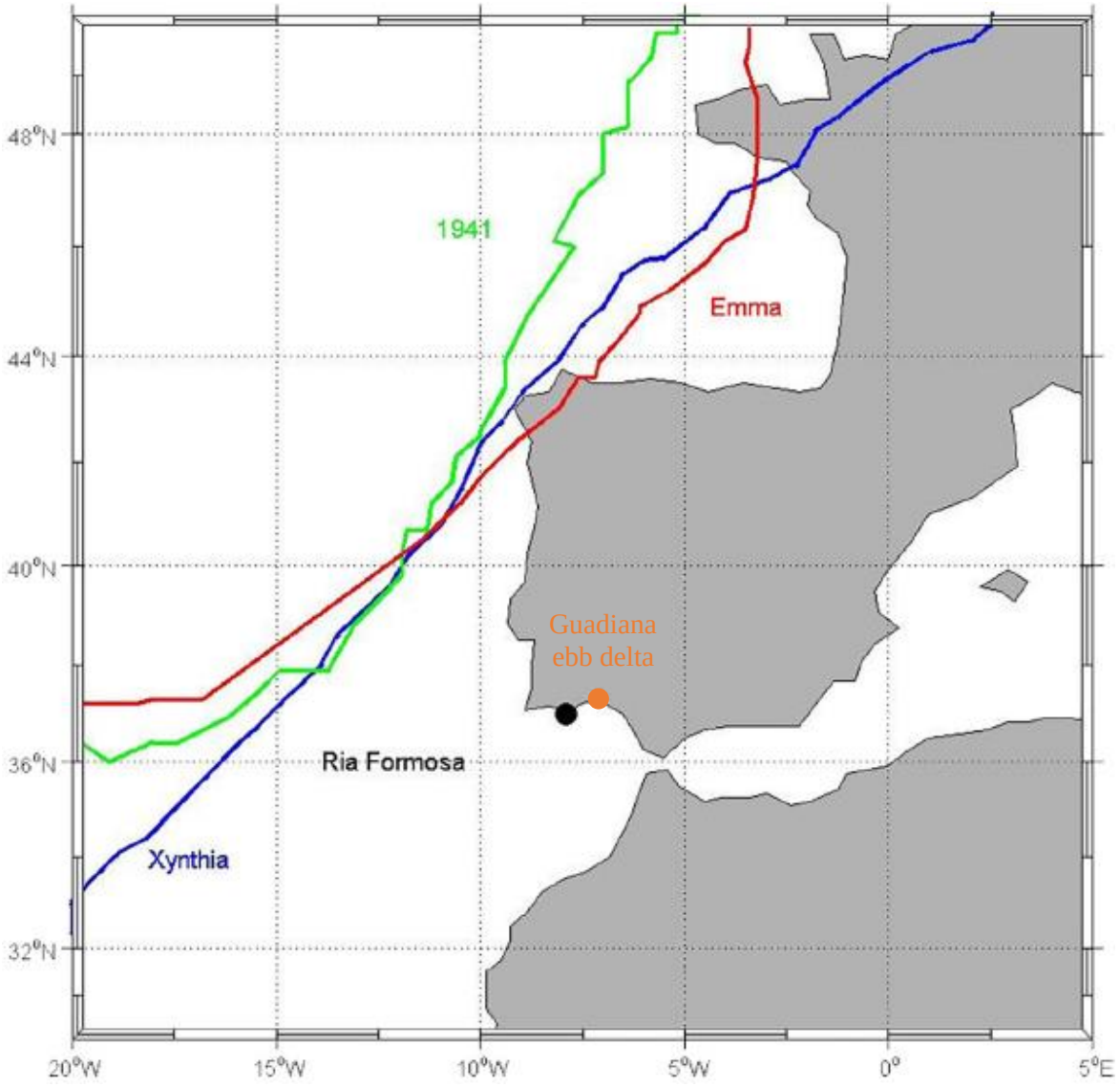

Figure 32.- Storm track of Emma storm(red) and of two of the most significant previous hazardous storms in the area (1941 storm in green and Xynthia storm in blue), modified from Ferreira et al. (2019).

8.4 Annex IV

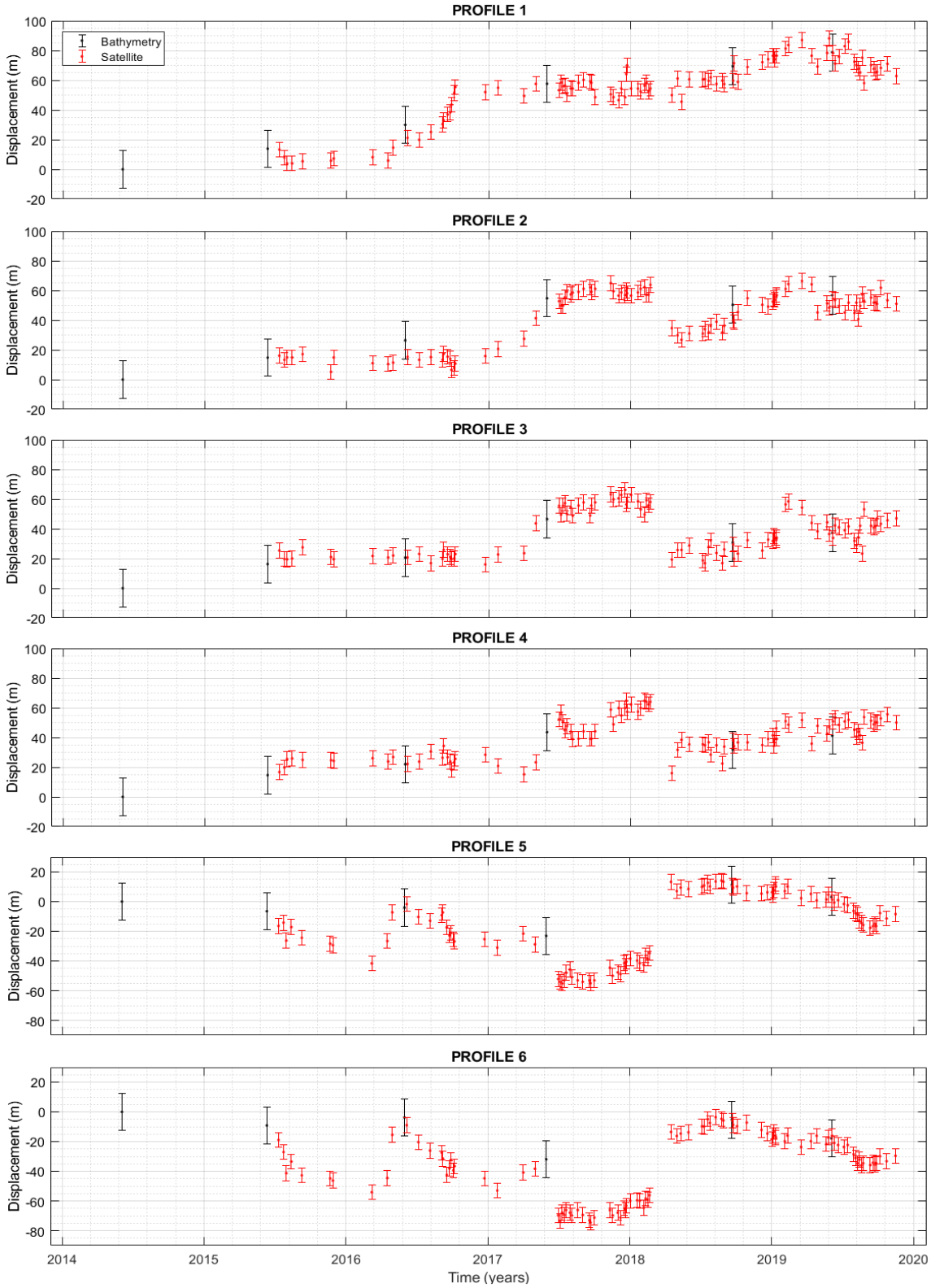

Figure 33.- Outer shoal displacement across the 6 profiles recorded through the satellite images (red error bar) ant the bathymetric maps (black error bars).

8.5 Annex V

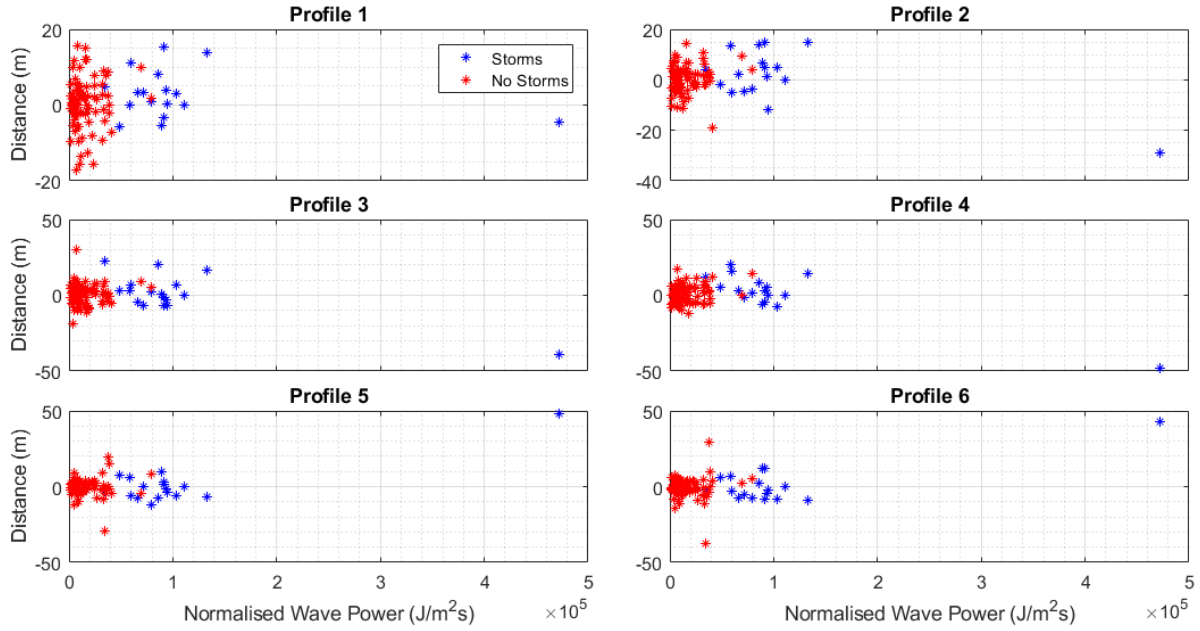

Figure 34.- Maximum Pn between samplings. Storm events are represented in blue while periods without storms are presented in red.

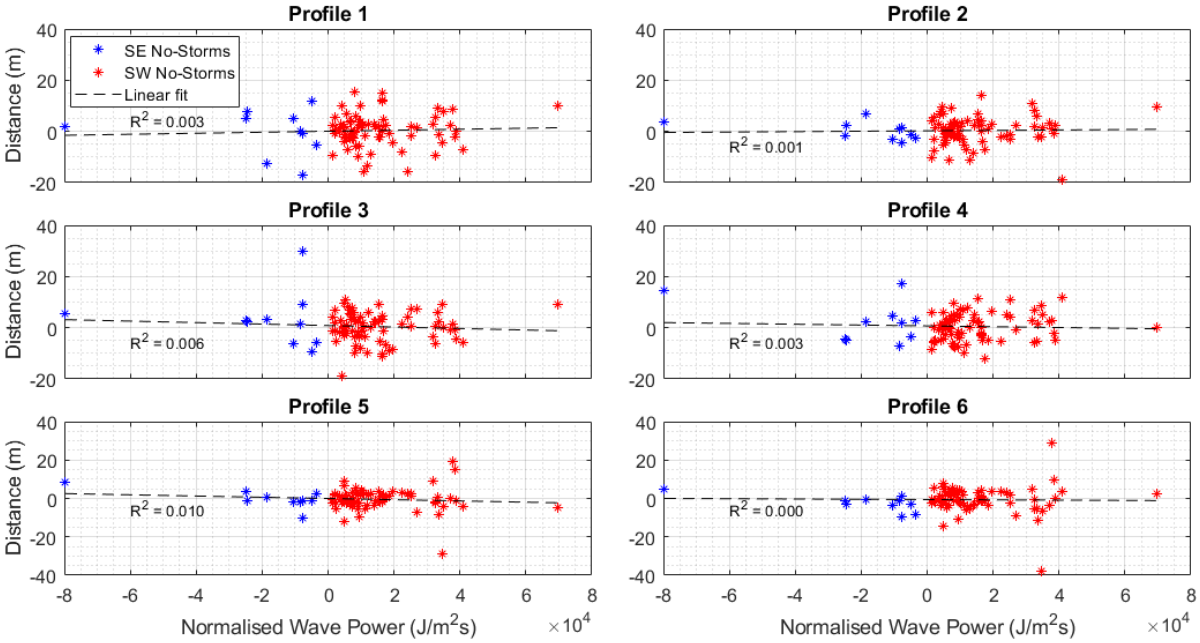

Figure 35.- Displacement of the shoal across the 6 profiles under normal conditions (without storm events). Maximum normalised wave power of the SE incoming waves represented in negative values(blue) and from the SW in positive (red). Dashed line illustrates the linear fit.

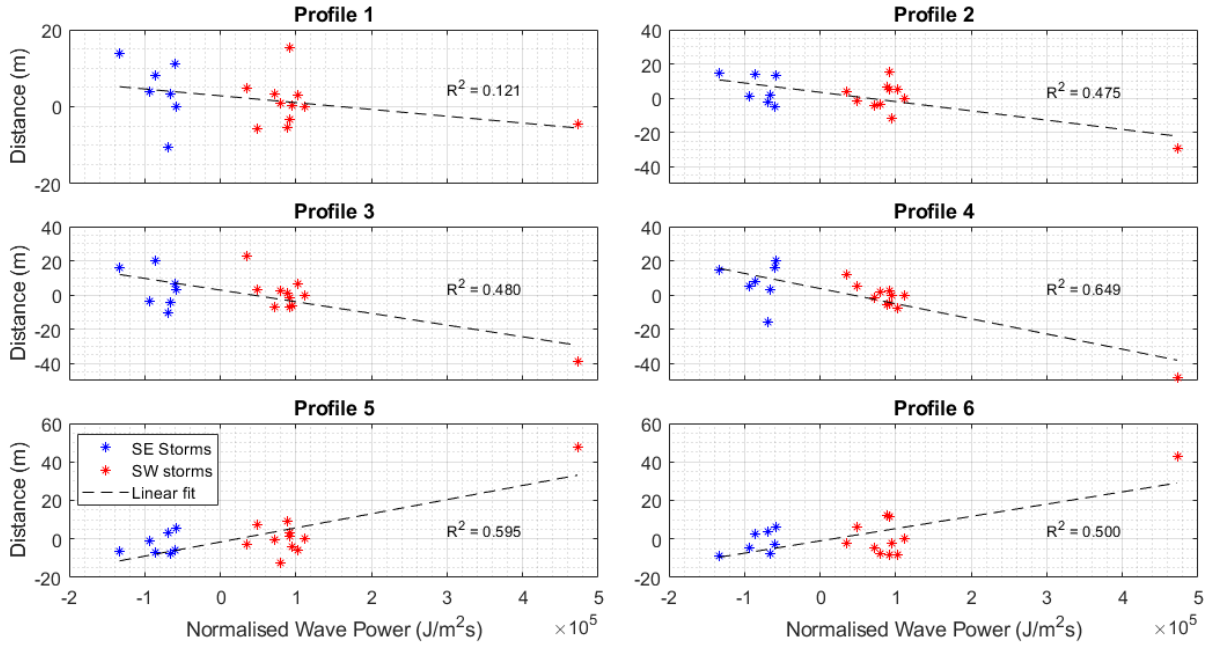

Figure 36.- Apparent displacement of the ebb-delta under storm conditions. Maximum normalised wave power from SE storm events represented in negative (blue) and from SW shown in positive (red). Dashed line illustrates the linear fit.

8.6 Annex VI

Table 8.- Dates of the datasets used for the study.

Date	Storm	Max Hs (m)	Mean Dir (°)	Dir	P (J/m^2s)	Max Pn (J/m^2s)
04/06/2014	X	4.79	253.15	SW	204487.60	111172.37
12/06/2015	X	4.53	125.11	SE	199208.40	133230.29
12/07/2015		1.44	-1.00	SE	9951.20	7673.96
25/07/2015		1.08	168.75	SE	5140.61	3668.35
01/08/2015		1.12	257.71	SW	6288.61	4960.93
14/08/2015		0.97	230.08	SW	5713.34	4955.10
10/09/2015		1.91	235.33	SW	28583.23	26911.70
22/11/2015	X	4.03	239.50	SW	167014.41	94781.86
29/11/2015		1.07	193.88	SW	5494.37	4528.37
08/03/2016	X	3.30	235.47	SW	107185.70	78895.40
17/04/2016		2.04	250.10	SW	40315.34	38422.66
30/04/2016		2.39	241.13	SW	55943.59	37916.79
31/05/2016	X	3.64	244.46	SW	103811.94	91706.29
06/06/2016		1.53	235.67	SW	15632.25	13078.15
06/07/2016		2.26	219.45	SW	40018.56	33480.07
05/08/2016		2.28	207.00	SW	40729.98	32402.00
04/09/2016		2.00	178.57	SE	29184.96	24976.65
07/09/2016		1.14	252.39	SW	18201.21	12409.07
17/09/2016		1.29	253.75	SW	11213.01	9513.53
24/09/2016		0.82	218.51	SW	9950.85	9002.17
27/09/2016		0.68	193.14	SW	4178.89	2098.83
04/10/2016		2.65	186.71	SW	48144.24	35083.90
07/10/2016		1.07	196.72	SW	11344.25	6908.43
23/12/2016	X	3.69	227.37	SW	166692.98	91780.60
25/01/2017	X	3.98	226.28	SW	170477.83	103014.02
02/04/2017	X	3.53	247.69	SW	111056.85	88625.20
02/05/2017	X	4.99	127.33	SE	256061.89	90917.46
31/05/2017	X	3.55	123.44	SE	123427.31	58510.71
01/07/2017		2.41	212.93	SW	39818.66	34561.92
06/07/2017		1.72	166.65	SE	21331.06	10417.82
11/07/2017		1.57	262.35	SW	11829.05	7743.00
16/07/2017		0.72	194.00	SW	3412.97	2263.31
21/07/2017		1.57	199.96	SW	13277.51	8332.74
31/07/2017		1.44	250.00	SW	11169.72	9725.50
05/08/2017		1.04	257.88	SW	5250.24	2552.06
20/08/2017		1.18	209.67	SW	9225.05	6789.32
02/09/2017		1.55	199.91	SW	16470.85	14318.55
19/09/2017		1.30	225.55	SW	23190.96	18642.34
22/09/2017		0.54	226.38	SW	2662.68	2176.81

02/10/2017		1.05	195.14	SW	12216.88	9177.53
11/11/2017		2.58	174.19	SE	93224.49	79673.39
18/11/2017		1.64	183.33	SW	16331.80	11060.20
01/12/2017		2.07	184.72	SW	38188.86	25371.56
08/12/2017		1.93	145.03	SE	28583.23	24618.51
18/12/2017	X	3.82	250.00	SW	119387.30	49005.44
21/12/2017		1.31	194.50	SW	12765.89	8138.48
23/12/2017		1.03	244.83	SW	14858.16	8447.65
02/01/2018		2.16	229.98	SW	28330.47	24033.31
20/01/2018		2.05	240.19	SW	43588.62	38742.35
27/01/2018		1.29	246.42	SW	25098.90	15774.78
06/02/2018	X	3.84	124.78	SE	131419.07	95794.82
11/02/2018		1.22	207.71	SW	10390.32	4891.00
16/02/2018		0.96	251.52	SW	13544.21	9516.44
21/02/2018		1.19	248.81	SW	21358.42	15577.75
17/04/2018	X	6.55	252.29	SW	525227.15	472470.16
02/05/2018	X	3.26	129.72	SE	94717.70	59061.27
12/05/2018		1.17	224.16	SW	16355.77	10813.97
01/06/2018		1.70	216.58	SW	19813.01	16341.05
06/07/2018		1.69	243.46	SW	19580.60	16630.08
11/07/2018		1.12	233.83	SW	5528.45	3528.84
21/07/2018		1.02	248.55	SW	5797.74	5170.38
26/07/2018		0.70	253.90	SW	2457.09	1358.08
10/08/2018		1.87	218.89	SW	27398.56	19558.43
25/08/2018		1.55	196.86	SW	18823.83	17532.71
30/08/2018		1.66	221.43	SW	21590.40	15501.80
21/09/2018		1.60	217.06	SW	17550.62	16337.85
22/09/2018		0.58	237.83	SW	2962.65	1471.97
24/09/2018		1.11	140.90	SE	7481.56	4837.63
04/10/2018		1.89	165.54	SE	24489.29	18455.65
29/10/2018		2.41	208.81	SW	81343.84	69772.85
06/12/2018	X	4.30	216.43	SW	164790.76	71976.20
21/12/2018		1.83	246.33	SW	35769.82	25140.86
02/01/2019		2.42	201.55	SW	44754.87	37230.66
05/01/2019		1.25	224.29	SW	12736.93	8136.87
07/01/2019		0.98	252.71	SW	11099.12	7357.18
11/01/2019		1.60	212.26	SW	15544.84	10018.96
12/01/2019		1.39	125.63	SE	16639.63	8466.11
04/02/2019	X	3.09	247.88	SW	74810.32	34941.15
11/02/2019		1.01	244.15	SW	15385.73	10449.52
18/03/2019	X	2.99	126.43	SE	105917.33	65961.35
12/04/2019	X	4.11	129.73	SE	165439.12	69758.33
27/04/2019		2.24	249.36	SW	46655.52	41088.28
22/05/2019		2.33	212.88	SW	42535.97	33406.97
27/05/2019		1.42	240.32	SW	16715.56	9895.97
04/06/2019		2.43	184.23	SW	44754.87	32665.39

06/06/2019	1.49	266.83	SW	10654.26	8067.03
11/06/2019	1.39	262.98	SW	8617.08	6083.26
21/06/2019	1.56	247.58	SW	23834.37	16849.81
06/07/2019	1.14	250.17	SW	7000.47	5729.71
16/07/2019	1.14	234.34	SW	5236.25	3951.19
31/07/2019	1.43	243.77	SW	16632.71	11849.43
05/08/2019	0.83	230.47	SW	5313.99	4812.20
10/08/2019	0.96	253.68	SW	8963.35	6636.66
15/08/2019	1.13	238.57	SW	11004.40	7271.47
20/08/2019	0.82	234.23	SW	6177.82	4328.43
25/08/2019	1.32	165.42	SE	13445.82	7637.31
12/09/2019	1.58	187.77	SW	17114.60	16449.33
19/09/2019	1.00	229.58	SW	7723.03	5485.47
24/09/2019	1.03	254.91	SW	10390.38	5427.70
27/09/2019	0.85	254.93	SW	9413.03	6859.33
07/10/2019	1.60	249.33	SW	33346.19	31805.71
24/10/2019	1.71	233.56	SW	20046.79	14099.54
16/11/2019	1.56	244.84	SW	25448.40	22354.36